ABSTRACT

Trends, Optical Properties, and Source Contributions to Elemental and Organic Carbon Influencing the North American Arctic

Tate E. Barrett, Ph.D.

Mentor: Rebecca J. Sheesley, Ph.D.

Atmospheric aerosols are one of the greatest sources of uncertainty in current global climate models. Aerosols affect the earth's radiative budget by scattering or absorbing incoming solar radiation and by acting as cloud condensation nuclei. Carbonaceous aerosols are dominated by two main components: organic carbon and elemental carbon. Traditionally, only elemental carbon aerosols acted as absorbing species in global climate models, causing models to underestimate warming in certain regions, particularly the Arctic. However, it is now known that a fraction of organic carbon, or brown carbon, absorbs incoming solar radiation mainly in the ultra-violet wavelengths, and is responsible for as much as 19% of total aerosol absorption resulting from anthropogenic activity globally. Primary aerosols are emitted directly into the atmosphere via natural and anthropogenic processes wildfires, fossil fuel combustion, and biomass burning, while secondary organic aerosols are formed in the atmosphere via gaseous emission partitioning into the condensed phase. Due to their short atmospheric lifespan, 1-2 weeks, it is thought that decreasing the emissions of elemental and brown carbon would immediately reduce climate forcing across the globe.

The Arctic is particularly sensitive to anthropogenic climate forcing. It is warming at a rate nearly twice the global mean, with temperature increases of nearly 2 °C since 1970. Aerosols play a vital role in the radiative budget of the Arctic due to their direct and indirect effects. For example, deposition of atmospheric aerosols on snow and ice reduces surface albedo, contributing to changing melt patterns. In order to determine the contributions of fossil and contemporary sources to organic and elemental carbon in the North American Arctic, a combination of source apportionment strategies, including radiocarbon abundance, was applied to samples collected at Barrow, Alaska. Optical properties were also explored to determine the overall efficiency of light-absorbing particles in the region. Results indicate that fossil sources dominate the elemental carbon burden for much of the year, while organic carbon has more equal contributions of fossil and contemporary sources throughout the year. These apportionment results are more tightly constrained than current climate models, and can be used to improve the overall accuracy of these models.

Trends, Optical Properties, and Source Contributions to Elemental and Organic Carbon Influencing the North American Arctic

by

Tate E. Barrett, B.S.

A Dissertation

Approved by the Institute of Ecological, Earth, and Environmental Sciences

_____

Joe Yelderman, Jr., Ph.D., Director

Submitted to the Graduate Faculty of
Baylor University in Partial Fulfillment of the
Requirements for the Degree
of

Doctor of Philosophy

Approved by the Dissertation Committee

_____

Rebecca J. Sheesley, Ph.D., Chairperson

_____

William C. Hockaday, Ph.D.

_____

Dennis A. Johnston, Ph.D.

_____

Sascha Usenko, Ph.D.

_____

Joseph D. White, Ph.D.

Accepted by the Graduate School

August 2016

_____

J. Larry Lyon, Ph.D., Dean

Page bearing signatures is kept on file in the Graduate School.

TABLE OF CONTENTS

LIST OF FIGURES

LIST OF TABLES

ABBREVIATION LIST

^{14}C	Radiocarbon
^{13}C	Stable carbon
AAE	Absorption Ängstrom exponent
AK	Alaska
ARM	Atmospheric Radiation Measurement
ARS	Agriculture Research Service
ASE	Accelerated solvent extractor
ATN	Optical attenuation
b_{abs}	Absorption coefficient
BC	Black carbon
BrC	Brown carbon
BSTFA	N,O-bis(trimethylsilyl)-trifluoroacetamide
BT	Back trajectory
CCN	Cloud condensation nuclei
CMB	Chemical mass balance
DCM	Dichloromethane
DISCOVER-AQ	Deriving Information on Surface Conditions from Column and Vertically Resolved Observations Relevant to Air Quality
EC	Elemental carbon
EPA	Environmental Protection Agency
$F_{biomass}$	Fraction biomass
F_{fossil}	Fraction fossil
FID	Flame ionization detector
F_m	Fraction modern
GC/MS	Gas Chromatography-Mass Spectrometry
GDAS	Global data assimilation system

GSA	Geographic source assessment
HYSPLIT	Hybrid Single-Particle Lagrangian Integrated Trajectory
IPCC	Intergovernmental Panel on Climate Change
KHP	Potassium hydrogen phthalate
MAC	Mass absorption cross-section
MAE	Mass absorption efficiency
MeOH	Methanol
NIOSH	National Institute of Occupational Safety and Health
NMHC	Non-methane hydrocarbons
NMVOC	Non-methane volatile organic compounds
NOAA	National Oceanic and Atmospheric Administration
NOSAMS	National Ocean Sciences Accelerator Mass Spectrometry
NSA	North Slope of Alaska
OC	Organic carbon
OM	Organic mass
PAH	Polycyclic aromatic hydrocarbon
PLE	Pressurized liquid extraction
PM	Particulate matter
PM_{10}	Particulate matter with an aerodynamic diameter of <10 μm
$PM_{2.5}$	Particulate matter with an aerodynamic diameter of <2.5 μm
PyrC	Pryolyzed carbon
QFF	Quartz fiber filter
SOA	Secondary organic aerosol
TCEQ	Texas Commission on Environmental Quality
TEOM	Tapered element oscillating microbalance
TexAQS	Texas Air Quality Study
TOC	Total organic carbon
TOR	Thermal optical reflectance
TOT	Thermal optical transmission
USDA	United States Department of Agriculture
VOC	Volatile organic compound

WIOC	Water insoluble organic carbon
WSOC	Water soluble organic carbon

ACKNOWLEDGMENTS

I would first like to thank my family, who have encouraged, supported, and believed in me throughout this research project. I am forever grateful to my parents, Dr. Robby and LaVon Barrett, who have always believed in me and allowed me to pursue my dreams. I want to thank my brother Tye for his friendship and always encouraging me and keeping me humble with his quick wit and humor. Most importantly, I would like to acknowledge my wife Danielle, whose unconditional love, encouragement, and sacrifice has allowed me to fully devote my time and energy to this project; what an honor it is to share life and this accomplishment with her.

I would also like to thank the people and agencies that have enabled me to pursue the research presented in this dissertation. First, I would like to thank my advisor, Dr. Rebecca Sheesley. She has pushed me to accomplish things I didn't think possible and her guidance has helped me to become a better scientist. Thanks to Dr. Sascha Usenko, for all of his work and suggestions on my research projects. Special thanks to the remaining members of my dissertation committee, Dr. Hockaday, Dr. Johnston, and Dr. White, for their support and suggestions for the development of this dissertation. Dr. Jeffrey Back has provided much help and guidance throughout my graduate studies and I am very grateful for not only his professional support, but his friendship as well. I would also like to thank my co-authors, Dr. Eleanor Robinson, Dr. Örjan Gustafsson, Patrik Winiger, and August Andersson for their collaboration and valuable suggestions during manuscript preparation.

I would also like to thank Dr. Örjan Gustafsson for financial support and for graciously hosting me at the University of Stockholm to perform sample preparation for radiocarbon analysis. Funding for my research was provided by the Gus C. Glasscock Jr. Endowed Fund for Excellence in Environmental Sciences, without this support this research would not have been possible. Also, a special thanks to my lab mates, both past and present. Thank you for your constant encouragement, support, and friendship.

DEDICATION

To my daughters, Evie Jacquelyn and Wilder Tate, anything is possible, and to my wife Danielle, for all that you mean to me.

PREFACE

The overall objective of this thesis was to investigate the sources, characteristics, and optical properties of atmospheric carbonaceous aerosols, including organic carbon (OC) and elemental carbon (EC), on the North Slope of Alaska (NSA), located within the Arctic Circle. This was accomplished using multiple techniques: abundance measurements of radiocarbon of total organic carbon particulate matter, isolation of EC and subsequent radiocarbon abundance measurements of isolates, analysis of water soluble organic carbon (WSOC), and light absorption measurements of both WSOC and EC. The specific objectives of each chapter and author contributions are highlighted below.

Chapter One introduces atmospheric aerosols and their effect on climate change and Chapter Two introduces the main sampling methods and analytical techniques used throughout the remaining chapters.

The main objective of Chapter Three was to investigate seasonal trends in bulk aerosol composition and water-soluble organic carbon concentrations and optical properties in central Texas and to determine the influence of major metropolitan areas on a regional background site. This chapter serves as a proof of concept for Chapters Four through Six, a local study used to develop the field, chemical, optical and spatial analysis tools to be applied in the Alaskan Arctic. This study was designed to establish a method for water-soluble organic carbon extraction and measurement, as well as UV-absorption measurements for carbonaceous aerosol filter samples. I am the primary author of this

chapter and performed all sample collection and analysis. Dr. Rebecca J. Sheesley was involved in all aspects of the project and writing the manuscript.

The main objective of Chapter Four was to determine the contributions of fossil fuel combustion and biomass burning sources to the atmospheric EC burden in Barrow, AK during the Arctic winter. Radiocarbon apportionment was compared to a chemical mass balance apportionment model to quantify the limitations of the application of the latter model to remote sites. Based on those comparisons, a novel method of calculating the half-life of levoglucosan, a biomass burning organic tracer, was also developed. I am the primary author of this chapter and coordinated sample collection and conducted all sample preparation and data analysis for the radiocarbon source apportionment. Dr. Eleanor M. Robinson performed the sample extractions and gas chromatography-mass spectrometry analysis (GC/MS). Dr. Sascha Usenko assisted with the GC/MS data analysis and writing the manuscript. Dr. Rebecca J. Sheesley was involved with all aspects of the project, in particular, she oversaw the quality assurance and quality control of the chemical mass balance model and the writing of the manuscript.

The main objective of Chapter Five was to perform year-round characterization of atmospheric OC in Barrow, AK, including its solubility (ie. WSOC), optical properties, and source apportionment. This characterization of WSOC was combined with radiocarbon abundance measurements of OC. I am the primary author of this chapter and coordinated sample collection and performed all sample and data analysis. Dr. Rebecca J. Sheesley was involved in all aspects of the project and writing the manuscript.

The main objective of Chapter Six was to perform a year-round assessment of the optical properties and the contributions of fossil fuel combustion and biomass burning to

atmospheric EC in Barrow, AK using radiocarbon abundance measurements and investigate the optical properties of Arctic EC. I am the primary author of this chapter and performed the radiocarbon sample preparation and source apportionment calculations. Dr. Jeffrey A. Back and Claire Moffett performed the IC analysis. Radiocarbon sample preparation was performed at Stockholm University under the guidance of Dr. Örjan Gustafsson and with the assistance of Patrik Winiger. Dr. Rebecca J. Sheesley was involved in all aspects of the project and writing the manuscript.

CHAPTER ONE

Introduction

Atmospheric Aerosols

By directly influencing the radiation balance of the earth through scattering or absorbing incoming solar radiation, aerosols introduce one of the greatest sources of uncertainty in global climate models (IPCC 2007; McComiskey, et al. 2008; Chen and Bond 2010). Atmospheric aerosols are a mixture of suspended solid and liquid particles originating from both natural and anthropogenic sources. Aerosols are typically classified based on their size, ranging from a few nanometers (typically from combustion sources) to around 100μm (Seinfeld and Pandis 2016). Aerosols are also of interest due to their negative effects on human health and can penetrate the lungs and leading to possible cardiovascular and respiratory diseases (Lin, Lee, and Eatough 2010; Lin, et al. 2011).

Aerosols are emitted directly into the atmosphere as primary particles from natural sources such as sea spray, volcanic emissions, wind-driven dust and emissions from naturally occurring wildfires (Pöschl 2005; Seinfeld and Pandis 2006). Anthropogenic sources of primary particles include combustion of fossil fuels as well as biomass/biofuel burning and industrial processes (Seinfeld and Pandis 2006). Secondary aerosols are particles formed in the atmosphere through the transformation of gaseous emissions such as sulfur- and nitrous oxides and volatile organic compounds (VOCs) into lower volatility species that partition into the condensed phase (Kroll and Seinfeld 2008; Kirillova 2013).

Compared to CO_2, aerosols have a very short lifespan in the atmosphere (approximately 1-2 weeks) due to their removal from the atmosphere by one of two mechanisms: dry deposition (deposition at the surface of the earth) and wet deposition (incorporation into precipitation) (Seinfeld and Pandis 2016). Concentrations of aerosols respond quickly to emissions reductions, therefore aerosol emission controls represent a possible strategy in reducing climate forcing from anthropogenic activities, and thus slowing the rate of climate change (Bond, et al. 2013).

Carbonaceous Aerosol Composition

Carbonaceous aerosol components in the atmosphere consist of two major components: black or elemental carbon (BC or EC) and organic carbon (OC). These two account for a large fraction of atmospheric particulate matter (Seinfeld and Pandis 2006; Pöschl 2005). Total organic carbon (TOC), the geochemical term, refers to the sum of all carbon contained in both the EC and OC fractions of carbonaceous aerosols (TOC = OC + EC).

Black Carbon

BC is emitted only through fossil fuel or biomass combustion processes and is therefore a primary pollutant (Bond, et al. 2013; Seinfeld 2008; Seinfeld and Pandis 2016). BC is distinguished from other forms of carbon in the atmosphere by the following physical properties: (1) it strongly absorbs light in the visible spectrum; (2) it is refractory, retaining its basic form at very high temperatures; (3) it is insoluble in water and organic solvents including methanol and acetone, and (4) it consists as an aggregate of small carbon spheres (Bond, et al. 2013). More than 90% of BC resides in fine

particulate matter (particulate matter with an aerodynamic diameter of less than 2.5 μm, $PM_{2.5}$) and undergoes little chemical transformation in the atmosphere; therefore, it can be used as an indicator for anthropogenic air pollution (Y. G. Wang, et al. 2011; B. Chen, et al. 2012).

Throughout the literature, BC is referenced to by a number of different names (i.e. black carbon, elemental carbon, equivalent black carbon, and refractory black carbon) depending on the measurement method used for quantification (Arctic Monitoring and Assessment Programme 2015). In order to maintain consistency with current literature, the nomenclature suggested by Petzold, et al. (2013) will be used. BC will be used to refer to light absorbing atmospheric aerosols, possessing the four previously mentioned physical properties, with no reference to a specific measurement method. Elemental carbon (EC) will be used to refer to light absorbing carbon evolved from thermal optical methods (Petzold, et al. 2013; Birch and Cary 1996). Further description of the determination of EC will be discussed in the methods section.

Organic Carbon

The organic carbon fraction of aerosols typically refers to aerosols associated with condensed organic compounds (Pöschl 2005; Seinfeld and Pandis 2006). OC is typically categorized into water-insoluble organic carbon (WIOC) and water-soluble organic carbon (WSOC) (Hecobian, et al. 2010). WIOC has been found to be emitted as a primary aerosol from combustion of both fossil fuel and biomass while WSOC can be emitted directly or result from atmospheric processes (Hecobian, et al. 2010; Zhang and Ying 2011; Zhang, et al. 2013). Water-soluble organic carbon (WSOC) is an important part of OC due to its ability to influence climate by increasing the hygroscopicity of

particles and their ability to act as CCN; WSOC can account for up to 70% of total organic aerosol (Kirillova, et al. 2014).

Aerosol Source Apportionment

In order to develop proper strategies for aerosol mitigation, it is imperative to understand source contributions to observations of ambient aerosol concentration (Hopke 2016). Source apportionment can be accomplished by including ion and organic tracer concentrations as input into receptor-based models (Kirillova 2013; Hopke 2016). One such receptor-based model commonly used is the chemical mass balance (CMB) model, which is most applicable to the apportionment of primary aerosols and has been used extensively for PM_{10} apportionment across the western United States (Watson, et al. 2002; Hopke 2016). While the CMB model has been used in remote locations (Barrett, et al. 2015; von Schneidemesser, et al. 2009), receptor-based apportionment modeling can be limited by the accuracy and appropriateness of the input emission source profiles for a particular study location; therefore, more accurate apportionment techniques are needed in remote areas such as the Arctic (Barrett, et al. 2015).

One such source apportionment technique is the measurement of the abundance of radiocarbon (^{14}C) in OC and EC samples (Heal 2014; Gustafsson, et al. 2009). This method distinguishes between fossil sources of carbon, which contain no ^{14}C, and modern sources of carbon, which contain an abundance of ^{14}C (Heal 2014). ^{14}C is present in the atmosphere and living material is at equilibrium with the atmosphere through the photosynthesis and respiration. Once living material dies, the uptake of ^{14}C ceases and the amount of ^{14}C begins to decrease with a half-life of 5,370 years; therefore, the carbon in fossil fuels contains no ^{14}C due to its age (Heal 2014). While the ^{14}C apportionment is

more precise than the CMB and other receptor-based models, the combination of the two can provide additional information over the ^{14}C alone, such as the relative contributions of subgroups of fossil carbon contributions (i.e. coal combustion, petroleum combustion, motor-vehicle exhaust) (Sheesley, Andersson, and Gustafsson 2011).

Aerosols and Climate Change

Atmospheric aerosols can affect the earth's radiative balance through direct effects (absorbing and scattering incoming solar radiation) and indirect effects (acting as cloud condensation nuclei, the cloud albedo effect, and decreasing surface albedo) (Chen and Bond 2010; Kirchstetter, Novakov, and Hobbs 2004; Lu, et al. 2015). BC has a total radiative forcing value (changes in the radiative balance of the earth due to increasing absorption of light within the atmosphere), including both direct and indirect effects, of +1.1 W m^{-2} with 90% uncertainty bounds of +0.17 to +2.1 W m^{-2}, making it the second most important atmospheric pollutant behind CO_2 (Bond, et al. 2013).

Typically, OC is treated as a light scattering species while EC is treated as the only light-absorbing species in climate models (Kirchstetter, Novakov, and Hobbs 2004; Cheng, et al. 2011). However, the effects of light-absorbing organic carbon, known as brown carbon (BrC), are becoming more apparent (Bahadur, et al. 2012). Recent modeling efforts including BrC suggest that it contributes up to +0.25 W m^{-2} globally to the earth's radiative budget, which is 19% of the total light absorption due to anthropogenic aerosols. The global atmospheric burden of BrC may be more than three times the burden of BC (Feng, Ramanathan, and Kotamarthi 2013). While there are multiple techniques to determine the presence and absorption properties of BrC, the

measurement of light absorption of liquid extracts of organic aerosols is a common method (Chen and Bond 2010; Kirillova, et al. 2014; Cheng, et al. 2011).

Aerosols at a Regional Background Site in Central Texas

Three major air quality studies have been conducted in the gulf region of Texas: the Texas Air Quality Study 2000 (TexAQS 2000), the Texas Air Quality Study 2006 (TexAQS 2006), and NASA's DISCOVER-AQ (Deriving Information on Surface Conditions from Column and Vertically Resolved Observations Relevant to Air Quality) in September 2013 (Barrett and Sheesley 2014). These studies showed the potential for outflow of organic contaminants and secondary aerosols from major metropolitan areas which could impact background regional aerosol concentrations (Fan, et al. 2005; Bates, et al. 2008; Bahreini, et al. 2009). Therefore, Riesel, TX, located in central Texas between two major metropolitan areas, Dallas/Fort Worth and Houston, TX, was chosen as a background measurement site. The assessment of background aerosols provides a broad assessment of the impact of atmospheric aerosols on the radiative budget of a region, helping to assess the possible impacts of major metropolitan areas in the region.

Aerosols in the Arctic

Wide-spread haze across the Arctic was first observed by explorers crossing the Greenland ice sheet in 1883, and also noted by pilots flying over the North American Arctic in the early 1950's; (Nordenskiöld 1883; Law and Stohl 2007). "Arctic Haze" is a phenomenon occurring each winter and spring consisting of particulate organic matter, sulfates, BC, and ammonium, nitrate and dust aerosols (Law and Stohl 2007; Quinn, et al. 2009). It was widely accepted in the 1970's that the majority of the air pollution in the

Arctic was transported from the middle latitudes (Law and Stohl 2007); however, the importance and possible underestimation of in-Arctic air pollution sources has recently been noted (Stohl, et al. 2013).

In addition to wide-spread haze events across the Arctic, the region's climate is rapidly changing, warming nearly 2 °C since 1970, at a rate nearly twice that of the global mean (Odemark, et al. 2012; Sand, et al. 2013a; Pistone, Eisenman, and Ramanathan 2014). Increased warming can lead to earlier spring melts, longer melt seasons, thawing permafrost and a reduction in sea ice thickness and extent (Sand, et al. 2013a; Peters, et al. 2011). Due to Arctic warming, Arctic sea ice cover has decreased by nearly 40%; this decline in sea ice extent is expected to continue with climate models predicting an ice free Arctic as early as the 2040's, unlocking the region for increased anthropogenic activity and the introduction of new aerosol emission sources (Odemark, et al. 2012; Pistone, Eisenman, and Ramanathan 2014; Wang and Overland 2012; Overland and Wang 2013).

More specifically, atmospheric aerosols, including OC, BC, and sulfates have been shown to have significant impacts on Arctic climate forcing, contributing to the current warming trend (Shindell and Faluvegi 2009; Serreze and Barry 2011; Odemark, et al. 2012). Recent model calculations have attributed 0.5-1.4 °C of warming in the Arctic to BC aerosols alone, leading to the idea that decreasing BC emissions within the Arctic will slow the warming trend in the region (Shindell and Faluvegi 2009).

Direction of the Dissertation

The goal of this dissertation, as previously stated, is to investigate the sources, characteristics, and optical properties of atmospheric carbonaceous aerosols, including

organic carbon (OC) and elemental carbon (EC), at the North Slope of Alaska (NSA), located within the Arctic Circle. This was accomplished through atmospheric aerosols sample collection in two field studies: a long-term sampling campaign at a regional background site in Riesel, Texas to test methods (Chapter Three), and a year-round Arctic aerosols sampling campaign in Barrow, AK (Chapters Four-Six). The regional background sampling campaign and sample analysis served as a pilot study for the subsequent sample collection and analysis during the Arctic sampling campaign in Barrow, AK.

During the pilot study, I successfully established several analytical methods for our lab at Baylor University including the WSOC extraction and analysis method, EC and WSOC absorption method, and the source region identification method. Additionally, I established sample preparation methods for radiocarbon analysis of OC and TOC, as well as a method to isolate EC for radiocarbon analysis. All methods are discussed in Chapter Two and are currently the standard methods for the Sheesley research lab. Following the discussion of the methods, the results of the two field campaign are presented in Chapters Three though Six.

CHAPTER TWO

Methods

The research presented in this dissertation is comprised of full environmental chemistry studies: field sampling/collection, analytical chemistry, spatial analysis, source apportionment modeling and statistical analysis. This chapter will give a brief overview of these components with additional, specific, relevant details presented in each chapter (Three through Six). This chapter is intended to introduce the readers to the methods that are present across several chapters and to indicate the methods utilized to complete this work.

Field Sampling

Two aerosol size fractions were routinely collected for off-line chemical analysis: particulate matter with an aerodynamic diameter less than 2.5 μm ($PM_{2.5}$) and particulate matter with an aerodynamic diameter less than10 μm (PM_{10}). All aerosol samples were collected on quartz fiber filters (QFF, Pall Corporation, Ann Arbor, MI) with an assumed collection efficiency of at least 99% of suspended particles that are passed through the filters. QFFs were chosen for their chemical, mechanical and thermal stability (Chow 1995). PM_{10} samples were collected on 20 x 25 cm QFFs (Tissuquartz™ Filters 2500, QAT-UP, Pall Corporation, Ann Arbor, MI) using a Tisch high volume PM_{10} sampler (TE-6070; Tish Environmental, Cleves, Ohio). $PM_{2.5}$ samples were collected on 90 mm QFFs (Pall Corporation, Ann Arbor, MI) using a URG medium volume $PM_{2.5}$ sampler (URG-3000b, URG Corporation, Research Triangle Park, NC). Prior to sample

collection, all filters were baked for 12 hours at 500 °C to and stored in baked foil packets. Field blanks were collected during each sampling campaign and were handled in the same manner as samples. Prior to and post sampling, QFFs were placed in freezers for storage.

Riesel, TX

$PM_{2.5}$ samples were collected at the United States Department of Agriculture-Agriculture Research Service (USDA-ARS) Grassland, Soil, and Water Research Laboratory's Riesel Watersheds site in Riesel, TX (31°28'30"N, 96°55'64"W). Samples were collected once every six days following the U.S. Environmental Protection Agency (EPA) 1-in-6 day monitoring schedule using a URG 300b medium volume air sampler (URG Corporation, Research Triangle Park, NC). Samplers were operated for 24 hours from midnight to midnight at a flow rate of 92 L min^{-1} with a dual sampling train for a Teflon filter and a 90mm QFF. Additional details and the results of this campaign are included in Chapter Three.

Barrow, AK

Atmospheric particulate matter samples were collected from June 2012 to May 2013 at the Department of Energy Atmospheric Radiation Measurement (ARM) Climate Research Facility. The NSA ARM research site is located 7.4 km northeast of the village of Barrow, AK in order to reduce the impact of local sources. Two size fractions of PM were collected during the sampling campaign, $PM_{2.5}$ and PM_{10}. Additional details of this campaign are included in Chapters Four through Six.

PM_{10} sample duration was approximately one week at a flow rate of 1.2 m^3 min^{-1}. $PM_{2.5}$ sampling duration was one to two weeks at a flow rate of 0.092 m^3 min^{-1}. The total volume per filter was normalized using the BC concentration from a co-located $PM_{2.5}$ sampler which had weekly flow rate checks.

Laboratory Measurements and Calculations

Organic Carbon and Elemental Carbon Measurements and Radiocarbon Measurement Sample Preparation

OC and EC concentration measurements were performed using the NIOSH 5040 protocol on a thermal-optical transmission (TOT) carbon analyzer from Sunset Laboratory (Tigard, OR) (Birch and Cary 1996). Using this method, the speciation of OC and EC is accomplished by controlling the temperature and atmosphere of the sample while continuous monitoring of filter light transmittance, achieved with a He-Ne laser at 678 nm. A 1.5 cm^2 punch from each QFF is loaded into the OC/EC analyzer, where OC and EC concentrations are determined in two steps. During the first, OC is volatilized from the sample in a 100% He atmosphere as the temperature in the oven is increased, stepwise, to 820 °C. The evolved carbon is then oxidized to CO_2 by MnO_2, and reduced to CH_4 in a methanator oven. The CH_4 is then detected and quantified by a flame ionization detector (FID). The oven temperature is then reduced to 525 °C, and a 10% oxygen/helium mixture is introduced to the system, and the temperature is again increased to 850 °C. During the He phase, EC can be produced *in-situ* through a process called charring, causing filter transmission to decrease (Schauer, et al. 2003). The char is burned off as O_2 is introduced into the oven and once the artificially generated EC has volatilized the transmittance value through the filter returns to its original value. This

point in the sample run is defined as the "split" point between OC and EC. Any carbon evolving prior to this point is classified as OC, and any carbon evolving after this point is considered EC. An instrument blank and sucrose standard were run with every batch of 10 samples and all samples were blank corrected.

Two fractions of the aerosol samples were submitted for radiocarbon abundance measurements: the total organic carbon fraction (TOC) and the EC fraction. For total organic carbon, an area containing approximately 100 μg of carbon was cut and subjected to acid fumigation in a desiccator over 1N HCl^- for at least 12 hours to remove carbonates and then placed in a drying oven at 60 °C for one hour. Samples were then sealed in pre-leaned glass petri-dishes.

In order to perform radiocarbon analysis on the EC fraction of aerosols, it must be isolated from the OC. Two different methods were used to accomplish this separation. The first method, the "filter pull" method (Chapter Four), involves truncating the above TOT method on the carbon analyzer, removing the OC and preserving the EC on the filter. In the second method, the "CO_2 capture" method (Chapters Five and Six), a full TOT run on the carbon analyzer is completed, and the resulting CO_2 from the evolving EC is collected via cryotrap. A full description of each method is below:

Filter-pull method. This method is used to isolate EC on individual 1.5 cm^2 punches from each sample. First, a filter punch is analyzed using a full NIOSH 5040 run on the Sunset carbon analyzer, and the split time between OC and EC is recorded. The NIOSH protocol is then adjusted to stop at the split time, causing only OC to evolve off of the filter, leaving 90-95% of EC on the filter (Gustafsson, et al. 2009). This is repeated with successive filter punches until a cumulative 100 μg of EC has been

isolated. The prepared filter punches are then acidified by fumigation over 1N HCl^- for at least 12 hours to remove any carbonate carbon and dried for one hour in an oven at 60 °C. The filters are then sealed in pre-cleaned glass petri-dishes.

CO_2 capture method. This method is used to capture the evolved CO_2 from the EC fraction of aerosol samples for radiocarbon measurement. The CO_2 that is produced during EC combustion is moved out of the Sunset TOT system and taken through a silver trap (Ag wool heated to 600 °C) to remove any halogen and sulfur containing gases that can inhibit the formation of graphite from CO_2 as well as a water trap filled with magnesium perchlorate ($Mg(ClO_4)_2$. The gas is trapped in steel tubing immersed in liquid nitrogen. Additional filter punches are analyzed, collecting only EC, until a cumulative 60 µg is trapped. This EC as CO_2 is then transferred under vacuum to a glass tube with silver and copper oxide added to remove any water or halogen impurities (Chen, et al. 2013).

All carbon isotope measurements were performed at the US National Ocean Sciences Accelerator Mass Spectrometry (NOSAMS) facility at the Woods Hole Oceanographic Institute (Woods Hole, MA).

Solvent Extraction and Chemical Mass Balance Model

Organic tracers were extracted from filter sections using pressurized liquid extraction (PLE) with dichloromethane (DCM) and methanol (MeOH) followed by analysis with a gas chromatograph 7890 coupled to a 5975C mass spectrometer in electron impact mode. The PLE methods are adapted from a previous study (Nallathamby, et al. 2014). Accelerated solvent extractor (ASE) cells were be pre-cleaned

using 1:1 (v/v) DCM:MeOH under the following ASE conditions: 100 °C, 1500 psi, 3 cycles (5 min each), and 120% rinse volume. Filter areas corresponding to ~300 μg organic carbon were placed in the cleaned cells and spiked with isotopically labeled surrogate standards (standard source: Wisconsin State Laboratory of Hygiene, for quantification of target analytes). Filters were extracted twice using 1) DCM and 2) MeOH using the same conditions described above. Combined filter extracts were then concentrated to ~65 μL at 40 °C and spiked with an isotopically labeled PAH internal standard (for quantification of PAH surrogate standards) prior to analysis using gas chromatography mass spectrometry (GC/MS) in electron impact mode. GC/MS methods are based on Usenko et al., 2005 with slight modifications. The final hold time was 19 min and the injection pulse pressure was 20 psi until 0.75 min. The target analyte list consisted of 28 PAHs, eight steranes and hopanes, and 25 alkanes. Levoglucosan was also identified and quantified through derivatization by using N,O-bis(trimethylsilyl)-trifluoroacetamide (BSTFA) as a silylation agent.

The EPA Chemical Mass Balance version 8.2 was used for apportionment of OC from wood smoke and motor vehicle exhaust (Schauer, et al. 1996). The wood smoke source profile is an average of spruce and pine with greens emissions while the motor vehicle exhaust apportionment uses includes three profiles: spark ignition exhaust, lubricating oil impacted exhaust, and diesel exhaust (von Schneidemesser, et al. 2009; Sheesley, et al. 2009; Iinuma, et al. 2007). Fitting statistics (r^2, χ^2, and a calculated to measured ratio for species included in the model) are used to validate the CMB model. The chi-square is the weighted sum of squares of the differences between the calculated and measured concentrations of the fitting species. A chi-square value less than 1

indicates a very good fit, values between 1 and 2 are considered acceptable and values over 4 indicate that the source contribution estimates do not explain one or more of the species concentrations (EPA 2004). In a perfect model, there would be no difference between the calculated and measured concentrations of the fitting species and the chi-square would be zero. The r-square given is the fraction of variance in the measured concentration that is explained by the variance in the calculated species concentrations. A value less than 0.8 indicates that the source contribution estimates do not explain the observations with the source profiles used for fitting (EPA 2004).

WSOC Extractions

WSOC analysis was performed using an established water extraction method (Barrett and Sheesley 2014). Sample aliquots were placed in 50 ml centrifuge tubes (Bio-Link Scientific, Wimberly, TX) and sonicated in 30 mL of de-ionized water for 15 minutes. All tubes were pre-cleaned by triple rinsing with DI water. The extracts were then centrifuged for 10 minutes and decanted to separate out large filter pieces from the solutions. The extracts are filtered using disposable Iso-Disc PTFE-25-2 Filters with a pore size of 0.2 μm (Supelco Analytical, Bellefonte, PA), to remove any particles or QFF material. The filters and syringe are both triple rinsed with DI water prior to filtration. 60 μl of 6N HCl^- was added to remove any CO_2 present in the solution. WSOC concentrations were measured as dissolved organic carbon in the solution using a Shimadzu TOC analyzer (Model TOC-5000A, Shimadzu, Kyoto, Japan) (Yang, Li, and Yu 2003). Samples were run in groups with calibration standards (Potassium Hydrogen Phthalate (KHP), C8H5KO4, 1000 mg C/L), (concentrations of: 0, 0.5, 1, 2, 3, 4, and 5 mg L^{-1}) measured prior to analysis of each group and periodically throughout each group.

The reporting limit is 0.5 mg L^{-1}. Each sample was analyzed three times using 100 µl injections each time. All samples are blank subtracted using an average blank value from field blanks collected during the sampling campaign.

Absorption Parameters

Water-soluble organic carbon absorption. Light absorption measurement of the aqueous extracts were done using a recently proven method (Barrett and Sheesley 2014). Light absorption of the aqueous extracts is measured from 200 to 700 nm on an Agilent 8453 UV-Vis spectrometer (Santa Clara, CA), with deuterium and tungsten halogen light sources. Light absorption of the extracts is defined by Beer-Lambert as:

$$ATN_\lambda = -log_{10}\left(\frac{I}{I_0}\right) = L \times \sum_i (C_i \times \varepsilon_{i,\lambda})$$

where I_0 and I are the intensity of the incident and transmitted light, L is the absorbing path length, C_i is the concentration of light absorbing substances in solution, and $\varepsilon_{i,\lambda}$ is the wavelength dependent mass absorption efficiency. The absorption coefficient (b_{abs}) is then calculated from ATN using the following equation:

$$(b_{abs})_\lambda = (ATN_\lambda - ATN_{700}) \times \frac{V_w}{V \times L} \times \ln(10)$$

where V_w is the volume of water used for the extraction (30 ml), V is the volume of air sampled (m^3) and L is the path length (0.01 m). Since there is no absorption for ambient aerosol extracts at 700 nm, ATN_{700} accounts for baseline drift during analysis (Hecobian, et al. 2010; Cheng, et al. 2011). Mass absorption efficiency at a particular wavelength (MAE_λ) is then calculated as:

$$MAE_\lambda = \frac{(b_{abs})_\lambda}{WSOC}$$

Elemental carbon absorption. The optical attenuation (ATN) of a 678 nm laser source in the TOT analyzer will be used in the determination of b_{abs} and MAC for the filter based samples. ATN is defined by the Beer-Lambert law as:

$$ATN = -ln\left(\frac{I_0}{I}\right)$$

where I_0 and I are the transmittance signals before and after thermal optical analysis. ATN from the carbon analyzer is then used to determine b_{abs}:

$$b_{abs}(Mm^{-1}) = ATN \times \frac{A}{V}$$

where *A* is the filter area with particle loading (mm^2) and *V* is the volume of air sampled (m^3). MAC is then calculated as:

$$MAC\ (m^2/g) = \frac{ATN \times A}{EC \times V} \times \frac{1}{3.6}$$

where EC_s is the filter loading of EC. All MAC calculations will be corrected by an empirical correction factor, *C*= 3.6 (Weingartner, et al. 2003). Previous studies have shown equivalence in ATN as determined by the Aethalometer and the carbon analyzer when the wavelength is kept constant (Cheng, et al. 2011; Ram and Sarin 2009).

Back Trajectory Analysis

Back trajectories (BTs) were completed using the NOAA Hybrid Single-Particle Lagrangian Integrated Trajectory (HYSPLIT) Model version 4 May 2012 release (R.R. Draxler and G.D. Rolph 2010) and clustered using HYSPLIT. The HYSPLIT model is run using meteorological data from the Global Data Assimilation System (GDAS) produced by the National Oceanic and Atmospheric Administration. Ten-day back trajectories were calculated from the sampling location every 6 hours of each sampling day. Each back trajectory is set to run with a starting height of 10 meters above ground

level, using vertical velocity fields supplied with the GDAS meteorological data. The resulting clusters were mapped using ESRI's ArcGIS 10 software.

CHAPTER THREE

Urban Impacts on Regional Carbonaceous Aerosols: Case Study in Central Texas

This chapter published as: Barrett, Tate E., and Rebecca J. Sheesley. "Urban Impacts on Regional Carbonaceous Aerosols: Case Study in Central Texas." *Journal of the Air & Waste Management Association* 64, no. 8 (2014): 917-926.

Abstract

Rural and background sites provide valuable information on the concentration and optical properties of organic, elemental and water-soluble organic carbon (OC, EC and WSOC), which are relevant for understanding the climate forcing potential of regional atmospheric aerosols. To quantify climate- and air quality-relevant characteristics of carbonaceous aerosol in the Central USA, a regional background site in central Texas was chosen for long term measurement. Back trajectory (BT) analysis, ambient OC,EC and WSOC concentrations, and absorption parameters are reported for the first 15 months of a long-term campaign (May 2011-Aug. 2012). BT analysis indicates consistent North-South air flow connecting central Texas to the Central Plains. Central Texas aerosols exhibited seasonal trends with increased fine particulate matter (<2.5 μm aerodynamic diameter, $PM_{2.5}$) and OC during the summer ($PM_{2.5}$ = 10.8 μg m^{-3} and OC = 2.95 μg m^{-3}) and elevated EC during the winter (0.22 μg m^{-3}). When compared to measurements in Dallas and Houston, TX, central Texas OC appears to have mixed urban and rural sources. However, central Texas EC appears to be dominated by transport of urban emissions. WSOC averaged 63% of the annual OC, with little seasonal variability in this ratio. To monitor brown carbon (BrC), absorption was measured for the aqueous WSOC

extracts. Light absorption coefficients for EC and BrC were highest during summer (EC MAC = 10.6 m^2 g^{-1} and BrC MAE_{365} = 0.14 m^2 g^{-1}). Results from optical analysis indicate that regional aerosol absorption is mostly due to EC with summertime peaks in BrC attenuation. This study represents the first reported values of WSOC absorption, MAE_{365}, for the Central USA.

Introduction

Optical properties of aerosols are important in determining climatic impacts on both regional and global scales (Ram and Sarin 2009). Elemental carbon (EC, equivalent to black carbon) is thought to dominate light absorption by aerosols and is most efficient at absorbing visible light (Bond, et al. 2004) with a climate forcing value of +1.1 W m^{-2} with 90% uncertainty bounds of +0.17 to +2.1 W m^{-2}, resulting in a net global warming of up to 0.8°C (Ramanathan and Carmichael 2008; Chung, et al. 2005; B. Chen, et al. 2012; Chung and Seinfeld 2005; Bond, et al. 2013). Among atmospheric pollutants it is second only to CO_2 in potential forcing (Bond, et al. 2013). It has also been proposed that atmospheric heating as a result of EC may affect large scale circulation and the hydrological cycle, leading to significant regional climate effects (Cheng, et al. 2011). Typically, EC is treated as the only light absorbing species in climate models (Cheng, et al. 2011; Kirchstetter, Novakov, and Hobbs 2004). However, the effects of light-absorbing organic brown carbon, or BrC, are becoming more apparent and have been reported at 28% of total absorption at lower wavelengths for California (Bahadur, et al. 2012; Doherty, et al. 2010). BrC absorbs light from the UV to lower visible wavelengths, with absorption greatly increasing as wavelength decreases. Sources of BrC include primary emissions (e.g. incomplete and smoldering combustion) as well as products of

photochemical reactions in the atmosphere (Zhang, et al. 2011; Hecobian, et al. 2010; Zhang, et al. 2013). The presence of BrC in atmospheric particulate matter is often determined through the spectral properties of water soluble organic carbon (WSOC) in aqueous solutions; however not all WSOC is BrC (Hoffer, 2006). BrC can also be present in the water insoluble fraction of organic carbon. For this study, BrC refers only to water-soluble, light-absorbing organic carbon.

Absorption due to carbonaceous aerosols, both the organic and elemental fractions, is currently one of the greatest sources of uncertainty in the global radiative budget (Chen and Bond 2010; Anderson, et al. 2003; McComiskey, et al. 2008). Absorption coefficient for WSOC absorption (b_{abs}) and mass absorption cross section measurements for the USA have been made in the Southeast and on the West Coast, including Atlanta, GA ($b_{abs} = 0.61 \pm 0.38$ Mm^{-1}) and Pasadena, CA ($b_{abs} = 0.88 \pm 0.71$ Mm^{-1}) but are needed for the Central USA, particularly for BrC (Zhang, et al. 2011; Hecobian, et al. 2010). Aerosol absorption measurements are needed in this region to improve regional accuracy and reduce uncertainty in global climate models (Cheng, et al. 2011; Thompson, et al. 2012; Bond and Bergstrom 2006).

To characterize carbonaceous aerosols in the Central USA, a rural background site in central Texas was chosen. Central Texas is frequently impacted by atmospheric pollution from major metropolitan centers (Dallas-Fort Worth, the Texas Coast including Houston, and the Interstate-35 corridor including Austin). Depending upon the season, these metroplexes can impact regional aerosol concentrations and radiative forcing up through the Central Plains. Two major air quality studies have been conducted in the gulf coast region of Texas: the Texas Air Quality Study 2000 (TexAQS 2000) and the Texas

Air Quality Study 2006 (TexAQS 2006). These studies indicate high potential for urban outflow of organic matter and secondary aerosol from Texas metropolitan areas (Zhang and Ying 2010; Bahreini, et al. 2009; Massoli, et al. 2009; Russell, et al. 2009; Bates, et al. 2008; Fan, et al. 2005). A more recent study characterizing $PM_{2.5}$ in Houston, TX identifies industrial activities and traffic in and around the Houston Ship Channel as major sources of $PM_{2.5}$ (Sullivan et al. 2013). With this outflow of major urban areas combining with regional agricultural and biogenic sources, central Texas is a natural laboratory for characterizing EC and BrC from mixed urban/rural sources.

Measurement of organic carbon (OC), elemental carbon (EC) and water-soluble organic carbon (WSOC) provides a broad perspective on carbonaceous aerosol sources and variability (Schauer, et al. 2003; Currie, et al. 2002; Birch and Cary 1996). WSOC can comprise 20-70% of carbonaceous aerosol (Kirillova, et al. 2010). WSOC is emitted by primary sources (biomass burning), produced in the atmospheric by gas to particle conversion processes (secondary organic aerosol formation) and can be used to track aging of particulate carbon (Hecobian, et al. 2010; Kirillova, et al. 2013; Zhang, et al. 2012b). Several campaigns have measured WSOC concentrations in the central United States; however, these campaigns do not include absorption parameters for WSOC (Anderson, et al. 2008; Asa-Awuku, et al. 2011; Snyder, et al. 2009). This study is the first in the central United States to include long-term WSOC absorption measurements.

This study presents filter-based ambient concentrations and absorption of OC, EC, and WSOC combined with calculation of b_{abs} and MAC for both the filter samples and aqueous extract. Statistical analysis combined with clustering of HYSPLIT back

trajectories (BTs) was used to understand seasonal and source region influence on ambient concentrations.

Materials and Methods

Sampling Site

A fifteen month long sampling campaign was conducted at the United States Department of Agriculture-Agricultural Research Service (USDA-ARS) Grassland, Soil, and Water Research Laboratory's Riesel Watersheds, Riesel, Texas (31°28'30"N, 96°55'64"W). USDA-ARS Riesel Watersheds is a part of the Agriculture Research Service and managed by the United States Department of Agriculture and has been in operation since the mid-1930s (Harmel, Bonta, and Richardson 2007; Harmel, et al. 2003; Harmel, et al. 2006). Riesel is 29 km southeast of Waco, Texas (Figure 3.1). The primary local sources are agricultural activities. The USDA-ARS site is located approximately 4 km off of Texas Highway 6, the primary route between Waco and Houston, annual average daily traffic count of 12,000 vehicles (2011, http://www.txdot.gov/inside-txdot/division/transportation-planning/maps/traffic.html).

Sample Collection

$PM_{2.5}$ samples were collected once every six days from May 2011 through August 2012, following the United States Environmental Protection Agency (US EPA) 1-in-6 day monitoring schedule, on a URG 3000b medium volume sampler (URG Corporation, Research Triangle Park, North Carolina). Teflo® Teflon Membrane Disc Filters (47 mm) and quartz fiber filters (QFF, 90 mm) (Pall Corporation, Ann Arbor, Michigan) were used for sample collection. The sampler operated for 24 hours at 92 l min^{-1}, split at 10 l min^{-1} for the 47 mm filters and 82 l min^{-1} for the 90 mm filters, with a total of 132.48 m^3 of air

sampled from midnight to midnight each day. Prior to sampling, the QFF were baked at 500°C for 12 hours and were individually stored in petri-dishes lined with baked aluminum foil. All samples were stored in a freezer prior to and post sampling. Blanks were handled in the same manner as the sampled filters. Summer and winter intensives were conducted in August 2011 and January 2012. 24-hour samples were taken every other day over a two-week period.

$PM_{2.5}$ data from Houston (Clinton St.), Dallas (Hinton St.), and Waco (Mazanec) monitoring stations was accessed via the Texas Commission on Environmental Quality's (TCEQ) air quality monitoring website available at http://www.tceq.texas.gov/cgi-bin/compliance/monops/site_photo.pl. Houston Clinton and Dallas Hinton St. OC and EC data was downloaded via the US EPA Air Quality systems data mart available at http://www.epa.gov/ttn/airs/aqsdatamart/access/interface.html.

Bulk Carbon and $PM_{2.5}$ Analysis for Riesel

OC and EC concentrations were determined on a thermo-optical transmission (TOT) carbon analyzer (Sunset Laboratories, Tigard, OR) using the NIOSH 5040 method (Birch and Cary 1996). An instrument blank and sucrose standard were run with every batch of ten samples. All samples were blank subtracted using an average blank value of 0.19 μg cm^{-2}. For use in $PM_{2.5}$ mass balance, the OC concentrations need to be converted to organic mass (OM). This factor is dependent upon emission source composition and photochemical aging. Different factors have been recommended in the literature, for example, a factor of 2.1 ± 0.2 is recommended for aged aerosols at rural sites downwind of urban areas (Polidori, et al. 2008). In this case, an OM:OC factor determined by Fourier transform infrared (FTIR) fluorescence during the TexAQS 2006 study in

Houston (Russell, et al. 2009) was used. A factor of 1.8 ± 0.14 was estimated for northerly air masses impacting Houston and this factor will be uniformly applied to estimate OM for Riesel (Russell, et al. 2009). This factor is potentially biased high during winter seasons which have less photochemical activity and biased low for aged air masses impacting Riesel during summer months.

Prior to April 2009, the reported OC and EC values from the Dallas Hinton site were determined using the NIOSH protocol. The NIOSH protocol was also used at the Houston Clinton site prior to January 2010. After these dates, OC and EC concentrations for the Houston Clinton and Dallas Hinton sites were determined using the IMPROVE method. The two methods have been shown to report equivalent total carbon concentrations; however, EC concentrations from the NIOSH method have been shown to be lower than those from the IMPROVE method depending on emission sources (Chow, et al. 2001; Zhang, et al. 2013; Wright, et al. 2010). In order to address the possible bias in EC concentrations due to differences between the NIOSH and IMPROVE protocols, long term trends in the EC and OC averages at the two urban sites were examined (Figures A.1 and A.2). 1-in-6 24 hour EC and OC concentrations from January 2006 through March 2009 were compared to concentrations from April 2009 to 2012 for the Dallas Hinton site while measurements from 2006 through 2009 were compared to those for 2010 and 2011 for the Houston Clinton site using an unpaired t-test ($\alpha = .05$). No significant differences in the EC concentrations from the NIOSH and IMPROVE methods were found using the statistical analysis at either the Houston Clinton (p-value = 0.06) or the Dallas Hinton (p-value = 0.08) site.

$PM_{2.5}$ mass was determined gravimetrically using the 47mm Teflon filters. All filters were weighed in a humidity and temperature controlled room at the Wisconsin State Laboratory of Hygiene prior to and post sampling. $PM_{2.5}$ mass for Riesel was compared to data collected by the TCEQ at the Waco (Mazanec) air quality monitoring station ($r^2 = 0.55$). The Waco (Mazanec), Houston Clinton, and Dallas Hinton monitoring sites determine $PM_{2.5}$ mass using a tapered element oscillating microbalance (TEOM). The TEOM has been shown to underestimate $PM_{2.5}$ mass when compared to gravimetrical measurements (Li, et al. 2012) and this may explain the positive bias in the comparison between Riesel and Waco (Supplemental Materials figure S3.) Despite the possible underestimation by the TEOM, $PM_{2.5}$ concentrations in Dallas and Houston are, on average, greater than Riesel and Waco $PM_{2.5}$ concentrations.

WSOC Analysis

Water-soluble organic carbon (WSOC) analysis was performed on sub-samples of the QFF's. WSOC extraction methods largely followed established protocols (specific extraction techniques are further outlined in the supplemental materials) (Kirillova, et al. 2010; Ram and Sarin 2010). Briefly, soluble compounds on the QFF were extracted by sonication using 30 mL of deionized water. Blank levels were on average 6% of the sample. WSOC concentrations were measured as dissolved organic carbon in the solution using a Shimadzu total organic carbon (TOC) analyzer (Model TOC-5000A, Shimadzu, Kyoto, Japan) (Yang, Li, and Yu 2003) (Appendix A).

Absorption Parameters

Elemental carbon absorption. The optical attenuation (Wood, et al. 2010) using the 678 nm laser source in the TOT analyzer was used to determine b_{abs} and MAC as described by Ram and Sarin (2009) and Cheng et al. (2011). All MAC calculations in this study have been corrected by an empirical correction factor, C= 3.6, used to correct the measured absorption for multiple scattering and shadowing effects (Weingartner, et al. 2003; Ram and Sarin 2009) (Appendix A).

Brown carbon absorption. Light absorption of the WSOC extracts was measured at 200 to 700 nm on an Agilent 8453 UV-Vis spectrometer (Santa Clara, CA), with deuterium and tungsten halogen light sources. Absorption coefficients were calculated at 365 nm (MAE_{365}) in order to avoid possible interferences from inorganic compounds, and to remain consistent with previously published BrC absorption parameters (Cheng, et al. 2011; Hecobian, et al. 2010). Further details on absorption calculations for BC and BrC are included in Appendix A.

Back Trajectory and Seasonal Analysis

48-hour back trajectories (BTs) were calculated for Riesel every 6 hours for each sampling day over the entire field campaign in order to determine the geographic source region of air masses impacting the site. BTs were completed using the NOAA Hybrid Single-Particle Lagrangian Integrated Trajectory (HYSPLIT) Model version 4 May 2012 release (R.R. Draxler and G.D. Rolph 2010) and clustered using HYSPLIT. The HYSPLIT model was run using meteorological data from the Global Data Assimilation System (GDAS) produced by the National Oceanic and Atmospheric Administration.

Each back trajectory was set to run with a starting height of 10 meters above ground level, using vertical velocity fields supplied with the GDAS meteorological data. The resulting clusters were mapped using ESRI's ArcGIS 10 software on a map of Texas counties provided by ESRI (Figure 3.1). There are intrinsic uncertainties characteristic of the HYSPLIT model concerning modeling of terrain height; however, uncertainties of the current application are minimized due to the short duration of the back trajectories (48 hours) and the flat terrain of the region.

The field campaign was divided into four seasons (spring, summer, fall, and winter) based on examination of daily maximum temperatures rather than a traditional three-month division in order to capture the effect of high photochemistry in the late summer months in Texas. Each day was assigned to a season based on its maximum temperature to differentiate between seasons. Winter was defined as daily maximum temperatures from 0-15° C, spring from 15-30° C, summer from 30-42° C, and fall from 30-15°C (blue, red, green and purple, respectively in Figure 3.1). Fall and spring have the same temperature range because they are transition seasons between the summer and winter and are distinguished by the time of year. This temperature range was chosen in order to capture the extended period of high photochemistry during the summer.

Results and Discussion

Seasonal Analysis

Carbon and $PM_{2.5}$ mass measurements were grouped by time of year to assess effects of season on regional background aerosol concentrations in central Texas.

Seasonal concentrations for the regional site are compared to values reported by TCEQ for Dallas, Houston and Waco, TX.

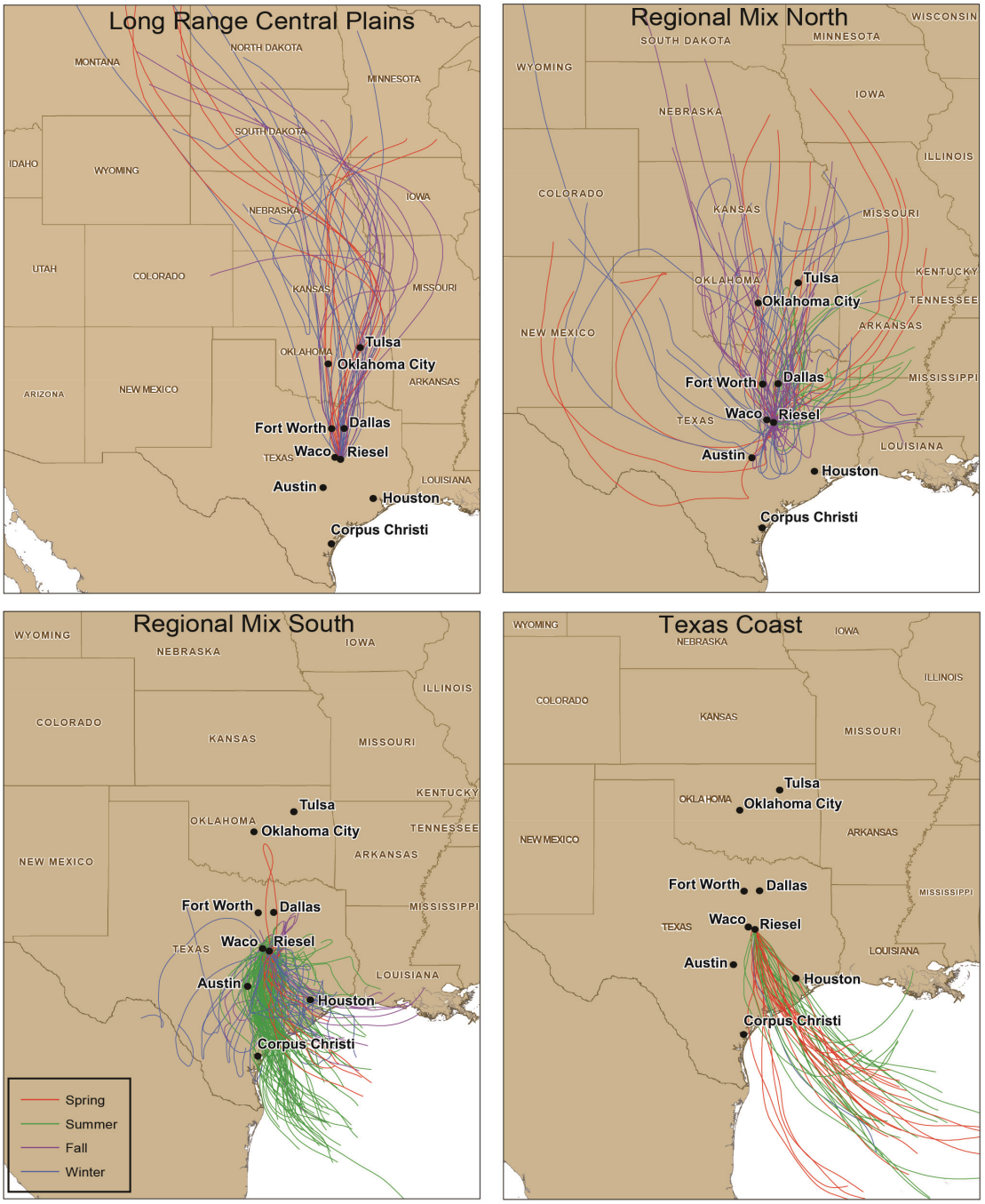

Figure 3.1: Forty-eight hour back trajectory plots showing the path of air arriving at Riesel, TX. Spring is shown in red, summer in green, fall in purple, and winter in blue.

Seasonal PM2.5 and OC Results. There are distinct seasonal trends for concentrations of $PM_{2.5}$ mass and OC in central Texas (Tables 3.1 and 3.2). Mean $PM_{2.5}$ concentrations for Riesel ranged from a springtime average of 6.8 ± 2.5 μg m^{-3} to a summertime average of 10.9 ± 4.7 μg m^{-3}. Studies of particulate matter in the southeastern United States have shown similar seasonal trends with maximum $PM_{2.5}$ concentrations occurring in warmer months and the lowest concentrations for the cooler winter months (Zhang, et al. 2012b; Y. J. Chen, et al. 2012). This summertime peak is consistent with $PM_{2.5}$ monitoring stations in Waco and Dallas (Table 3.1). Houston peaks in spring, but has the second highest $PM_{2.5}$ in the summer months. The Houston Clinton monitoring site historically has one of the highest annual $PM_{2.5}$ concentrations in Texas; however, $PM_{2.5}$ concentrations have steadily declined since 2006 (Sullivan, et al. 2013). Riesel differs from these three urban Texas sites in that springtime has the lowest $PM_{2.5}$ values. The Riesel results indicate important seasonal differences between urban and regional background $PM_{2.5}$.

The OC concentrations at Riesel ranged from 1.9 ± 0.7 μg m^{-3} in the spring to 3.0 ± 1.6 μg m^{-3} in the summer; however, the differences among the seasons were not statistically significant (p-values = 0.19, 0.21, 0.06, and 0.34 for winter, spring, summer and fall, respectively). OC accounts for 27% of summer $PM_{2.5}$ mass (OM is 49%); this contribution is consistent for springtime and summer at Riesel. OC concentrations in Dallas were consistent through winter, spring, and summer and decreased in the fall. Houston displays opposite trends for OC, with the lowest average value in the summer months and highs in the spring.

Table 3.1: Comparison of fine particulate matter (PM2.5), organic carbon (OC), elemental carbon (EC), and EC/OC ratios for four sampling sites across Texas for 2011 and 2012.

	Riesel (2011 & 2012)	Waco (2011 & 2012)	Houston Clinton (2011)				Dallas Hinton (2011 & 2012)			
Season	$PM_{2.5}$ ($\mu g/m^3$)	$PM_{2.5}$ ($\mu g/m^3$)	$PM_{2.5}$ ($\mu g/m^3$)	OC ($\mu g/m^3$)	EC ($\mu g/m^3$)	EC/OC Ratio	$PM_{2.5}$ ($\mu g/m^3$)	OC ($\mu g/m^3$)	EC ($\mu g/m^3$)	EC/OC Ratio
Spring (13)	6.77	9.78	14.1	3.73	0.67	0.19	11.9	2.26	0.42	0.19
Summer (39)	10.9	10.0	13.4	2.88	0.69	0.27	12.5	2.27	0.38	0.18
Fall (15)	8.50	7.43	10.4	3.58	0.78	0.23	10.6	2.00	0.51	0.25
Winter (18)	7.85	6.79	10.7	3.59	0.81	0.21	11.5	2.28	0.49	0.21

Back trajectory analysis can help to explain some of these regional differences; Houston has dominant southerly winds in the summer which have lower documented OC than northerly air masses due to fewer upwind anthropogenic sources (Bates, et al. 2008). Absolute OC concentrations are very similar for Dallas and Riesel while Houston is 40% higher on average (Tables 3.1 and 3.2).

For both Houston and Dallas sites, $PM_{2.5}$ concentrations have the highest correlation to OC and sulfate when compared to correlations with nitrate, ammonium or EC (Figures A.4-A.6). Regression analysis for Houston-Clinton indicates roughly one-third of the variability in $PM_{2.5}$ concentrations can be explained by either sulfate or OC (r^2 = 0.32 and 0.39, respectively when regressed with $PM_{2.5}$). This correlation between sulfate and $PM_{2.5}$ is confirmed by Sullivan et al. (2013) who showed sulfate as one of the main contributors to $PM_{2.5}$ mass at Houston-Clinton. For Dallas-Hinton, sulfate and OC are also highly correlated with $PM_{2.5}$ concentrations (r^2 = 0.57 and 0.36, respectively when regressed with $PM_{2.5}$). When summing the bulk inorganic and carbon components, 65% of the $PM_{2.5}$ variability can be explained at Texas urban sites (r^2 = 0.65 for sum of sulfate, nitrate, ammonium, OM and EC when regressed with $PM_{2.5}$ at both Dallas and Houston sites) (Figures A.4-A.6). The TexAQS campaigns also documented significant contribution from sulfate to $PM_{2.5}$ in the Houston region (Bates, et al. 2008), and related this to coal-fired electricity generation from upwind/northerly sources (Zhang and Ying 2010).

The OC and $PM_{2.5}$ concentrations are correlated at Riesel on an annual scale with a correlation coefficient of 0.48, which is higher than either Dallas or Houston (Figure A.7). On average, the OC accounts for 31% of the $PM_{2.5}$ mass at Riesel (OM accounts for

56%), with seasonal peaks in both summer and fall. Although sulfate measurements are not yet available for Riesel, it would be expected that regional sulfate would also be important to $PM_{2.5}$ concentrations at Riesel. Based on these differences in seasonal OC and $PM_{2.5}$ between Riesel and urban areas in Texas (Houston, Dallas, Waco), it is hypothesized that central Texas OC is impacted by a combination of transported urban and regional rural emissions.

Seasonal EC Results. EC concentrations at Riesel are much lower than Dallas and Houston (factor of 2.4 and 4 respectively) (Tables 3.1 and 3.2). Despite this difference, EC at Riesel displays similar seasonal trends to Houston and Dallas, with fall/winter maximums and spring/summer minimums (Table 3.2). This is very different than the $PM_{2.5}$ and OC trends discussed in the *Seasonal $PM_{2.5}$ & OC results section*, where OC at Riesel had different trends than urban centers but similar absolute concentrations. Dallas and Houston EC concentrations are typical of large urban areas throughout the United States (i.e. Pasadena and Atlanta) while the Riesel concentrations are much lower (Zhang, et al. 2011). Houston EC concentrations are generally higher than Dallas and Riesel for all seasons, potentially due to the large amount of diesel combustion sources in the Houston shipping channel in addition to urban traffic sources (Wu, et al. 2009; Kuwayama, et al. 2013). The Riesel EC/OC ratio was highest in the winter (0.10) and lowest in the summer (0.05). This difference could be driven by increased EC emissions during the winter months, possibly from residential wood burning or motor vehicle exhaust in the colder winter months. In addition to emission source changes, the back trajectory analysis indicates a shift to dominant northerly air masses in the winter. These northerly air masses consistently pass over the Dallas-Fort

Worth metroplex before arriving in Riesel. Based on this seasonal analysis, EC concentrations at Riesel are likely dominated by transport and dilution from urban areas which may include areas with industrial as well as gas and oil production emissions such as the Houston shipping channel. If EC is considered a tracer for urban impacts on Riesel, it further supports the notion that urban OC is supplemented by regional rural sources in central Texas.

Table 3.2: Seasonal organic carbon (OC), elemental carbon (EC), organic mass (OM), EC/OC ratio, water soluble organic carbon (WSOC) and WSOC/OC ratio concentrations for Riesel, TX for the 15 month sampling campaign from May 2011 to August 2012. The number of sampling days for each season is shown in parentheses next to each season.

Season	OC ($\mu g/m^3$) ± s.d.	EC ($\mu g/m^3$) ± s.d.	OM ($\mu g/m^3$) ± s.d.	EC/OC Ratio	WSOC ± s.d.	WSOC/OC Ratio
Spring (13)	1.9 ± 0.73	0.17 ± 0.04	3.4 ± 0.74	0.09	1.3 ± 0.55	0.66
Summer (39)	3.0 ± 1.6	0.14 ± 0.07	5.3 ± 1.6	0.05	2.0 ± 1.3	0.66
Fall (15)	2.9 ± 2.4	0.22 ± 0.14	5.2 ± 2.4	0.08	1.9 ± 1.6	0.64
Winter (18)	2.3 ± 1.3	0.22 ± 0.09	4.2 ± 1.3	0.10	1.3 ± 0.76	0.55

Seasonal WSOC Results. To better understand the bulk carbon in central Texas, the water-soluble fraction was quantified. Mean WSOC concentrations ranged from 1.3 ± 0.55 μg m^{-3} in the spring to 2.0 ± 1.30 μg m^{-3} in the summer and showed similar seasonal trends as OC with maximum concentrations in the summer and fall (Table 3.2, Figure 3.2). However, the differences among seasons were not statistically significant (p-values = 0.10, 0.17, 0.31, and 0.08 for winter, spring, summer and fall, respectively). Summer WSOC values for Riesel are higher than summer WSOC concentrations in Pasadena, CA (1.0 ± 0.72), and similar to summer WSOC concentrations in Atlanta, GA

(2.0 ± 1.0), which has known high biogenic contributions (Zhang, et al. 2011). The small increase in WSOC concentrations in the summer and fall are potentially due to an enhancement of secondary chemical processes due to increased solar radiation and biogenic VOC emissions (Zhang, et al. 2012b; Chow, et al. 2009; Zhang and Ying 2011). Photo-oxidation of non-methane hydrocarbons (NMHC) from oil and gas production in the source regions could also contribute to the higher concentrations (Carlton, et al. 2010; Berkowitz, Spicer, and Doskey 2005). However, at a rural site like Riesel, it is also likely that high WSOC is related to aging of OC during transport from source areas (Kirillova, et al. 2013). WSOC/OC ratios were lowest in the winter months, at 0.55, and increased to 0.66 during the spring and summer (Table 3.2). Regression of WSOC with OC gives a correlation coefficient of $r^2 = 0.90$ with a slope of 0.70. Given the small difference among seasons and the consistent relationship to OC, WSOC is likely a mixture of aged urban and aged regional rural aerosol.

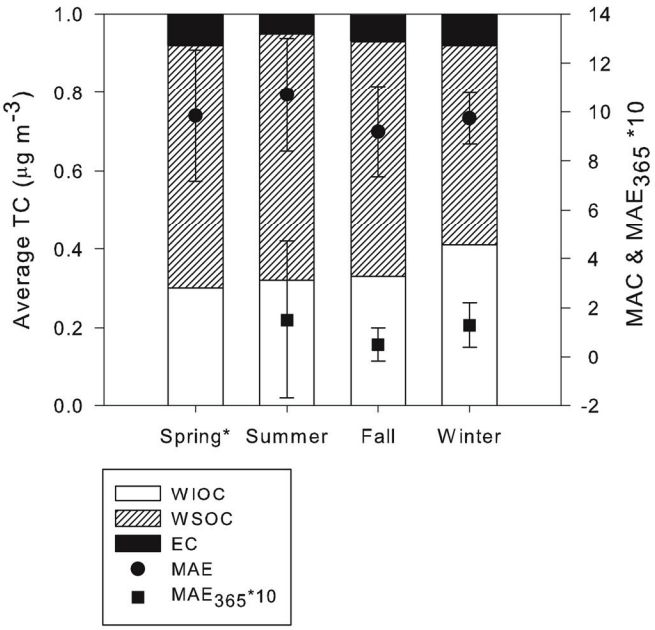

Figure 3.2: Contributions of water-insoluble organic carbon (WIOC), water-soluble organic carbon (WSOC) and elemental carbon (EC) by season at Riesel, TX. Average MAC and MAE_{365}*10 values are also presented. The WSOC MAE_{365}*10 is not available for spring.

Back Trajectory Cluster Analysis

48-hour BT's showed that air masses impacting the sampling site could be divided into 4 distinct clusters: the Long Range Central Plains cluster, the Regional Mix North cluster, the Texas Coast cluster and the Regional Mix South cluster (Figure 3.1). This annual BT analysis indicates that the Central Plains and Central Texas can be considered to be connected airsheds. Geographic source analysis of contributions of OC, EC, and WSOC showed no significant difference by BT cluster with the exception of lower EC concentrations from air masses originating in the Regional Mix South Cluster (p-value = 0.002) (Appendix A, Table A.1). It has previously been shown that Houston, TX, a coastal city, exhibits a pronounced dependence on BT's for OC concentration

(Bates, et al. 2008);however, there is a higher dependence on season rather than source region in explaining the variability in carbon components in central Texas.

Absorption

Seasonal Absorption. EC light attenuation is consistent throughout the year, ranging from 0.21 ± 0.13 in the summer to 0.32 ± 0.15 in the winter, indicative of a steady source of dilute urban EC (Table 3.3). ATN and EC filter loadings exhibit a strong correlation for all seasons other than spring (r^2= 0.9 for summer, fall and winter, r^2= 0.42 for spring, Figure 3.3), indicating that EC is the principal absorbing component for most of the year. The weak correlation in spring (r^2=0.42) indicates contribution of absorption from other species (possibly BrC or mineral dust). There is no significant difference in the slopes for summer, winter, and fall at the 95% confidence interval according to the Student's T test (n=3). The MAC calculated at 678 nm ranged from 8.5 to 14.6 with a mean standard deviation of ± 1.0 m^2 g^{-1} in the summer. In the winter the MAC ranged from 8.3 to 12.1 with a mean standard deviation of ± 2.3 m^2 g^{-1}. It has been shown that MAC is influenced by mixing state and when EC is internally mixed with components such as sulfate and OC, these coatings can focus light into the EC core increasing the MAC (Cheng, et al. 2011). Maximum MAC values coincide with maximum OC and WSOC concentrations during the summer (Figure 3.2), potentially indicating the intensification of MAC by organic aerosol coating, including SOA.

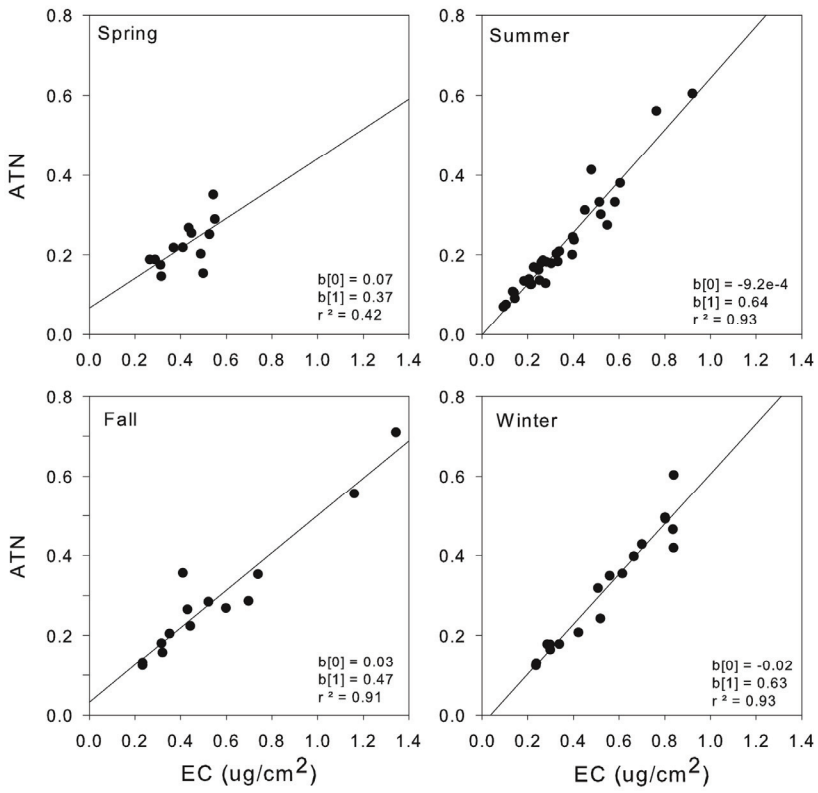

Figure 3.3: Light attenuation vs. filter elemental carbon (EC) loading by season; b(0) is equal to the y-intercept and b(1) is equal to the slope of the regression.

Seasonal BrC Absorption. Light absorption of the WSOC aqueous solutions was explored in order to determine the presence and potential regional climate effects of BrC (Table 3). WSOC ATN is much higher in the summer, 0.013 ± 0.05, than fall and winter, 0.002 ± 0.002 and 0.004 ± 0.003 respectively and is likely connected to summer photochemical events. The WSOC MAE_{365} averaged 0.15 ± 0.32 m^2 g^{-1} for summer and 0.13 ± 0.09 m^2 g^{-1} for winter (Figure 3.2). BrC has been shown to rapidly form in high NO_x (urban) environments and nitrogen containing aromatic compounds are effective light absorbers at 365 nm, with urban WSOC MAE_{365} values generally higher than those of biogenic SOA (Zhang, et al. 2013). Average WSOC MAE_{365} in Riesel is much lower than the reported average value of 0.71 m^2 g^{-1} for summer 2010 in Los Angeles, CA, a

high NO_x environment (Zhang, et al. 2013). Average WSOC b_{abs} values were 0.17 ± 0.14 and 0.35 ± 0.14 Mm^{-1} for the winter and summer respectively. The summer maximum seen in Riesel is lower than summer values reported for the Atlanta, GA (0.61 ± 0.38 Mm^{-1}) and Pasadena, CA (0.88 ± 0.71 Mm^{-1}) urban areas (Zhang, et al. 2011). This difference may be due to a lower number of anthropogenic mobile sources and higher biogenic or NMHC sources of BrC at Riesel. WSOC and WSOC b_{abs} were positively correlated during the winter (r^2= 0.62). The correlation was low during summer, but this may be due to variable WSOC:WSOC b_{abs} ratios during this time (Figure 3.4). The absorption spectrum of the WSOC extracts for both the summer and winter are typical of BrC, with absorption decreasing sharply as wavelength increases (Figure 3.5) (Andreae and Gelencser 2006; Hoffer, et al. 2006; Cheng, et al. 2011).

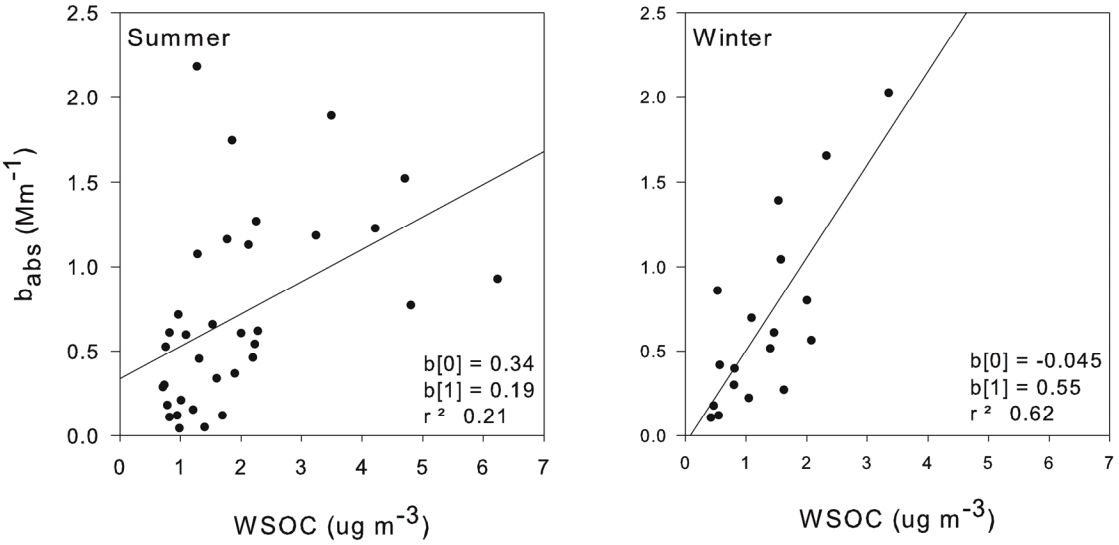

Figure 3.4: scatter plots showing the correlation of WSOC babs (365nm) and WSOC concentrations for summer and winter at Riesel, TX; b(0) is equal to the y-intercept and b(1) is equal to the slope of the regression.

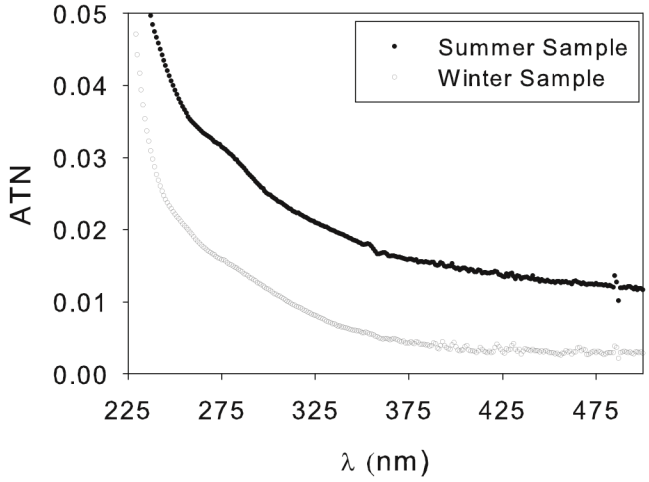

Figure 3.5: Example of water-soluble absorption spectra for one summer (08/13/2012) and one winter (02/15/2015) sample from Riesel, TX. The Ängrstrom absorption exponent for the summer sample is 5.8, and 4.8 for the winter sample.

Conclusion

Absolute OC concentrations are in the same annual range for Riesel, Dallas, and Houston throughout the study period. Strong correlation of OC and $PM_{2.5}$ at Riesel and differing seasonal trends between Riesel and Texas urban areas supports the notion that dispersed rural OC sources contribute significantly to regional $PM_{2.5}$ concentrations in the Central USA. Based on the BT analysis, these rural sources of OC could impact baseline $PM_{2.5}$ concentrations for urban areas including Houston and Dallas-Fort Worth. WSOC:OC ratios remain consistent at Riesel regardless of season or source region. A consistent annual relationship of WSOC to OC points to the importance of aged atmospheric aerosols arriving at Riesel. OC reaching Riesel is likely a mixture of aged urban and aged regional rural aerosol.

Absolute EC concentrations in Dallas and Houston are 4-7 times higher than Riesel for the study period. The EC:OC ratio decreases from the urban sites (Dallas and Houston) relative to Riesel by a factor of 2. Low EC concentrations at Riesel are likely

due to a dilution of urban EC during transport with minimal EC contributions from regional rural/agricultural sources as compared to OC.

Absorption due to both EC and BrC was explored in this study in order to provide a regional perspective on potential climate forcing by atmospheric aerosols. Biogenic SOA predominance, in addition to SOA from NMHC sources, may contribute to the lower WSOC MAE_{365} values as compared to urban sites (Zhang, et al. 2013). These WSOC MAE_{365} results also support the notion of rural OC impacting Riesel. BrC ATN peaked during the summer. The combined optical results indicate the dominance of aerosol absorption by EC in central Texas. BrC does contribute to absorption in the summer at Riesel; however, the lower WSOC MAE_{365} indicates less absorption by unit mass for the WSOC in Riesel compared to the southeast US and California. Continued monitoring of this site will improve understanding of regional aerosol absorption in the Central USA.

Acknowledgments

This work was supported by the Baylor University Department of Environmental Science. We thank the Baylor University Center for Reservoir and Aquatic Systems Research for WSOC analysis, Daren Harmel and the United States Department of Agriculture Agricultural Research Service for site access, Jeff DeMinter at the Wisconsin State Laboratory of Hygiene for gravimetric analysis, and Punith Dev Nallathamby at Baylor University for help with sample collection. We also thank August Andersson at the University of Stockholm for his valuable comments and Kasey Savanich and Jim Price of the TCEQ and David Sullivan of the University of Texas for their help with data acquisition.

(2012). "2011 Traffic Maps." Retrieved August 9, 2013, from http://www.txdot.gov/inside-txdot/division/transportation-planning/maps/traffic.html.

(2012). "US Environmental Protection Agency. Air Quality System Data Mart. Retrieved February 15, 2013, from http://www.epa.gov/ttn/airs/aqsdatamart/access/interface.htm.

(2013). "Texas Commission on Environmental Quality Monitoring Site Information." Retrieved March 15, 2013, from http://www.tceq.texas.gov/cgi-bin/compliance/monops/site_photo.pl.

Anderson, C., J. E. Dibb, et al. (2008). "Simultaneous measurements of particulate and gas-phase water-soluble organic carbon concentrations at remote and urban-influenced locations." Geophysical Research Letters **35**(13).

Anderson, T. L., R. J. Charlson, et al. (2003). "Climate forcing by aerosols - a hazy picture." Science **300**(5622): 1103-1104.

Andreae, M. O. and A. Gelencser (2006). "Black carbon or brown carbon? The nature of light-absorbing carbonaceous aerosols." Atmospheric Chemistry and Physics **6**: 3131-3148.

Asa-Awuku, A., R. H. Moore, et al. (2011). "Airborne cloud condensation nuclei measurements during the 2006 Texas Air Quality Study." Journal of Geophysical Research-Atmospheres **116**.

Bahadur, R., P. S. Praveen, et al. (2012). "Solar absorption by elemental and brown carbon determined from spectral observations." Proceedings of the National Academy of Sciences of the United States of America **109**(43): 17366-17371.

Bahreini, R., B. Ervens, et al. (2009). "Organic aerosol formation in urban and industrial plumes near Houston and Dallas, Texas." Journal of Geophysical Research-Atmospheres **114**.

Bates, T. S., P. K. Quinn, et al. (2008). "Boundary layer aerosol chemistry during TexAQS/GoMACCS 2006: Insights into aerosol sources and transformation processes." Journal of Geophysical Research-Atmospheres **113**.

Berkowitz, C. M., C. W. Spicer, et al. (2005). "Hydrocarbon observations and ozone production rates in Western Houston during the Texas 2000 Air Quality Study." Atmospheric Environment **39**(19): 3383-3396.

Birch, M. E. and R. A. Cary (1996). "Elemental carbon-based method for monitoring occupational exposures to particulate diesel exhaust." Aerosol Science and Technology **25**(3): 221-241.

Bond, T. C. and R. W. Bergstrom (2006). "Light absorption by carbonaceous particles: An investigative review." Aerosol Science and Technology **40**(1): 27-67.

Bond, T. C., S. J. Doherty, et al. (2013). "Bounding the role of black carbon in the climate system: A scientific assessment." Journal of Geophysical Research-Atmospheres **118**(11): 5380-5552.

Bond, T. C., D. G. Streets, et al. (2004). "A technology-based global inventory of black and organic carbon emissions from combustion." Journal of Geophysical Research-Atmospheres **109**(D14).

Carlton, A. G., R. W. Pinder, et al. (2010). "To What Extent Can Biogenic SOA be Controlled?" Environmental Science & Technology **44**(9): 3376-3380.

Chen, B., K. Du, et al. (2012). "Emission and Transport of Carbonaceous Aerosols in Urbanized Coastal Areas in China." Aerosol and Air Quality Research **12**(3): 371-378.

Chen, Y. and T. C. Bond (2010). "Light absorption by organic carbon from wood combustion." Atmospheric Chemistry and Physics **10**(4): 1773-1787.

Chen, Y. J., M. Zheng, et al. (2012). "PM2.5 source apportionment in the southeastern U.S.: Spatial and seasonal variations during 2001-2005." Journal of Geophysical Research-Atmospheres **117**.

Cheng, Y., K. B. He, et al. (2011). "Mass absorption efficiency of elemental carbon and water-soluble organic carbon in Beijing, China." Atmospheric Chemistry and Physics **11**(22): 11497-11510.

Chow, J. C., J. G. Watson, et al. (2001). "Comparison of IMPROVE and NIOSH carbon measurements." Aerosol Science and Technology **34**(1): 23-34.

Chow, J. C., J. G. Watson, et al. (2009). "Aerosol light absorption, black carbon, and elemental carbon at the Fresno Supersite, California." Atmospheric Research **93**(4): 874-887.

Chung, C. E., V. Ramanathan, et al. (2005). "Global anthropogenic aerosol direct forcing derived from satellite and ground-based observations." Journal of Geophysical Research-Atmospheres **110**(D24).

Chung, S. H. and J. H. Seinfeld (2005). "Climate response of direct radiative forcing of anthropogenic black carbon." Journal of Geophysical Research-Atmospheres **110**(D11).

Currie, L. A., B. A. Benner, et al. (2002). "A critical evaluation of interlaboratory data on total, elemental, and isotopic carbon in the carbonaceous particle reference material, NIST SRM 1649a." Journal of Research of the National Institute of Standards and Technology **107**(3): 279-298.

Doherty, S. J., S. G. Warren, et al. (2010). "Light-absorbing impurities in Arctic snow." Atmospheric Chemistry and Physics **10**(23): 11647-11680.

Draxler, R. R. and G. D. Rolph (2010). HYSPLIT (HYbrid Single-Particle Lagrangian Integrated Trajectory) Model access via NOAA ARL READY Website (http://ready.arl.noaa.gov/HYSPLIT.php). Silver Spring, MD, NOAA Air Resources Laboratory.

Fan, J. W., R. Y. Zhang, et al. (2005). "Simulations of fine particulate matter (PM2.5) in Houston, Texas." Journal of Geophysical Research-Atmospheres **110**(D16).

Harmel, R. D., J. V. Bonta, et al. (2007). "The original USDA-ARS experimental watersheds in Texas and Ohio: Contributions from the past and visions for the future." Transactions of the ASABE **50**(5): 1669-1675.

Harmel, R. D., K. W. King, et al. (2003). "Long-term precipitation analyses for the central Texas Blackland Prairie." Transactions of the Asae **46**(5): 1381-1388.

Harmel, R. D., C. W. Richardson, et al. (2006). "Runoff and soil loss relationships for the Texas Blackland Prairies ecoregion." Journal of Hydrology **331**(3-4): 471-483.

Hecobian, A., X. Zhang, et al. (2010). "Water-Soluble Organic Aerosol material and the light-absorption characteristics of aqueous extracts measured over the Southeastern United States." Atmospheric Chemistry and Physics **10**(13): 5965-5977.

Hoffer, A., A. Gelencser, et al. (2006). "Optical properties of humic-like substances (HULIS) in biomass-burning aerosols." Atmospheric Chemistry and Physics **6**: 3563-3570.

Kirchstetter, T. W., T. Novakov, et al. (2004). "Evidence that the spectral dependence of light absorption by aerosols is affected by organic carbon." Journal of Geophysical Research-Atmospheres **109**(D21).

Kirillova, E. N., A. Andersson, et al. (2013). "13C- and 14C-based study of sources and atmospheric processing of water-soluble organic carbon (WSOC) in South Asian aerosols." Journal of Geophysical Research: Atmospheres **118**(2): 614-626.

Kirillova, E. N., R. J. Sheesley, et al. (2010). "Natural Abundance C-13 and C-14 Analysis of Water-Soluble Organic Carbon in Atmospheric Aerosols." Analytical Chemistry **82**(19): 7973-7978.

Kuwayama, T., J. R. Schwartz, et al. (2013). "Particulate Matter Emissions Reductions due to Adoption of Clean Diesel Technology at a Major Shipping Port." Aerosol Science and Technology **47**(1): 29-36.

Li, Q. F., W. L. Lingjuan, et al. (2012). "Field evaluation of particulate matter measurements using tapered element oscillating microbalance in a layer house." Journal of the Air & Waste Management Association **62**(3): 322-335.

Massoli, P., T. S. Bates, et al. (2009). "Aerosol optical and hygroscopic properties during TexAQS-GoMACCS 2006 and their impact on aerosol direct radiative forcing." Journal of Geophysical Research-Atmospheres **114**.

McComiskey, A., S. E. Schwartz, et al. (2008). "Direct aerosol forcing: Calculation from observables and sensitivities to inputs." Journal of Geophysical Research-Atmospheres **113**(D9).

Polidori, A., B. J. Turpin, et al. (2008). "Organic PM2.5: Fractionation by polarity, FTIR spectroscopy, and OM/OC ratio for the Pittsburgh aerosol." Aerosol Science and Technology **42**(3): 233-246.

Ram, K. and M. M. Sarin (2009). "Absorption Coefficient and Site-Specific Mass Absorption Efficiency of Elemental Carbon in Aerosols over Urban, Rural, and High-Altitude Sites in India." Environmental Science & Technology **43**(21): 8233-8239.

Ram, K. and M. M. Sarin (2010). "Spatio-temporal variability in atmospheric abundances of EC, OC and WSOC over Northern India." Journal of Aerosol Science **41**(1): 88-98.

Ramanathan, V. and G. Carmichael (2008). "Global and regional climate changes due to black carbon." Nature Geoscience **1**(4): 221-227.

Russell, L. M., S. Takahama, et al. (2009). "Oxygenated fraction and mass of organic aerosol from direct emission and atmospheric processing measured on the R/V Ronald Brown during TEXAQS/GoMACCS 2006." Journal of Geophysical Research-Atmospheres **114**.

Schauer, J. J., B. T. Mader, et al. (2003). "ACE-Asia intercomparison of a thermal-optical method for the determination of particle-phase organic and elemental carbon." Environmental Science & Technology **37**(5): 993-1001.

Snyder, D. C., A. P. Rutter, et al. (2009). "Insights into the Origin of Water Soluble Organic Carbon in Atmospheric Fine Particulate Matter." Aerosol Science and Technology **43**(11): 1099-1107.

Sullivan, D. W., J. H. Price, et al. (2013). "Field study and source attribution for PM2.5 and PM10 with resulting reduction in concentrations in the neighborhood north of the Houston Ship Channel based on voluntary efforts." Journal of the Air & Waste Management Association **63**(9): 1070-1082.

Thompson, J. E., P. L. Hayes, et al. (2012). "Aerosol optical properties at Pasadena, CA during CalNex 2010." Atmospheric Environment **55**: 190-200.

Weingartner, E., H. Saathoff, et al. (2003). "Absorption of light by soot particles: determination of the absorption coefficient by means of aethalometers." Journal of Aerosol Science **34**(10): 1445-1463.

Wood, E. C., M. R. Canagaratna, et al. (2010). "Investigation of the correlation between odd oxygen and secondary organic aerosol in Mexico City and Houston." Atmospheric Chemistry and Physics **10**(18): 8947-8968.

Wright, M. E., D. B. Atkinson, et al. (2010). "Extensive aerosol optical properties and aerosol mass related measurements during TRAMP/TexAQS 2006-Implications for PM compliance and planning." Atmospheric Environment **44**(33): 4035-4044.

Wu, J., D. Houston, et al. (2009). "Exposure of PM2.5 and EC from diesel and gasoline vehicles in communities near the Ports of Los Angeles and Long Beach, California." Atmospheric Environment **43**(12): 1962-1971.

Yang, H., Q. F. Li, et al. (2003). "Comparison of two methods for the determination of water-soluble organic carbon in atmospheric particles." Atmospheric Environment **37**(6): 865-870.

Zhang, H. L. and Q. Ying (2010). "Source apportionment of airborne particulate matter in Southeast Texas using a source-oriented 3D air quality model." Atmospheric Environment **44**(29): 3547-3557.

Zhang, H. L. and Q. Ying (2011). "Secondary organic aerosol formation and source apportionment in Southeast Texas." Atmospheric Environment **45**(19): 3217-3227.

Zhang, X., Z. Liu, et al. (2012). "Spatial and seasonal variations of fine particle water-soluble organic carbon (WSOC) over the southeastern United States: implications for secondary organic aerosol formation." Atmospheric Chemistry and Physics **12**(14): 6593-6607.

Zhang, X. L., Y. H. Lin, et al. (2013). "Sources, Composition and Absorption Angstrom Exponent of Light-absorbing Organic Components in Aerosol Extracts from the Los Angeles Basin." Environmental Science & Technology **47**(8): 3685-3693.

Zhang, X. L., Y. H. Lin, et al. (2011). "Light-absorbing soluble organic aerosol in Los Angeles and Atlanta: A contrast in secondary organic aerosol." Geophysical Research Letters **38**.

CHAPTER FOUR

Source Contributions to Wintertime Elemental and Organic Carbon in the Western Arctic Based on Radiocarbon and Tracer Apportionment

This chapter published as: T.E. Barrett, E.M. Robinson, S. Usenko, and R.J. Sheesley (2015). "Source Contributions to Wintertime Elemental and Organic Carbon in the Western Arctic Based on Radiocarbon and Tracer Apportionment." *Environmental Science & Technology* **49**(19): 11631-11639.

Abstract

Rapid warming and sea ice reduction has enabled intensified petroleum and natural gas exploration and commercial shipping in certain areas of the Arctic, potentially increasing elemental and organic carbon concentrations across the region. To quantify the contributions of fossil and biomass sources, radiocarbon source apportionment is reported for elemental (EC) and organic carbon (OC) fractions of six PM_{10} samples collected during a wintertime (2012-2013) campaign in Barrow, AK. Radiocarbon apportionment of EC indicates that fossil sources contribute an average of 68.4 ± 9,2% (0.01 – 0.07 μg m^{-3}) in mid-winter decreasing to 49.1 ± 5.6% (0.02 μg m^{-3}) in late winter. The mean contribution of fossil sources to OC for the campaign was a stable contribution at 38.3 ± 8.0% (0.04 – 0.32 μg m^{-3}). Samples also underwent pressurized liquid extraction and GC/MS analysis to identify polycyclic aromatic hydrocarbons, hopanes, and levoglucosan concentrations for use in a chemical mass balance (CMB) source apportionment model. The CMB model was able to apportion 24-53% and 99% of the OC and EC burdens during the campaign, with fossil OC contributions ranging from 25-74% (0.016-0.089 μg m^{-3}) and fossil EC contributions ranging from 73-94% (0.03-0.07

μg m^{-3}). HYSPLIT back trajectory analysis identified two major source regions to Barrow during the campaign: the Russian and North American Arctic regions. Novel quantification of atmospheric lifetimes of levoglucosan, ranging from 20 to 230 h, revealed variability in wintertime atmospheric processing of this biomass burning tracer. This study is the first application of radiocarbon source apportionment of EC in the North American Arctic, and allows for unambiguous apportionment of EC to fossil fuel and biomass combustion sources and validation of CMB modeling.

Introduction

Black carbon (BC) and organic carbon (OC) emissions within the Arctic (north of 66° N latitude) are expected to increase with intensifying petroleum and natural gas exploration and extraction combined with increased Arctic shipping (Odemark, et al. 2012; Browse, et al. 2013; Peters, et al. 2011; Fuglestvedt, et al. 2014). The recent acceleration of biomass burning in the Alaska Arctic could also lead to increased BC and OC burdens in the region (Turetsky, et al. 2011). These region-specific BC emissions could potentially create areas of enhanced near-surface solar heating downwind of the new emission sources (Sand, et al. 2013b). An increase in point source OC emissions within the Arctic (i.e. new drilling and shipping locations), in conjunction with inorganic ion composition, is relevant for understanding potential spatial heterogeneities in aerosol-cloud interactions across the Arctic (Sand, et al. 2013b; Hoffmann, et al. 2010). Carbonaceous aerosols, particularly OC, increase in hygroscopicity via atmospheric processing during transport; hygroscopicity of aerosols plays an important role in aerosol-cloud interactions (Hoffmann, et al. 2010; Fu, Kawamura, and Barrie 2009). It has been estimated that carbonaceous aerosols have contributed 1.09 ± 0.81 °C to the

observed Arctic temperature increase of 1.48 ± 0.28 °C from 1976-2007 (Shindell and Faluvegi 2009). Seasonal BC burdens are of particular interest in the Arctic due to its radiative impacts both in the atmosphere and at the surface. BC absorbs shortwave radiation in the atmosphere with estimated global direct radiative forcing values of +0.4 W m^{-2} as reported by the Intergovernmental Panel on Climate Change,(IPCC 2013) similarly, Bond et al. reported global direct radiative forcing of +0.71 W m^{-2} (with 90% uncertainty bounds of +0.08 to +1.27) (Bond, et al. 2013). Wintertime deposition of BC reduces snow albedo for a positive radiative forcing value of +0.13 W m^{-2} (with 90% uncertainty bounds of +0.04 to +0.33) (Bond, et al. 2013; Hegg, et al. 2009). Surface albedo feedback is the additional absorption of incoming shortwave radiation as ice and snow melts and the surface becomes less reflective (Winton 2006). A recent study from Tibet points to the need for also investigating the impact of OC on surface albedo in snow covered regions (Wang, et al. 2015). Finally, differences in source contributions can also affect the forcing values, as it has also been shown that BC plumes dominated by fossil fuel combustion sources are approximately 100% more efficient warming agents than those dominated by biomass burning sources (Ramana, et al. 2010). Therefore, for mitigation and modeling, it is necessary that fossil fuel and biomass combustion contributions to BC and OC emissions from in-Arctic source regions be defined (i.e. Russian, Scandinavian, and North American Arctic contributions) (Sand, et al. 2013b; Browse, et al. 2013; Peters, et al. 2011; Octaviani, et al. 2015).

Despite emitting less mass than mid-latitude sources, in-Arctic sources have higher relative impact than distant sources due to high transport efficiency and near 100% direct input within the Arctic dome (Bond, et al. 2013; Stohl, et al. 2013; Koch and

Hansen 2005). The phenomenon known as the Arctic Dome forms when surfaces of constant potential temperature form a dome over the colder Arctic lower troposphere, causing warmer air traveling northward to ascend (Law and Stohl 2007; Stohl 2006). The formation of the dome during the winter and spring isolates the Arctic lower troposphere from the rest of the atmosphere which makes understanding in-Arctic sources very important in the winter. This dome extends to the mid-latitudes in the central Eurasian continent; emission sources will not be evenly distributed across the Arctic (Bond, et al. 2013; Stohl, et al. 2013). Therefore, assumptions that concentrations of OC and EC are evenly mixed within the Arctic atmosphere could lead to inaccuracies in assessing potential climate forcing. Northern Russia has significant flaring emissions, estimated at nearly one-third of all flaring globally, associated with the petroleum and natural gas industry, which have been suggested as major sources of surface BC in the Arctic (Stohl, et al. 2013).

Despite the fact that flaring accounts for only 3% of global BC emissions, it has been modeled to contribute up to 42% of the mean annual Arctic surface concentrations (Stohl, et al. 2013). A recent emission inventory from Stohl et al. (2013) modeled BC concentrations in Barrow from flaring and other fossil sources (including transport, industry and energy sectors) to be 0.03 μg m^{-3} in January, decreasing to 0.02 μg m^{-3} in March 2008-10. This was equally split between flaring and all other fossil sources for the mid- to late winter period. In addition, Stohl et al. (2013) predicted biomass burning BC concentrations for Barrow of 0.02 μg m^{-3} for January decreasing to 0.01 μg m^{-3} in March for 2008-10. For the mid- to late winter period, the dominant predicted biomass BC source was domestic combustion, with a potential for increased wildfires by late winter

according to modeled results (Stohl, et al. 2013; Warneke, et al. 2010; Q. Wang, et al. 2011). While BC emissions and their sources have been modeled extensively in the Arctic, their results have not been validated by observation of fossil and biomass burning contribution and detailed OC modeling is still needed. To improve regional models of Arctic BC and climate impacts, measurements of atmospheric concentrations and processing are needed based on geographic region, season and emission source.

Previous receptor-based source apportionment of BC in the Arctic has relied on a combination of elemental and organic tracers (von Schneidemesser, et al. 2009). The accuracy of receptor-based source apportionment modeling is limited by the appropriateness and completeness of the input emission source profiles for the study location and by the atmospheric lifetime of the organic tracers; the latter has been documented as increasing uncertainty in source apportionment of OC at remote sites in the Arctic (Yttri, et al. 2014) and in the Indian Ocean (Sheesley, Andersson, and Gustafsson 2011). In this study, ^{14}C abundance and organic tracer measurements were applied to apportion and characterize both the OC and elemental carbon (EC) fractions of six, week-long winter Arctic aerosol samples from the North Slope of Alaska (NSA) in Barrow, Alaska (AK). In order to perform isotope analysis on the EC fraction of the sample, it must be isolated from the OC fraction. During the isolation process, OC can be charred to form pyrolyzed carbon (PyrC), which could be inadvertently included in the isolated EC. Different methods have been widely published to address this potential bias. Some EC isolation protocols add a water extraction pretreatment prior to thermal volatilization in a helium-oxygen atmosphere, which has documented 20% EC loss prior to EC isolation (Dusek, et al. 2014). Other protocols utilize post-analysis sensitivity tests

to report potential bias of pyrolyzed OC included in the ^{14}C of isolated EC using isolation based on truncation of the thermal optical transmission protocol (Chen, et al. 2013; Budhavant, et al. 2015; August Andersson, et al. 2015). For the current study we have utilized the latter method to enable better comparison with published emission source profiles and ambient EC studies which have utilized thermal optical transmission OCEC analysis.

The large difference in end members between fossil and contemporary carbon allows precise quantification of fossil fuel combustion and biomass burning contribution (Gustafsson, et al. 2009; R. J. Sheesley, et al. 2012; Lewis, Klouda, and Ellenson 2004). Contemporary carbon is used to define all carbon (elemental and organic) that is derived from biomass combustion (wildfires, biofuels, agricultural fuel and residential firewood combustion) and biogenic emission (primary biogenic emissions and secondary organic aerosols produced from biogenic volatile organic carbon). The precision in the radiocarbon apportionment can be used to validate the accuracy of source apportionment utilizing organic tracers. This study applied ^{14}C source apportionment to evaluate atmospheric processing of organic tracers in the Arctic; ^{14}C source apportionment of EC was combined with biomass burning emission profiles to calculate wintertime half-lives ($\tau_{1/2}$) for the biomass burning tracer levoglucosan (Zangrando, et al. 2013). Levoglucosan is a commonly measured organic tracer which is used to track contributions of biomass burning. In the current study, levoglucosan half-lives are used to understand 1) differences between the two receptor-based source apportionment models: radiocarbon and CMB, and 2) relative differences in atmospheric processing for the filter samples. This combination of ^{14}C, organic tracer, and ten-day Hybrid Single Particle Lagrangian

Integrated Trajectory Model (HYSPLIT) back trajectory analysis is applied here to understand wintertime source contributions and transport processing of fossil and contemporary carbonaceous aerosols in the North American Arctic.

Experimental

Field Collection

Wintertime particulate matter (aerodynamic diameter of <10 μm; PM_{10}) samples were collected from December 28, 2012 to March 11, 2013 at the NSA Atmospheric Radiation Measurement (ARM) Climate Research Facility, 7.4 km northeast of Barrow, AK (71°19'23.73" N, 156°36'56.70" W); see Figure 4.1. Samples from Dec 28-Feb 15 were labeled mid-winter, while Feb 25-Mar 11 were labeled late winter. For mid-winter, 93% of the total sampling time had local wind direction from the clean sector of 0-130º (Shaw, et al. 2010), and 91% of the total sampling time during the late winter was from the clean sector. A comparison of co-located BC (aethalometer, Magee Scientific, Berkeley, CA) and wind direction revealed no significant differences between clean and dirty sector BC concentrations during this campaign.

PM_{10} samples were collected on quartz fiber filters (QFF; Tissuquartz™ Filters 2500 QAT-UP; 20 x 25 cm.) using a Tisch high volume PM_{10} sampler (TE-6070; Tisch Environmental, Cleves, Ohio). QFFs were baked at 500 °C for 12 hours (h) prior to sampling. All samples and blanks were stored in aluminum foil packets and storage bags in a freezer. Sampling duration was approximately one week at a flow rate of approximately 1.2 m^3 min^{-1}. The total volume per filter was normalized using two co-located measurements: a $PM_{2.5}$ sampler, which had weekly flow rate checks, and an aethalometer. EC from the $PM_{2.5}$ correlated well with the aethalometer BC (r^2 = 0.91)

which was located at the adjacent National Oceanic and Atmospheric Administration (NOAA) site in Barrow.

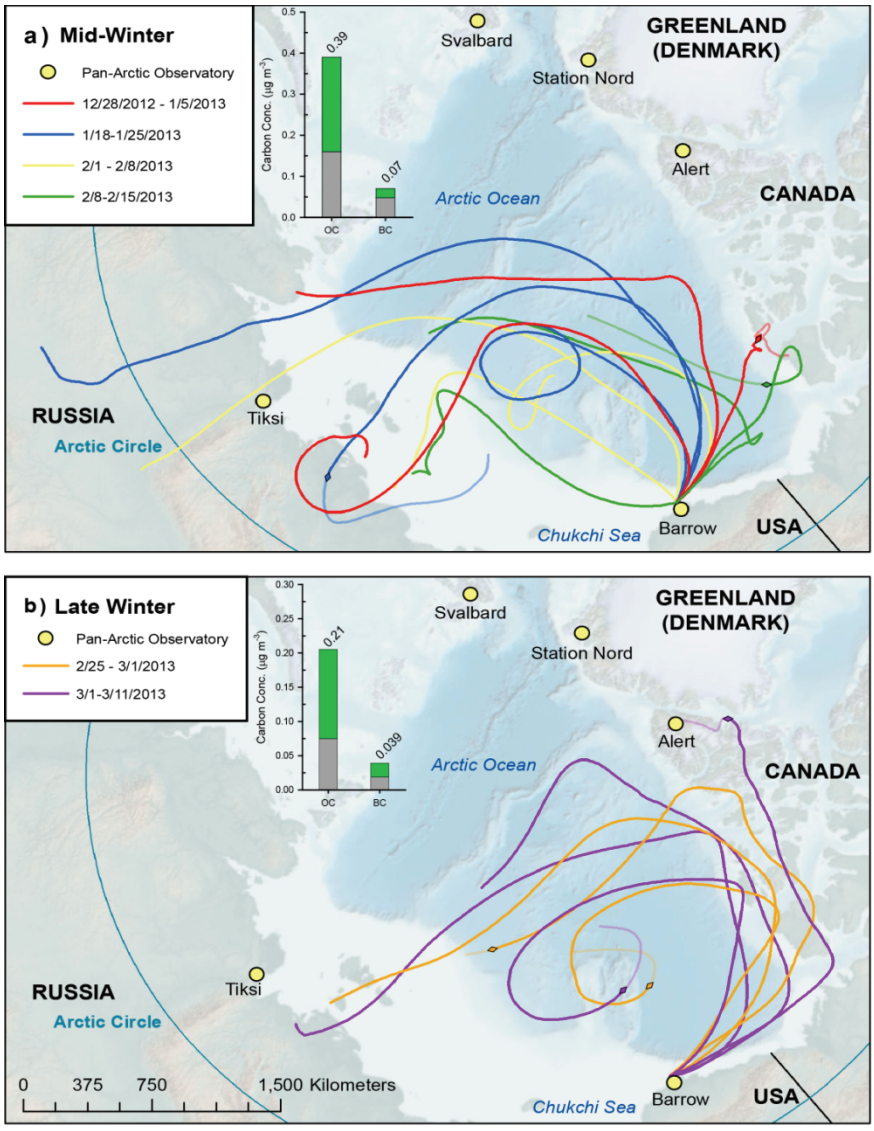

Figure 4.1: Ten-day HYSPLIT back trajectories of air masses arriving in Barrow, AK: a) mid-winter and b) late winter. Early winter trajectories are dominated by Arctic Ocean and Russian sources. Late winter trajectories were dominated by North American sources and the Arctic Ocean. Inlays: bar graphs represent the mean organic carbon (OC) and elemental carbon (EC) concentrations: green represents the contemporary carbon contribution while gray represents the fossil carbon contribution to particulate carbon. Transparent back trajectories indicate that the back trajectory is above the surface boundary layer, diamonds and then opaque lines represent the point where the back trajectories remain below the boundary layer.

Carbon and Isotope Analysis

Six samples were chosen for measurement of the ambient ^{14}C signal of the total organic carbon (Zaveri, et al.) and EC fractions based on available mass (Table B.1 & Figure 4.1). Prior to ^{14}C analysis, OC and EC filter concentrations were determined using a thermo-optical transmittance carbon analyzer (Sunset Laboratories, Tigard, OR) using the NIOSH 5040 method (Birch and Cary 1996). Instrument blanks and a sucrose standard were run with each batch of ten samples. Samples were blank subtracted using a value of 0.18 μg cm^{-2} of OC. EC was isolated on the filters for ^{14}C analysis on the carbon analyzer to remove OC and preserve 90-95% of EC on the filter (Andersson, et al. 2011). The NIOSH 5040 method was truncated at the split time between OC and EC for each sample. It is known that a fraction of OC is pyrolyzed during the He phase of the NIOSH 5040 method, potentially leading to a fraction of the OC being included in the isolated EC fraction. The inclusion of this PyrC with the EC fraction could affect the isotopic signature of the EC. Sensitivity analysis for the current study shows a maximum underestimation of fossil contribution to EC by 14-22% in the mid-winter and 10-11% in the late winter, maintaining the difference in EC fossil contribution between the two processing regimes (Table B.7). The average percent difference of the sensitivity tests has been included as the radiocarbon apportionment uncertainty as it far exceeds uncertainty associated with the accelerator mass spectrometry measurement and blank subtraction (Gustafsson, et al. 2009; Chen, et al. 2013; A. Andersson, et al. 2015; Budhavant, et al. 2015).

For the ^{14}C of TOC, the QFFs were cut to give ~100 μg of TOC for the accelerator mass spectrometry measurement of the ^{14}C signal. The TOC and isolated EC

filter sections were acidified in a desiccator over hydrochloric acid for 12 h and then dried in a drying oven and stored in pre-baked glass petri-dishes (Gustafsson, et al. 2009). Radiocarbon analysis was performed at the National Oceanic Sciences Accelerator Mass Spectrometry facility.

Organic Tracer Analysis

Organic tracers were measured using pressurized liquid extraction (Hung, et al. 2005; Nallathamby, et al. 2014) of filter sections with dichloromethane (DCM) and methanol (MeOH) followed by analysis with a gas chromatograph 7890 coupled to a 5975C mass spectrometer in electron ionization mode (GC/MS) (Hung, et al. 2005). GC/MS methods are based on Usenko et al.(Usenko, et al. 2005) with slight modifications to final hold time and injection pulse pressure outlined below; PLE methods were adapted from a previous study (Nallathamby, et al. 2014) and extractions were performed using an accelerated solvent extractor (ASE 350; Dionex, Sunnyvale, CA, USA). Extraction cells were pre-cleaned using 1:1 (v/v) DCM:MeOH under the following PLE conditions: 100 °C, 1500 psi, 3 cycles (5 min each), and 120% rinse volume. Filter areas corresponding to ~300 μg organic carbon were placed in the cleaned cells and spiked with isotopically labeled surrogate standards (standard source: Wisconsin State Laboratory of Hygiene, see Supplemental Information-Target Analyte list). Filters were extracted twice using 1) DCM and 2) MeOH using the same conditions described above. Combined filter extracts were concentrated to ~65 μL at 40 °C and spiked with an isotopically-labeled polycyclic aromatic hydrocarbon (PAH) internal standard (for quantification of PAH surrogate standards) prior to analysis using GC/MS. The final hold time was 19 min and the injection pulse pressure was 20 psi until 0.75

min. For levoglucosan, silylation derivatization, using N,O-bis(trimethylsilyl)-trifluoroacetamide (BSTFA, with 1% trimethylchlorosilane as a catalyst; Sigma-Aldrich, St. Louis, MO) was required prior to GC/MS analysis. The target analyte list consisted of 28 PAHs, eight steranes and hopanes, 25 alkanes and levoglucosan.

Source Apportionment Modeling

Two different types of source apportionment modeling were used: radiocarbon source apportionment and CMB modeling using organic tracers. The $\Delta^{14}C$ end member for contemporary carbon (carbon resulting from biomass combustion and biogenic emissions) used was +107.5‰, based on wood burning from a 2010 reference for temperate regions.(Zotter, et al. 2014) The ^{14}C end member for fossil fuels used here was -1000‰ (Q. Wang, et al. 2011; Gustafsson, et al. 2009; R. J. Sheesley, et al. 2012). End members were applied in the following equation:

$$\Delta^{14}C\text{-}EC = (\Delta^{14}C_{biomass})(F_{biomass}) + (\Delta^{14}C_{fossil})(1\text{-}F_{biomass})$$

The contribution from fossil carbon (F_{fossil}) is (1- $F_{biomass}$). The $\Delta^{14}C$ for OC was calculated from $\Delta^{14}C$ for EC and $\Delta^{14}C$ for TOC, using TOC = OC + EC.

The EPA CMB model version 8.2 was used for apportionment of OC from wood smoke, motor vehicle exhaust (spark and compression ignition) and lubricating oil-impacted exhaust (von Schneidemesser, et al. 2009; Sheesley, et al. 2009; Iinuma, et al. 2007). Source emission profiles along with ambient concentrations from the receptor site were used as input into the model; all model inputs used compatible techniques for OCEC analysis (thermal optical transmittance) and organic tracer analysis. As in von Schneidemesser et al. (2009), the fossil fuel combustion source profiles were nominally for North American motor vehicle exhaust, but also functioned to apportion high PAH-

(spark ignition), high EC- (compression ignition) and high heavy oil- (lubricating oil-impacted exhaust) emitting sources. These were combined to give "CMB fossil." Fitting statistics (r^2, χ^2, and a calculated to measured ratio for modeled species) of the model results with respect to input matrix (ambient concentrations and ratios or organic tracers to organic carbon for the emission sources) were used to determine if model results were acceptable (Watson, et al. 2002). Results were not accepted with an r^2 less than 0.8 and chi-square greater than 3.5. CMB OC results were converted to EC by using the EC to OC ratios from the emission source profiles in the CMB model, allowing a modeled assessment of contributions of fossil and contemporary carbon to Arctic EC (Table B.2) (Sheesley, et al. 2009).

Back Trajectories and Boundary Layer Height

Ten-day back trajectories were calculated for Barrow every six hours for each sampling day over the entire sampling campaign. Back trajectories were completed using the NOAA HYSPLIT model, version 4, May 2012 release (R.R Draxler and G.D. Rolph 2010). The model was run using meteorological data from the Global Data Assimilation System (GDAS) produced by NOAA (http://www.emc.ncep.noaa.gov/gmb/gdas/). Each back trajectory was set to run with a starting height of 10 m above ground level using vertical velocity fields provided in the GDAS data. Resulting trajectories were clustered using the clustering function in the HYSPLIT model and mapped using ESRI's ArcGIS 10 software. Back trajectories are imprecise in the Arctic due to a limited number of meteorological monitoring stations in the region, but are used here to provide a broad description of the source region of the air masses and are used to track large shifts. In order to evaluate this potential uncertainty, a sensitivity analysis was conducted by

completing back trajectories for two additional, nearby locations with three different starting heights (50, 100 and 500 m). The sensitivity analysis results showed that the HYSPLIT model is robust and the shift in potential source region detected by the model is reproducible (Supplemental Information figures B.2-B.10). Boundary layer height was determined by analysis of skew-t charts for Barrow, AK (http://weather.uwyo.edu/upperair/sounding.html). To determine the height of the boundary layer, two skew-t charts for each day of sampling, from 00z and 12z, were analyzed. The boundary layer was 623 m to 967 m during this study. Areas where the temperature and dew point readings deviate indicate dry areas, with the height of the dry area indicating the strength of the cap.

Levoglucosan Half-life Calculations and Wood smoke Profile Sensitivity Analysis

Under the assumption that EC is conserved through atmospheric transport and that the ^{14}C signal of contemporary carbon in EC is also conserved, initial levoglucosan concentration at the source can be calculated. This is achieved by multiplying the contemporary EC concentrations by known levoglucosan/EC ratios from different wood smoke types ($Levoglucosan_{source}/EC_{source}$). Published levoglucosan/EC ratios from seven different wood smoke profiles (Table B.3) were used for calculating initial levoglucosan concentration (eq. 2) for samples from the mid- and late winter. The different wood smoke profiles cover a range of wood types and composites of multiple wood types, but all utilize the same thermal optical transmittance method for EC analysis. Equation 2 below was used to determine the initial levoglucosan concentration ($Levoglucosan_{initial}$; μg m^{-3}) at the source:

$$Levoglucosan_{initial} = EC_{contemporary} \times Levoglucosan_{source}/EC_{source}$$

The half-life ($\tau_{1/2}$) of levoglucosan was then determined from the calculated initial levoglucosan concentration and the measured levoglucosan concentration ($Levoglucosan_{measured}$; μg m^{-3}) at the sampling site (Table B.4). Transit time, t, of the wood smoke aerosol will systematically affect the calculated reaction rate coefficient of levoglucosan. With wind direction consistently from the clean sector, transit times of 2 and 5 days are reported for the $\tau_{1/2}$ calculations. The decay of levoglucosan follows first-order kinetics (Hoffmann, et al. 2010); therefore the half-life ($\tau_{1/2}$) was determined using the integrated rate law (eq. 3) and the half-life equation for first order reactions (eq. 4);

$$\ln[A]=-kt+\ln[A_o]$$

where *k* is the reaction rate coefficient and is determined graphically by plotting the *ln* of $Levoglucosan_{initial}$ and *ln* of $Levoglucosan_{measured}$ [A] vs. t (Figure B.1), the slope of the line is expressed in terms of *k*, and is then used in equation 4 to determine the $\tau_{1/2}$ of levoglucosan;

$$\tau_{1/2} = \frac{ln2}{k}$$

The calculated levoglucosan half-lives were then used to determine an appropriate wood smoke profile for use in the CMB apportionment (Table B.2 and B.4). The identification of an appropriate wood smoke profile for use in CMB is key for accurate apportionment of fossil and contemporary source (Sheesley, et al. 2007). Multiple wood smoke profiles were examined for use in the CMB; 1) Pine, 2) Pine w/greens, 3) Spruce, 4) Average of Pine w/greens and Spruce, 5) California (pine and fir), 6) Maine (spruce and birch), and 7) Washington (fir and hemlock). The Pine w/greens profile is the same wood smoke profile as used by von Schneidemesser et al. (2009) in CMB analysis of summertime aerosols from Summit, Greenland, originally from Iinuma et al. (2007). The

Pine profile is also from Iinuma et al. (2007). The Spruce wood smoke profile was taken from Schmidl et al. (2008) and the Average of Pine w/greens and Spruce is an average of the Pine w/greens and the Spruce profiles (Schmidl, et al. 2008). The California, Maine, and Washington wood smoke profiles are from emission inventories from Fine et al. (2004; 2002) and are based on tree stand inventories from the U.S. Forestry Service. The Pine w/greens, Spruce, and Pine w/greens and Spruce Avg. profiles all had negative $\tau_{1/2}$ values and were excluded from CMB analysis. The Maine wood smoke profile was identified as an appropriate wood smoke profile based on $\tau_{1/2}$ calculations and tree stand makeup. The atmospheric lifetime test of levoglucosan in the Arctic enabled the identification of an appropriate wood smoke profile for use in the CMB, improving the overall accuracy of the CMB apportionment.

Results and Discussion

Carbonaceous Aerosols and Source Apportionment

In this study, the mean EC burden (fossil plus contemporary) for the mid-winter period was 0.07 ± 0.02 μg m^{-3}, ranging from 0.04 to 0.1 ± 0.01 μg m^{-3} (Dec 28-Feb 15, Figure 4.1a Inlay, Table B.1). During this time, back trajectories indicate air masses arriving at Barrow generally originate in northern Russia and the Arctic Ocean with limited time over the North American Arctic. Back trajectory analysis also showed that air masses arriving at Barrow were predominantly within the atmospheric surface layer (Figure 4.1a; boundary height 780 meters above ground level). ^{14}C fossil EC concentrations range from 0.03 to 0.07 ± 0.016 μg m^{-3} in January and early February (Figure 4.2a), which accounted for 66.4 to 71.1% ± 1.9% of total EC during mid-winter. When comparing to 2010 emissions inventories, we find Stohl et al. (2013) is within 5%

of ^{14}C fossil EC for early January and underestimates fossil BC by up to 62% throughout mid- and late winter, which is possibly due to a combination of an underestimation of BC emissions by fossil sources within the model and/or increased fossil fuel combustion in 2013. Year to year variability in meteorological conditions such as atmospheric transport patterns and wet and dry deposition could also be responsible for the reported differences. However, the contemporary signal is more stable (0.023 ± 0.014 μg m^{-3} of EC from contemporary sources from January to early March), which closely matches previously described early winter models (Stohl, et al. 2013) (Figure 4.2a).

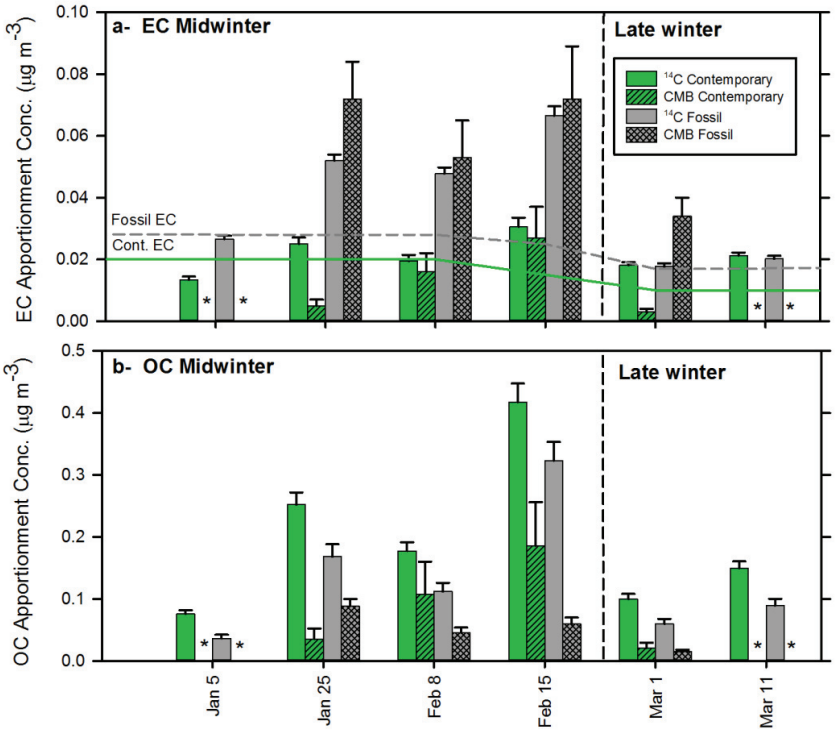

Figure 4.2: Contemporary and fossil a) elemental carbon (EC) and b) organic carbon (OC) concentrations measured during the study period. Also shown are the chemical mass balance (CMB) modeled concentrations of EC and OC. The fossil EC line (- - - -) and contemporary EC line (——) in (a) are from emissions inventories used in Stohl et al.(Stohl, et al. 2013) * indicate that CMB results are not available.

In the late winter (Feb 25-Mar 11) there were shifts in the carbonaceous aerosol concentration, ^{14}C source apportionment of EC, and back trajectory source regions (Figure 4.1b). Mean fossil contribution to the Arctic EC burden drops from 68.4 ± 9.2% (mid-winter) to 49.1 ± 5.6% (late winter). This drop in fossil contribution coincides with a shift in back trajectories; all late winter ten-day back trajectories pass over the North American Arctic and do not penetrate into northern Russia (Figure 4.1b; boundary height 900 meters above ground level). During late winter, mean fossil EC concentration drops from 0.048 ± 0.016 to 0.019 ± 0.001 μg m^{-3}, while mean contemporary EC concentration remains relatively stable at 0.019 ± 0.002 μg m^{-3} (Figure 4.1b Inlay). We attribute this late winter decrease in fossil EC to regional differences in fossil fuel combustion emissions; this shift in fossil EC concentration was predicted for Barrow by Stohl et al (2013). Previously discussed uncertainties associated with EC isolation for isotope analysis only widens the difference between the two winter regimes, with the reported fraction fossil of EC representing the lowest possible fossil contributions to EC during the study (Table B.7). Previous long-term monitoring studies have documented equivalent BC (aethalometer) concentrations decreasing significantly from winter into spring and summer, but did not distinguish between fossil and contemporary BC contributions (Sharma, et al. 2006).

The mean OC burden (fossil plus contemporary) for the study period was 0.33 ± 0.07 μg m^{-3}, ranging from 0.11 ± 0.01 to 0.74 ± 0.04 μg m^{-3} (Figure 4.1a and 4.1b Inlay). Fossil contribution to OC is much lower and relatively stable throughout the winter despite back trajectory shifts, with a mean contribution of 38.3 ± 8.0% (Figure 4.1). The remaining 61.7% of OC was contemporary, potentially representing a combination of

biomass burning and biogenic source contributions. Oxidation products for biogenic volatile organic carbon, specifically monoterpene and sesquiterpene, have been reported to contribute up to 12% of late winter/early spring secondary organic carbon at Alert, Canada (Fu, et al. 2009). Fossil OC concentrations ranged from 0.04 ± 0.01 μg m^{-3} to 0.32 ± 0.02 μg m^{-3} with contemporary OC concentrations ranging from 0.08 ± 0.01 μg m^{-3} to 0.42 ± 0.02 μg m^{-3} for the winter (Figure 4.2b). Previous OC apportionment could only estimate source contributions for 4% of the mass (1.5% fossil, 1% biomass, and 1.5% vegetative detritus) with 96% of the OC remaining unapportioned (von Schneidemesser, et al. 2009). Our radiocarbon apportionment allows for a precise split between fossil and contemporary sources, effectively apportioning 100% of the mass to give ambient concentrations of fossil OC and contemporary OC.

^{14}C results were also compared to the modeled EC concentration values from an organic tracer CMB (Table B.2). Mid-winter EC concentrations from the CMB model were inconsistent with the ^{14}C EC apportionment results (Figure 4.2a). Percent differences for fossil and contemporary sources show best agreement between ^{14}C and CMB apportionment during the Feb 8 and 15 samples (Figure 4.3). The effectiveness of the organic tracer CMB model can also be evaluated based on the fraction of the ambient mass that was able to be apportioned and by how closely that apportionment matches the ^{14}C source apportionment for OC. The CMB apportioned mass ranged from 24% in late winter to 53% in mid-winter for OC, which is 6-13 times higher mass apportioned than previous studies (von Schneidemesser, et al. 2009). For OC apportionment, the contemporary ^{14}C and CMB also show the best agreement for Feb 8 and 15, but the fossil ^{14}C and CMB have the best agreement for the Jan 25 sample (Figure 4.3). This

variability in agreement between the CMB model and ^{14}C apportionment could be due to previously unrecognized differential degradation of organic tracers by photochemistry and cloud processing during atmospheric transport to Barrow, a remote receptor site.

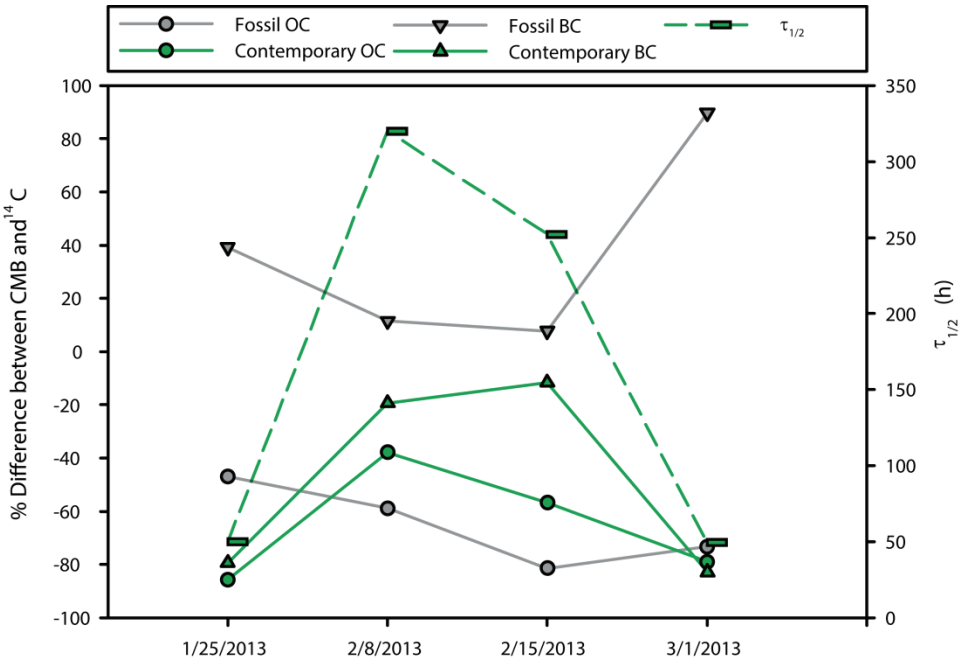

Figure 4.3: Percent differences between ^{14}C apportioned elemental carbon (EC) and organic carbon (OC) for fossil and contemporary source contributions are compared to atmospheric lifetimes ($\tau_{1/2}$, 5-day transit time) for levoglucosan, a biomass burning tracer.

Atmospheric Lifetime of Levoglucosan

Organic tracers can undergo significant degradation during transport in the Arctic, but field-based estimations of $\tau_{1/2}$ have been elusive. Laboratory and modeling studies by Hoffman et al. (2010) estimated $\tau_{1/2}$ values for levoglucosan, a biomass burning tracer, ranging from 12.7 to 83.2 h for a polluted continental plume model. The range in $\tau_{1/2}$ values was due to variations in OH radical concentrations, temperature, cloudiness, and season; shorter atmospheric half-lives were dominated by cloud processing (Hoffmann, et al. 2010). Yttri et al. (2014) tested Hoffman et al.'s (2010) atmospheric half-lives for

levoglucosan using ambient data and emissions inventories and generally concluded that to achieve reasonable comparison with emissions inventories, the $\tau_{1/2}$ of levoglucosan would need to be at least 96 h. In the current study, the ^{14}C apportioned EC was combined with reported ratios for levoglucosan/EC to calculate $\tau_{1/2}$ for levoglucosan at 2 and 5 day transit times (Figure 4.3 and Tables B.4 and B.5). This enabled examination of relative atmospheric processing over the Arctic winter; processing will likely increase aerosol hygroscopicity. The atmospheric half-lives of levoglucosan increased for a period during mid-winter, which reveals short-term variability in atmospheric processing during the winter season. For the four weeks of ambient levoglucosan measurement, two weeks were identified as relatively high degradation and two weeks as low degradation. These differences in atmospheric lifetime did not coincide with changes in source contribution or back trajectory source region. HYSPLIT back trajectory estimates of residence time above the atmospheric surface layer and residence time with over 90% relative humidity were also not conclusive in determining meteorological impacts on atmospheric lifetimes of levoglucosan in this study. More detailed atmospheric characterization and shorter sampling times are needed to determine which factor drives the atmospheric lifetime of levoglucosan in the Arctic winter.

During periods of high degradation (Jan 25 and Mar 1), $\tau_{1/2}$ values were 20 h and 50 h, for 2-day and 5-day transit times respectively. However, during periods of apparent low degradation (Feb 8 and Feb 15) the $\tau_{1/2}$ averaged 114 ± 19 h and 286 ± 48 h, for 2-day and 5-day transit times respectively (Figure 4.3 and Tables B.4 and B.5). The high degradation periods fall within previously reported estimates of atmospheric lifetimes (13-83 h) for levoglucosan (Hoffmann, et al. 2010), while the low degradation periods are

significantly longer. The difference in atmospheric half-lives of levoglucosan throughout the campaign matches the percent differences seen between ^{14}C and CMB for contemporary EC and OC (Figure 4.3), which indicates that lifetime of levoglucosan is the limiting factor in the ability of the CMB to apportion biomass burning. However, the ability of organic tracer CMB to model fossil OC does not follow the same $\tau_{1/2}$ trends for levoglucosan, which may indicate that improvements in fossil emission profiles for the Arctic are also needed. Although not all aerosol components will age at the same rate as levoglucosan, these results demonstrate that organic tracer half-lives show potential for use in tracking atmospheric processing (i.e. aging) of Arctic aerosols. Further investigation is needed to understand which factors drive changes in the observed half-life of levoglucosan before these half-lives can be effectively applied to systematically characterize atmospheric processing of Arctic aerosols.

^{14}C source apportionment of wintertime PM_{10} samples confirms high fossil contribution to EC in mid-winter (68.4 ± 9.2%) and lower contribution in the later winter (49.1 ± 5.6%) from in-Arctic sources impacting the North American Arctic. Back trajectory analysis revealed potential spatial differences in fossil fuel combustion activities within the Russian and North American Arctic which could be driving differences in fossil contribution to the winter EC burden in Barrow. Over the course of the sampling campaign, shifts in atmospheric processing of levoglucosan were identified. Variations in atmospheric processing provide an opportunity to identify temporal differences in aerosol-cloud interaction during the winter. Results from this study represent a six week wintertime campaign in the North American Arctic; therefore, additional analysis on a larger spatial and temporal scale is needed to accurately quantify

source contributions and processing across the Arctic. Unambiguous apportionment of fossil and contemporary sources of EC coupled with atmospheric lifetime measurements of aerosols can be used to improve global climate models in this region.

Author Contributions

The manuscript was written through contributions of all authors. All authors have given approval to the final version of the manuscript.

Funding Sources

Financial support provided by the United States Department of Energy (Atmospheric Radiation Measurement Field Campaign #2010-05876) and the C. Gus Glasscock, Jr. Endowed Fund for Excellence in Environmental Sciences.

Acknowledgment

Financial support provided by the United States Department of Energy (Atmospheric Radiation Measurement Field Campaign #2010-05876) and the C. Gus Glasscock, Jr. Endowed Fund for Excellence in Environmental Sciences. The authors would like to thank Dr. George Cobb of Baylor University for use of the PM_{10} sampler, Walter Brower and Jimmy Ivanoff of the Ukpeagvik Inupiat Corporation for sample collection and field assistance along with Fred Helsel, Dan Lucero, and Jeffrey Zirzow of the Sandia National Laboratory for site access and preparation, and Aaron Jones for assistance with spatial analysis. The authors gratefully acknowledge the NOAA Air Resources Laboratory for the provision of the HYSPLIT transport and dispersion model used in this publication. The authors also acknowledge Dr. Anne Jefferson and Matthew Martinsen of NOAA for their valuable comments and insight.

Odemark, K.; Dalsoren, S. B.; Samset, B. H.; Berntsen, T. K.; Fuglestvedt, J. S.; Myhre, G., Short-lived climate forcers from current shipping and petroleum activities in the Arctic. *Atmos. Chem. Phys.* **2012,** *12*, (4), 1979-1993.

Browse, J.; Carslaw, K. S.; Schmidt, A.; Corbett, J. J., Impact of future Arctic shipping on high-latitude black carbon deposition. *Geophys. Res. Lett.* **2013,** *40*, (16), 4459-4463.

Peters, G. P.; Nilssen, T. B.; Lindholt, L.; Eide, M. S.; Glomsrod, S.; Eide, L. I.; Fuglestvedt, J. S., Future emissions from shipping and petroleum activities in the Arctic. *Atmos. Chem. Phys.* **2011,** *11*, (11), 5305-5320.

Fuglestvedt, J. S.; Dalsoren, S. B.; Samset, B. H.; Berntsen, T.; Myhre, G.; Hodnebrog, O.; Eide, M. S.; Bergh, T. F., Climate Penalty for Shifting Shipping to the Arctic. *Environ. Sci. Technol.* **2014,** *48*, (22), 13273-13279.

Turetsky, M. R.; Kane, E. S.; Harden, J. W.; Ottmar, R. D.; Manies, K. L.; Hoy, E.; Kasischke, E. S., Recent acceleration of biomass burning and carbon losses in Alaskan forests and peatlands. *Nat. Geosci.* **2011,** *4*, (1), 27-31.

Sand, M.; Berntsen, T. K.; Seland, O.; Kristjansson, J. E., Arctic surface temperature change to emissions of black carbon within Arctic or midlatitudes. *J. Geophys. Res.-Atmos.* **2013,** *118*, (14), 7788-7798.

Hoffmann, D.; Tilgner, A.; Iinuma, Y.; Herrmann, H., Atmospheric Stability of Levoglucosan: A Detailed Laboratory and Modeling Study. *Environ. Sci. Technol.* **2010,** *44*, (2), 694-699.

Fu, P.; Kawamura, K.; Barrie, L. A., Photochemical and Other Sources of Organic Compounds in the Canadian High Arctic Aerosol Pollution during Winter-Spring. *Environ. Sci. Technol.* **2009,** *43*, (2), 286-292.

Shindell, D.; Faluvegi, G., Climate response to regional radiative forcing during the twentieth century. *Nat. Geosci.* **2009,** *2*, (4), 294-300.

IPCC, *Climate Change 2013: The Physical Science Basis. Contribution of Working Group I to the Fifth Assessment Report of the Intergovernmental Panel on Climate Change*. Cambridge University Press: 2013.

Bond, T. C.; Doherty, S. J.; Fahey, D. W.; Forster, P. M.; Berntsen, T.; DeAngelo, B. J.; Flanner, M. G.; Ghan, S.; Karcher, B.; Koch, D.; Kinne, S.; Kondo, Y.; Quinn, P. K.; Sarofim, M. C.; Schultz, M. G.; Schulz, M.; Venkataraman, C.; Zhang, H.; Zhang, S.; Bellouin, N.; Guttikunda, S. K.; Hopke, P. K.; Jacobson, M. Z.; Kaiser, J. W.; Klimont, Z.; Lohmann, U.; Schwarz, J. P.; Shindell, D.; Storelvmo, T.; Warren, S. G.; Zender, C. S., Bounding the role of black carbon in the climate system: A scientific assessment. *J. Geophys. Res.-Atmos* **2013,** *118*, (11), 5380-5552.

Hegg, D. A.; Warren, S. G.; Grenfell, T. C.; Doherty, S. J.; Larson, T. V.; Clarke, A. D., Source Attribution of Black Carbon in Arctic Snow. *Environ. Sci. Technol.* **2009,** *43*, (11), 4016-4021.

Winton, M., Amplified Arctic climate change: What does surface albedo feedback have to do with it? *Geophys. Res. Lett.* **2006,** *33*, (3).

Wang, M.; Xu, B.; Cao, J.; Tie, X.; Wang, H.; Zhang, R.; Qian, Y.; Rasch, P. J.; Zhao, S.; Wu, G.; Zhao, H.; Joswiak, D. R.; Li, J.; Xie, Y., Carbonaceous aerosols recorded in a southeastern Tibetan glacier: analysis of temporal variations and model estimates of sources and radiative forcing. *Atmos. Chem. Phys.* **2015,** *15*, (3), 1191-1204.

Ramana, M. V.; Ramanathan, V.; Feng, Y.; Yoon, S. C.; Kim, S. W.; Carmichael, G. R.; Schauer, J. J., Warming influenced by the ratio of black carbon to sulphate and the black-carbon source. *Nat. Geo.* **2010,** *3*, (8), 542-545.

Octaviani, M.; Stemmler, I.; Lammel, G.; Graf, H. F., Atmospheric transport of persistent organic pollutants to and from the Arctic under present-day and future climate. *Environ. Sci. Technol.* **2015,** *49*, (6), 3593-602.

Stohl, A.; Klimont, Z.; Eckhardt, S.; Kupiainen, K.; Shevchenko, V. P.; Kopeikin, V. M.; Novigatsky, A. N., Black carbon in the Arctic: the underestimated role of gas flaring and residential combustion emissions. *Atmos. Chem. Phys.* **2013,** *13*, (17), 8833-8855.

Koch, D.; Hansen, J., Distant origins of Arctic black carbon: A Goddard Institute for Space Studies ModelE experiment. *J. Geophys. Res.-Atmos.* **2005,** *110*, (D4).

Law, K. S.; Stohl, A., Arctic air pollution: Origins and impacts. *Science* **2007,** *315*, (5818), 1537-1540.

Stohl, A., Characteristics of atmospheric transport into the Arctic troposphere. *J. Geophys. Res.-Atmos.* **2006,** *111*, (D11), D11306.

Warneke, C.; Froyd, K. D.; Brioude, J.; Bahreini, R.; Brock, C. A.; Cozic, J.; de Gouw, J. A.; Fahey, D. W.; Ferrare, R.; Holloway, J. S.; Middlebrook, A. M.; Miller, L.; Montzka, S.; Schwarz, J. P.; Sodemann, H.; Spackman, J. R.; Stohl, A., An important contribution to springtime Arctic aerosol from biomass burning in Russia. *Geophys. Res. Lett.* **2010,** *37*.

Wang, Q.; Jacob, D. J.; Fisher, J. A.; Mao, J.; Leibensperger, E. M.; Carouge, C. C.; Le Sager, P.; Kondo, Y.; Jimenez, J. L.; Cubison, M. J.; Doherty, S. J., Sources of carbonaceous aerosols and deposited black carbon in the Arctic in winter-spring: implications for radiative forcing. *Atmos. Chem. Phys.* **2011,** *11*, (23), 12453-12473.

von Schneidemesser, E.; Schauer, J. J.; Hagler, G. S. W.; Bergin, M. H., Concentrations and sources of carbonaceous aerosol in the atmosphere of Summit, Greenland. *Atmos. Environ.* **2009,** *43*, (27), 4155-4162.

Yttri, K. E.; Myhre, C. L.; Eckhardt, S.; Fiebig, M.; Dye, C.; Hirdman, D.; Strom, J.; Klimont, Z.; Stohl, A., Quantifying black carbon from biomass burning by means of levoglucosan - a one-year time series at the Arctic observatory Zeppelin. *Atmos Chem Phys* **2014,** *14*, (12), 6427-6442.

Sheesley, R. J.; Andersson, A.; Gustafsson, O., Source characterization of organic aerosols using Monte Carlo source apportionment of PAHs at two South Asian receptor sites. *Atmos. Environ.* **2011,** *45*, (23), 3874-3881.

Dusek, U.; Monaco, M.; Prokopiou, M.; Gongriep, F.; Hitzenberger, R.; Meijer, H. A. J.; Röckmann, T., Evaluation of a two-step thermal method for separating organic and elemental carbon for radiocarbon analysis. *Atmos. Meas. Tech.* **2014,** *7*, (7), 1943-1955.

Chen, B.; Andersson, A.; Lee, M.; Kirillova, E. N.; Xiao, Q. F.; Krusa, M.; Shi, M. N.; Hu, K.; Lu, Z. F.; Streets, D. G.; Du, K.; Gustafsson, O., Source Forensics of Black Carbon Aerosols from China. *Environ. Sci. Technol.* **2013,** *47*, (16), 9102-9108.

Budhavant, K.; Andersson, A.; Bosch, C.; Krusa, M.; Kirillova, E. N.; Sheesley, R. J.; Safai, P. D.; Rao, P. S. P.; Gustafsson, O., Radiocarbon-based source apportionment of elemental carbon aerosols at two South Asian receptor observatories over a full annual cycle. *Environ. Res. Lett.* **2015,** *10*, (6).

Andersson, A.; Deng, J.; Du, K.; Zheng, M.; Yan, C.; Skold, M.; Gustafsson, O., Regionally-Varying Combustion Sources of the January 2013 Severe Haze Events over Eastern China. **2015,** *49*, (4), 2038-2043.

Gustafsson, O.; Krusa, M.; Zencak, Z.; Sheesley, R. J.; Granat, L.; Engstrom, E.; Praveen, P. S.; Rao, P. S. P.; Leck, C.; Rodhe, H., Brown Clouds over South Asia: Biomass or Fossil Fuel Combustion? *Science* **2009,** *323*, (5913), 495-498.

Sheesley, R. J.; Kirillova, E.; Andersson, A.; Krusa, M.; Praveen, P. S.; Budhavant, K.; Safai, P. D.; Rao, P. S. P.; Gustafsson, O., Year-round radiocarbon-based source apportionment of carbonaceous aerosols at two background sites in South Asia. *J. Geophys. Res.-Atmos.* **2012,** *117*.

Lewis, C. W.; Klouda, G. A.; Ellenson, W. D., Radiocarbon measurement of the biogenic contribution to summertime PM-2.5 ambient aerosol in Nashville, TN. *Atmos. Environ.* **2004,** *38*, (35), 6053-6061.

Zangrando, R.; Barbaro, E.; Zennaro, P.; Rossi, S.; Kehrwald, N. M.; Gabrieli, J.; Barbante, C.; Gambaro, A., Molecular Markers of Biomass Burning in Arctic Aerosols. *Environ. Sci. Technol.* **2013,** *47*, (15), 8565-8574.

Shaw, P. M.; Russell, L. M.; Jefferson, A.; Quinn, P. K., Arctic organic aerosol measurements show particles from mixed combustion in spring haze and from frost flowers in winter. *Geophys. Res. Lett.* **2010,** *37*, (10), L10803.

Zaveri, R. A.; Shaw, W. J.; Cziczo, D. J.; Schmid, B.; Ferrare, R. A.; Alexander, M. L.; Alexandrov, M.; Alvarez, R. J.; Arnott, W. P.; Atkinson, D. B.; Baidar, S.; Banta, R. M.; Barnard, J. C.; Beranek, J.; Berg, L. K.; Brechtel, F.; Brewer, W. A.; Cahill, J. F.; Cairns, B.; Cappa, C. D.; Chand, D.; China, S.; Comstock, J. M.; Dubey, M. K.; Easter, R. C.; Erickson, M. H.; Fast, J. D.; Floerchinger, C.; Flowers, B. A.; Fortner, E.; Gaffney, J. S.; Gilles, M. K.; Gorkowski, K.; Gustafson, W. I.; Gyawali, M.; Hair, J.; Hardesty, R. M.; Harworth, J. W.; Herndon, S.; Hiranuma, N.; Hostetler, C.; Hubbe, J. M.; Jayne, J. T.; Jeong, H.; Jobson, B. T.; Kassianov, E. I.; Kleinman, L. I.; Kluzek, C.; Knighton, B.; Kolesar, K. R.; Kuang, C.; Kubatova, A.; Langford, A. O.; Laskin, A.; Laulainen, N.; Marchbanks, R. D.; Mazzoleni, C.; Mei, F.; Moffet, R. C.; Nelson, D.; Obland, M. D.; Oetjen, H.; Onasch, T. B.; Ortega, I.; Ottaviani, M.; Pekour, M.; Prather, K. A.; Radney, J. G.; Rogers, R. R.; Sandberg, S. P.; Sedlacek, A.; Senff, C. J.; Senum, G.; Setyan, A.; Shilling, J. E.; Shrivastava, M.; Song, C.; Springston, S. R.; Subramanian, R.; Suski, K.; Tomlinson, J.; Volkamer, R.; Wallace, H. W.; Wang, J.; Weickmann, A. M.; Worsnop, D. R.; Yu, X. Y.; Zelenyuk, A.; Zhang, Q., Overview of the 2010 Carbonaceous Aerosols and Radiative Effects Study (CARES). *Atmos. Chem. Phys.* **2012,** *12*, (16), 7647-7687.

Birch, M. E.; Cary, R. A., Elemental carbon-based method for monitoring occupational exposures to particulate diesel exhaust. *Aerosol Sci. Technol.* **1996,** *25*, (3), 221-241.

Andersson, A.; Sheesley, R. J.; Krusa, M.; Johansson, C.; Gustafsson, O., C-14-Based source assessment of soot aerosols in Stockholm and the Swedish EMEP-Aspvreten regional background site. *Atmos. Environ.* **2011,** *45*, (1), 215-222.

Hung, H.; Blanchard, P.; Halsall, C. J.; Bidleman, T. F.; Stern, G. A.; Fellin, P.; Muir, D. C. G.; Barrie, L. A.; Jantunen, L. M.; Helm, P. A.; Ma, J.; Konoplev, A., Temporal and spatial variabilities of atmospheric polychlorinated biphenyls (PCBs), organochlorine (OC) pesticides and polycyclic aromatic hydrocarbons (PAHs) in the Canadian Arctic: Results from a decade of monitoring. *Sci. Total Environ.* **2005,** *342*, (1-3), 119-144.

Nallathamby, P. D.; Lewandowski, M.; Jaoui, M.; Offenberg, J. H.; Kleindienst, T. E.; Rubitschun, C.; Surratt, J. D.; Usenko, S.; Sheesley, R. J., Qualitative and quantitative assessment of unresolved complex mixture in PM2.5 of Bakersfield, CA. *Atmos. Environ.* **2014,** *98*, 368-375.

Usenko, S.; Hageman, K. J.; Schmedding, D. W.; Wilson, G. R.; Simonich, S. L., Trace analysis of semivolatile organic compounds in large volume samples of snow, lake water, and groundwater. *Environ. Sci. Technol.* **2005,** *39*, (16), 6006-6015.

Zotter, P.; El-Haddad, I.; Zhang, Y.; Hayes, P. L.; Zhang, X.; Lin, Y.-H.; Wacker, L.; Schnelle-Kreis, J.; Abbaszade, G.; Zimmermann, R.; Surratt, J. D.; Weber, R.; Jimenez, J. L.; Szidat, S.; Baltensperger, U.; Prevot, A. S. H., Diurnal cycle of fossil and nonfossil carbon using radiocarbon analyses during CalNex. *J. Geophys. Res.-Atmos.* **2014,** *119*, (11), 6818-6835.

Sheesley, R. J.; Schauer, J. J.; Garshick, E.; Laden, F.; Smith, T. J.; Blicharz, A. P.; Deminter, J. T., Tracking personal exposure to particulate diesel exhaust in a diesel freight terminal using organic tracer analysis. *J. Expo. Sci. Environ. Epidemiol.* **2009,** *19*, (2), 172-186.

Iinuma, Y.; Bruggemann, E.; Gnauk, T.; Muller, K.; Andreae, M. O.; Helas, G.; Parmar, R.; Herrmann, H., Source characterization of biomass burning particles: The combustion of selected European conifers, African hardwood, savanna grass, and German and Indonesian peat. *J. Geophys. Res.-Atmos.* **2007,** *112*, (D8).

Watson, J. G.; Zhu, T.; Chow, J. C.; Engelbrecht, J.; Fujita, E. M.; Wilson, W. E., Receptor modeling application framework for particle source apportionment. *Chemosphere* **2002,** *49*, (9), 1093-1136.

Draxler, R. R.; Rolph, G. D. HYSPLIT (HYbrid Single-Particle Lagrangian Integrated Trajectory) model access via NOAA ARL READY Website (http://ready.arl.noaa.gov/HYSPLIT.php).

Sheesley, R. J.; Schauer, J. J.; Zheng, M.; Wang, B., Sensitivity of molecular marker-based CMB models to biomass burning source profiles. *Atmos. Environ.* **2007,** *41*, (39), 9050-9063.

Schmidl, C.; Marr, L. L.; Caseiro, A.; Kotianova, P.; Berner, A.; Bauer, H.; Kasper-Giebl, A.; Puxbaum, H., Chemical characterisation of fine particle emissions from wood stove combustion of common woods growing in mid-European Alpine regions. *Atmos. Environ.* **2008,** *42*, (1), 126-141.

Fine, P. M.; Cass, G. R.; Simoneit, B. R. T., Chemical characterization of fine particle emissions from the fireplace combustion of wood types grown in the Midwestern and Western United States. *Environ. Eng. Sci.* **2004,** *21*, (3), 387-409.

Fine, P. M.; Cass, G. R.; Simoneit, B. R. T., Chemical characterization of fine particle emissions from the fireplace combustion of woods grown in the southern United States. *Environ. Sci. Technol.* **2002,** *36*, (7), 1442-1451.

Sharma, S.; Andrews, E.; Barrie, L. A.; Ogren, J. A.; Lavoue, D., Variations and sources of the equivalent black carbon in the high Arctic revealed by long-term observations at Alert and Barrow: 1989-2003. *J. Geophys. Res.-Atmos.* **2006,** *111*, (D14).

Fu, P.; Kawamura, K.; Chen, J.; Barrie, L. A., Isoprene, Monoterpene, and Sesquiterpene Oxidation Products in the High Arctic Aerosols during Late Winter to Early Summer. *Environ. Sci. Technol.* **2009,** *43*, (11), 4022-4028.

CHAPTER FIVE

Year-round Characterization of Sources and Optical Properties of Arctic Organic Aerosols in the North Slope of Alaska

Abstract

Long term data on organic aerosol concentration and optical properties is needed in the Arctic to improve characterization of radiative forcing by atmospheric aerosols. This study presents the annual trends of organic carbon (OC), water-soluble organic carbon (WSOC) and their optical properties from a year-long sampling campaign in Barrow, AK. Results show that ambient OC concentrations are highly variable with peaks in the summer (0.14 μg m^{-3}) and the winter (0.15 μg m^{-3}). Annual trends in WSOC concentrations follows the same trends (0.8 μg m^{-3} and 0.9 μg m^{-3} for the summer and winter, respectively). In order to understand the radiative impacts of light absorbing OC, or brown carbon (BrC), the light absorption properties of WSOC were determined. Seasonal averaging revealed that the highest average mass absorption efficiency value of 1.54 ± 0.75 m^2 g^{-1} was in the fall, with an annual range of 0.70 ± 0.44 to 1.54 ± 0.75 m^2 g^{-1}. To quantify the contributions of fossil and contemporary carbon sources to OC and total organic carbon (TOC), radiocarbon abundance measurements were performed. For both OC and TOC, fossil contributions were the greatest in the fall at 61.4 ± 9.8% and 67.4 ± 3.8%, respectively, with contemporary contributions to dominating OC in the spring and summer (68.9 ± 9.8% and 64.8 ± 9.8%, respectively). Back trajectories identified five major source regions to Barrow throughout the year, with a marine influence from the Arctic Ocean in all seasons. For 2012-2013, OC concentrations do not

follow the typical trends of black carbon in the Arctic, indicating impact from different, likely non-combustion sources.

Introduction

While the annual concentration and radiative impacts of some aerosols, such as sulfate and black carbon (BC) have been studied extensively in the Arctic, organic carbon (OC) is not as well monitored or modeled. There are several established monitoring sites across the Arctic which have produced long term BC trends: Svalbard, Norway; Alert, Canada; Barrow, Alaska, USA; and Summit, Greenland (Sharma, et al. 2006; Sharma, et al. 2004; Sharma, et al. 2013); however there is limited information on seasonal OC characterization at those same sites. In the Arctic, OC will be co-emitted from the same combustion sources as BC, but will also be emitted from marine and terrestrial biogenic sources and be produced from secondary reactions of anthropogenic and biogenic volatile organic carbon precursors. A previous study which focused on the wintertime OC and BC apportionment at Barrow, AK during the 2012-2013 campaign, found that the OC was significantly less fossil than BC (Barrett, et al. 2015). The current study will focus on OC concentration, sources and optical properties from an annual campaign at Barrow, AK for 2012-2013, which enables comparison with the long term BC trends available for that site.

Arctic OC could impact the radiative balance via direct and indirect effects, but there is still uncertainty associated with quantifying these effects. Light absorbing organic carbon, or brown carbon (BrC) has been shown to be responsible for up to 28% of total light absorption in California, and for up to 50% of the total light absorption for biomass burning aerosols (Bahadur, et al. 2012; Kirchstetter, Novakov, and Hobbs 2004; Chen

and Bond 2010). Recent modeling suggests that BrC contributes up to +0.25 W m^{-2} globally to the earth's radiative budget (19% of the total absorption due to anthropogenic aerosols) and that the global atmospheric burden of BrC is more than three times the burden of BC (Feng, Ramanathan, and Kotamarthi 2013). Emissions of BrC have been attributed to both primary sources (biomass burning, residential heating by wood and coal, and biogenic emission) and secondary sources (high-molecular weight light-absorbing compounds produced in atmospheric reactions) (Laskin, Laskin, and Nizkorodov 2015). While BC strongly absorbs light in the visible spectrum, BrC strongly absorbs light in the ultra-violet range (Srinivas and Sarin 2014). Light absorption in the ultraviolet range is also of significance because it may affect photolysis rates of gaseous compounds in the atmosphere by decreasing the amount of total incoming solar radiation, leading to reduced tropospheric concentrations of atmospheric oxidants such as ozone (Chen and Bond 2010; Laskin, Laskin, and Nizkorodov 2015). In terms of the indirect effect, the water soluble fraction of organic carbon (WSOC) may be important due to its ability to increase the hygroscopicity of particles and enable them to act as cloud condensation nuclei (CCN); WSOC can account for 20-70% of total organic aerosol (Kirillova, et al. 2014). While multiple techniques have been used to determine the presence and absorption properties of atmospheric BrC, the measurement of light absorption of liquid extracts of aerosol samples is a common method to determine the absorption properties of atmospheric BrC (Chen and Bond 2010; Kirillova, et al. 2014; Cheng, et al. 2011), and is utilized in this study.

As mentioned previously, long-term trends in OC, WSOC and BrC have not been as well characterized across the Arctic. Prior to this study, the only long-term collection

of organic carbon samples was in northern Finland from September 1997 to June 1999 (Ricard, et al. 2002). Studies of seasonal trends in ambient concentration, absorption properties and sources are needed to understand potential climate impacts of these aerosols (Kawamura, Kasukabe, and Barrie 2010; Anderson, et al. 2008; Hu, et al. 2013).

The goal of this manuscript is to report the results of an annual study of non-BC carbonaceous aerosols (OC, WSOC and BrC) including seasonal trends in optical properties, ambient concentrations, and sources for Barrow, Alaska. This is accomplished using multiple offline analytical chemistry techniques, including OC by thermal-optical transmission, WSOC measurements, absorption measurements of water extractable OC, and radiocarbon abundance measurements.

Materials and Methods

Sample Collection and Bulk Carbon Analysis

All samples were collected at the Department of Energy Atmospheric Radiation Measurement (ARM) Climate research facility (71°19'23.73" N, 156°36'56.70 W) on the North Slope of Alaska (NSA). The NSA-ARM facility, in operation since 1997, is located 7.4 km northeast of the village of Barrow, AK, 515 km north of the Arctic Circle.

PM_{10} samples were collected on quartz fiber filters (QFF, Tissuquartz^{TM} Filters 2500 QAT-UP, 20 x 25 cm) using a Tisch high-volume PM_{10} sampler (Tisch Environmental, Cleves, OH, USA). Prior to sampling, QFFs were baked at 500 °C for 12 hours and stored in baked aluminum foil packets and storage bags. Sampling duration was approximately one week. All blanks were treated in the same manner as samples. Samplers were located on a sampling platform approximately 10 m above ground level.

OC and elemental carbon (EC) concentrations were determined using a thermal-optical transmission (TOT) carbon analyzer (Sunset Laboratories, Tigard, OR) utilizing the NIOSH 5040 protocol (Birch and Cary 1996). Instrument blanks and sucrose standards were run with every batch of ten samples and all samples were blank subtracted using an average blank value of 0.18 μg OC cm^{-2}. Total organic carbon (TOC) is the sum of the OC and EC fractions for each sample. Following the nomenclature suggested by Petzold, et al. (2013), BC will be used to refer to non-OC light absorbing carbon with no reference to a specific measurement method, while EC will be used to refer to the concentration of non-OC light absorbing carbon evolved from the thermal optical method mentioned above.

Water-Soluble Organic Carbon & Absorption Measurements

Water soluble organic carbon (WSOC) analysis was performed using a previously described method (Barrett and Sheesley 2014). Briefly, filter areas corresponding to ~75 μg of OC, based on filter loading, were placed in 50 mL centrifuge tubes (Bio-Link Scientific, Wimberly, TX) and sonicated in 30 mL of deionized (DI) water for 15 minutes. All tubes were pre-cleaned by triple rinsing with DI water prior to extractions. The extracts were then centrifuged for 10 minutes and decanted. The sample is then split with 20 mL of the extracts filtered into glass vials using pre-cleaned disposable Millex® -GV syringe-driven filters (33 mm, pore size 0.22 μm, Merck Millipore, Ltd., Ireland). 40 μL of 6N HCl^- was added to remove any CO_2 trapped in solution. WSOC concentrations were measured as dissolved organic carbon in the solution using a Shimadzu total organic carbon (Zaveri, et al. 2012) analyzer (TOC-5000A, Shimadzu, Kyoto, Japan). Samples were run with calibration standards (Potassium Hydrogen Phthalate, KHP, $C_8H_5KO_4$,

Ultra Scientific, North Kingstown, RI) at 0, 0.5, 1, 2, 3, 4, and 5 mg L^{-1}, measured prior to analysis and periodically throughout each group. Each sample was analyzed three times (100 μL injection volume) and the reported value is the average of the three injections. All samples were blank subtracted using an average laboratory and field blank value of 0.26 mg L^{-1} prior to conversion to atmospheric concentrations. The remaining 10 mL of extract was filtered into a separate glass vial and reserved for absorption analysis.

Light absorption of the filtered aqueous extracts was measured from 200 to 700 nm on an Agilent 8453 ultraviolet-visible (UV-Vis) spectrometer (Santa Clara, CA), with tungsten and deuterium light sources. Acidification was not applied to sample extracts used in light absorption measurements. Absorption spectrums were determined relative to a reference cuvette containing the same solvent (Chen and Bond 2010). The mass absorption efficiency (MAE) of water extracts was calculated for each WSOC sample using equation 1:

$$MAE_{\lambda} = \frac{Abs_{\lambda}}{[WSOC]} = \frac{\left(ATN_{\lambda} - ATN_{700}\right) \times \frac{V_w}{V_a \times l} \times \ln(10)}{[WSOC]}$$

where Abs_{λ} represents the light absorption coefficient (Mm^{-1}); [WSOC] represents the ambient WSOC concentration of the sample (μg m^{-3}); ATN_{λ} is the light attenuation at the given wavelength measured by the spectrophotometer; V_w is the volume of the water extract (mL); V_a is the air volume (m^3), and l is the optical path length (0.01 m) (Yan, et al. 2015). MAE was calculated at 365 nm in order to avoid possible interference from inorganic compounds as done with previous WSOC absorption studies. The wavelength (λ) dependence of WSOC absorption, the absorption Ångström exponent (AAE), was investigated by the following relationship:

$$\frac{A(\lambda_1)}{A(\lambda_2)} = \left(\frac{\lambda_2}{\lambda_1}\right)^{AAE}$$

AAE was determined with a linear regression of ln (Abs_λ) against ln (λ) through the range of 330-400 nm, where the slope = AAE ($r^2 = 0.99$) (Kirillova, et al. 2014; Chen and Bond 2010; Yan, et al. 2015).

Carbon Isotope Analysis and Radiocarbon Source Apportionment

In addition to characterizing the optical properties of OC, it is also of importance to determine the source contributions of OC to the Arctic. For this determination, radiocarbon (^{14}C) abundance was used as a source apportionment tool. Typically, source apportionment of OC in the Arctic has relied on a combination of elemental and organic tracers; however, due to uncertainty of the atmospheric lifetime of certain organic tracers at remote sites, the accuracy of this method is uncertain (Yttri, et al. 2014; Barrett, et al. 2015; Sheesley, Andersson, and Gustafsson 2011). Due to the large difference in ^{14}C end members for biomass burning and fossil fuel combustion sources, accurate apportionment between the contributions of fossil and contemporary carbon to OC is possible (Gustafsson, et al. 2009; Lewis, Klouda, and Ellenson 2004; R. J. Sheesley, et al. 2012; Budhavant, et al. 2015). Here, contemporary carbon is defined as all OC derived from biogenic emissions and biomass combustion, including OC derived secondary aerosol.

Ambient PM_{10} samples were composited to give ~60 μg of total organic carbon (TOC) (Zaveri, et al.) for accelerator mass spectrometry measurement of the ^{14}C signal. Samples were composited by 10-day back trajectory analysis (Table C.1) with samples having similar air mass source region, and of the same season, composited together. For radiocarbon composites, each included sample was represented by equal mass of TOC.

Therefore, the radiocarbon source apportionment is a true average of the included samples and not one individual sample is biasing the apportionment. TOC filter samples were acidified in a desiccator over hydrochloric acid for 12 hours to remove and carbonate and dried in a drying oven at 60 °C for one hour. Samples were then placed in prebaked glass petri dishes. ^{14}C abundance measurements were performed at the National Oceanic Sciences Accelerator Mass Spectrometry facility at Woods Hole Oceanographic Institute (Woods Hole, MA).

In order to accurately apportion TOC based on ^{14}C abundance, $\Delta^{14}C$ end members must be defined and used in the following equation:

$$\Delta^{14}C_{TOC} = \left(\Delta^{14}C_{contemporary}\right)\left(F_{contemporary}\right) + \left(\Delta^{14}C_{fossil}\right)\left(1 - F_{contemporary}\right)$$

The $\Delta^{14}C$ end member for contemporary carbon (OC derived from biogenic emissions and biomass combustion) used was +107.5‰, based on wood burning from a 2010 reference from temperate regions (Zotter, et al. 2014; Barrett, et al. 2015). The $\Delta^{14}C$ end member for fossil fuels was -1000‰ (Gustafsson, et al. 2009). The contribution from fossil carbon is equal to 1-$F_{contemporary}$ and $\Delta^{14}C$ of OC was calculated from $\Delta^{14}C_{TOC}$ and $\Delta^{14}C_{EC}$ using TOC=OC + EC (Barrett, et al. 2015). TOC uncertainty calculations include instrumental standard error, blank correction uncertainty and end member uncertainty. OC uncertainty calculations are based on a sensitivity analysis performed in order to account for the inadvertent inclusion of pyrolysis carbon with the EC fraction when isolating the EC fraction from OC. For the current study, sensitivity analysis indicates an average uncertainty of 9.8%.

Normalization for Seasonal Analysis

Sample times ranged from seven to ten days throughout the year-round sampling campaign. In order to calculate seasonal averages despite the difference in sample duration, a normalization was applied based on sample duration (R. J. Sheesley, et al. 2012). The following equation was used to calculate averages based on sample volume, which is a means of tracking sample duration:

$$C_j = \left(\Sigma_i C_i v_i\right) / \left(\Sigma v_i\right)$$

where C_i is the OC concentration for sample i, and v_i is the sampled air volume for sample i, and C_j equals the normalized average concentration. The normalized concentrations are reported throughout the manuscript, and also used as input for source apportionment based on ^{14}C analysis. Seasonal and annual radiocarbon averages were normalized based on composite sample duration and concentration using the following equation:

$$F_j = \left(\Sigma_i C_i F_i t_i\right) / \left(\Sigma_i C_j t_i\right)$$

where F_i is the F_m for composite i, C_i is the normalized OC concentration for composite i, t_i is the sampling duration, and C_j is the normalized average concentration (R. J. Sheesley, et al. 2012). Seasonal averages were calculated based on the following seasonal definitions: summer (> 15 hrs. daylight), winter (<12 hrs. daylight) and the transitional seasons of spring and fall with 12-15 hrs. of daylight.

Back Trajectory Analysis

Back trajectory analysis was completed using the National Oceanic and Atmospheric Administration Hybrid Single Particle Lagrangian Integrated Trajectory

Model (HYSPLIT) model, version 4 (R.R Draxler and G.D. Rolph 2010) in order to broadly identify potential source regions of OC to the North American Arctic. Briefly, 10 day back trajectories starting every six hours were run for each sampling day during the study period. Further description of the model parameters is available in Barrett, et al. (2015). The resulting back trajectories were clustered for the time representing each filter sample using the clustering function available in the model. The results of this cluster analysis were used to group the filter samples for radiocarbon analysis into composites based on geographic source region by season. The cluster means were then mapped using ESRI ArcGIS 10 software. Due to the limited number of meteorological monitoring stations in the region, back trajectory models can be imprecise for this study area. A sensitivity analysis of back trajectories was conducted and results show the model to be robust (Barrett, et al. 2015). Here, back trajectories are used only to provide a broad description of source regions to the sampling site.

Results

Back Trajectory Analysis Results

Cluster means representing 10 day back trajectories for each filter sample revealed 5 major source regions to Barrow, AK throughout the study period: the Russian Arctic, Canadian Arctic, Alaskan Arctic, the Arctic Ocean and western Alaska (Figure 5.1a-d; back trajectories are colored by radiocarbon composite and depicted by season). There is a fraction of back trajectories originating over the Arctic Ocean in all sampled weeks, pointing to a potential marine/sea ice influence in OC in all seasons. Discussion will focus on the differences among seasonal back trajectory analysis.

Summer back trajectories mainly consisted of air masses originating along the Russian Arctic and western Alaska, with minor impact from the Canadian Arctic. Influence from interior and western Alaska increased into August 2012, while air masses from the Russian Arctic decreased. For the late summer, August 12 through August 31, back trajectories were dominated by interior Alaskan influence.

For the fall, back trajectories shifted from western Alaska/Canadian Arctic to mainly the Russian Arctic as the major source region: 41% of back trajectories for the first week of fall, September 21-28, passed over western Alaska; however, the influence of western Alaska decreases throughout the remainder of the season, with northern Alaska and the Russian Arctic as the major source regions to Barrow.

Winter back trajectories have been previously described by Barrett, et al. (2015). In the previous manuscript, back trajectories originating in both the Alaskan Arctic and the Canadian Arctic were combined and referred to as the North American Arctic; however, in this manuscript, we make the distinction between the two regions. Briefly, the winter is characterized by two major source regimes: the midwinter period with heavy influence from the Arctic Ocean and the Russian Arctic, and a shift in the late winter to air masses spending time over the Canadian Arctic. This back trajectory analysis represents the current annual campaign, but may not represent the long term annual trends in source regions for the NSA.

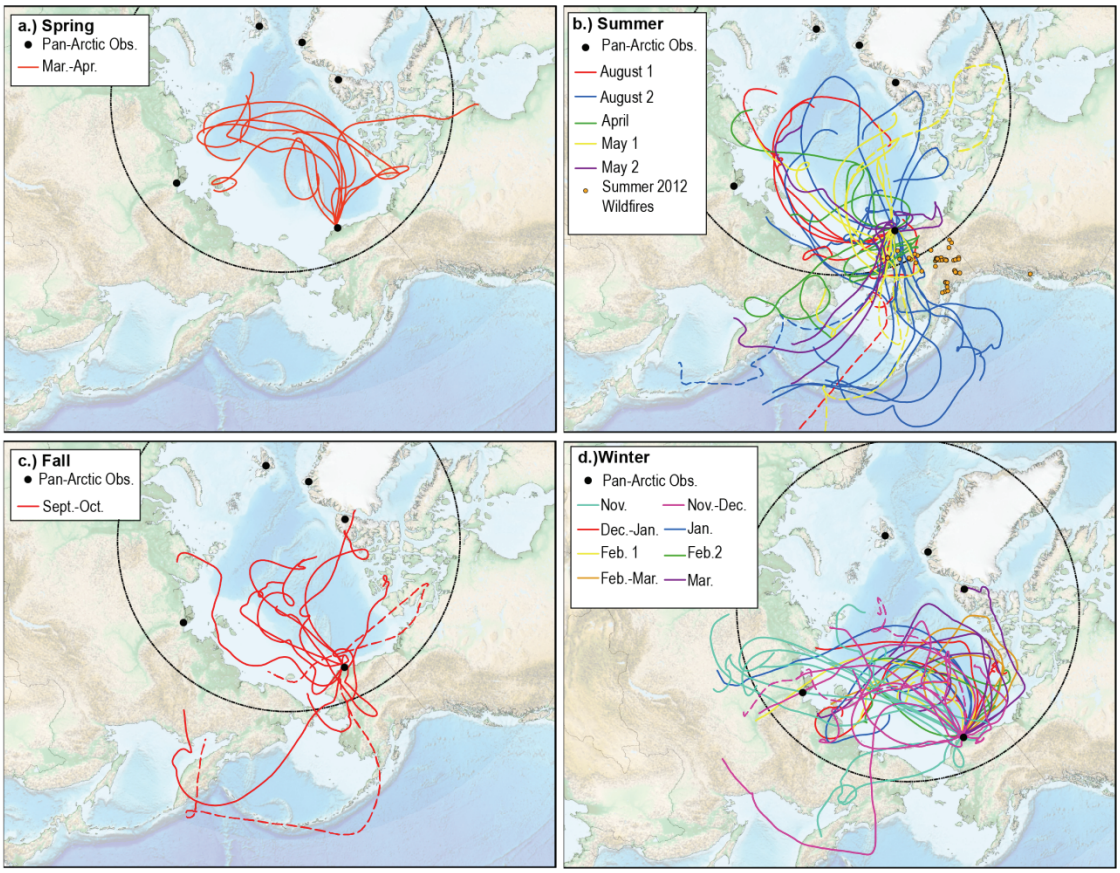

Figure 5.1: 10-day back trajectory cluster means for a) Spring b) Summer c) Fall and d) Winter for Barrow, AK. Back trajectories are colored according to composite for radiocarbon analysis with each line representing a cluster mean for each sample included in the composite. Wildfires for summer 2012 are shown in Figure b. Dashed lines indicate that <10% of the clusters are represented by that cluster mean. Date ranges for each composite are as follows: Mar.-Apr.: 3/20-4/12/2012; August 1: 7/16-7/23/2012 and 8/3-8/12/2012; August 2- 7/23-8/3/2012 and 8/12-8/31/2012; Sep.-Oct.: 9/7-10/26/2012; Nov.: 11/3-11/26/2012; Nov.-Dec.: 11/26-12/21/2012; Dec.-Jan.: 12/28/2012-1/5/2013; Jan.: 1/18-1/25/2013; Feb.1: 2/1-2/8/2013; Feb. 2: 2/8-2/15/2013; Feb.-Mar.: 2/25-3/1/2013; Mar.: 3/1-3/11/2013; April: 4/12-4/26/2013; May 1: 5/10-5/24/2013; May 2: 5/27-6/4/2013.

During the sampling campaign, the meteorology of Barrow was influenced by both positive and negative phases of the Arctic Oscillation (AO) (NOAA 2015). The positive phase of the AO is expected to increase wind transport from North America and Europe into the Arctic (L'Heureux, et al. 2010; Eckhardt, et al. 2003; Wu, et al. 2006). The positive phase of the AO occurred from May through September 2012, with the

exception of a negative phase during June 2012. A transition to the negative phase occurred in October 2012 persisting through March 2013. The strongest negative phase occurred in March 2013, prior to a return to the positive phase in April and May 2013. A negative phase of the AO during the winter would help isolate the region from emissions in the lower latitudes during this season, limiting the region to in-Arctic emissions.

Annual and Seasonal OC trends

It is well known that aerosol pollution in the Arctic, specifically BC, peaks in the late winter and early spring periods when the polar dome traps pollutants over the Arctic, in a phenomenon known as Arctic Haze (Q. Wang, et al. 2011; McNaughton, et al. 2011; Law and Stohl 2007; von Schneidemesser, et al. 2009). EC concentrations at Barrow, AK (an operational definition of BC as measured by thermal optical techniques) during the sampling campaign follow established BC trends for the Arctic with elevated concentrations in the winter and spring and very low concentrations during the summer (Figure 5.2). Further discussion of the optical and source characteristics of EC will be presented in a future manuscript. Our annual campaign results indicate that OC doesn't always follow the same trend as BC, with peaks in late summer and early fall in addition to the late winter. Ambient OC concentrations for the year range from 0.008 ± 0.002 μg m^{-3} to 0.95 ± 0.06 μg m^{-3} (Figure 5.2) with peaks in late summer, early fall and late winter. A prior study from 1997-1999 in northern Finland found that organic carbon concentrations peaked between July and September, with concentrations decreasing to a background level two to three times lower than the summer maximum (Ricard, et al. 2002). OC concentrations during our campaign did have maximum concentrations occurring between July and September, but had a second maximum in early February

(Figure 5.2). WSOC and water-insoluble carbon (WIOC) also had a wide range with WSOC values ranging from 0.005 ± 0.004 μg m^{-3} to 0.49 ± 0.05 μg m^{-3} (Figure 5.2). WSOC had similar trends to OC, with maximum concentrations occurring July through September, and a second high period in winter. However, average summer WSOC is lower than previously reported WSOC values Alert, Canada (0.19 μg m^{-3}, February to June, 1991) (Kawamura et al. 2010) and aerosol phase WSOC for the summer 2006 at Summit, Greenland (0.19 ± 0.17 μg m^{-3}) (Anderson et al. 2008), as well as lower than the average WSOC summer concentration reported for 2009 in the Beaufort Sea (0.373 μg m^{-3}) (Hu et al. 2013). On average, WSOC accounted for 56 ± 11% of the total OC burden throughout the sampling campaign, which is consistent with previous WSOC values. Average % WSOC values for our campaign are equivalent to average % WSOC in Alert, Canada from February to June, 1991 (56%) and similar to urban and rural values from the southeastern United States (51.9% and 55.8% annually) (Zhang, et al. 2012a); however, % WSOC values in our study were much greater than values for the Maldives, a long range transport site in the Indian Ocean, from 2008-2009 (15-29%) (Kirillova, et al. 2013). The spring transitional period accounted for the highest average WSOC/OC, 70.0% WSOC, pointing to the presence of aged aerosols at the site. The increased WSOC/OC ratio in the spring corresponds with a switch to the positive phase of the Arctic Oscillation which may transport more aged aerosols to Barrow via long-range transport.

Prior to this campaign, there were no year-round studies of Arctic OC and WSOC in the North American Arctic; it was not known whether OC would be dominated by transported combustion aerosol, like BC, or have large contributions from biogenic and

secondary organic aerosol sources. Regression analysis of EC vs. OC, EC vs. WSOC and EC vs. WIOC show no correlation (Figure C.2, C.3, and C.4), indicating different sources of EC compared to OC, WSOC, and WIOC. The lack of correlation between EC and OC indicates that OC is likely impacted by atmospheric processing and non-combustion sources including secondary organic aerosol and biogenic emissions; this is further supported by a strong correlation between OC and WSOC ($r^2 = 0.82$, Figure C.6). These results indicate greater complexity with regards to OC sources in the Arctic and the need for continued long term sample collection and modeling in the region.

Seasonal PM_{10} average OC burdens ranged from 0.04 ± 0.27 μg m^{-3} in the fall to 0.15 ± 0.19 μg m^{-3} in the winter (Table 5.1). Maximum weekly OC concentrations occurred in the summer (0.95 ± 0.06 μg m^{-3}) possibly due to increased contribution from lower latitudes and interior Alaskan sources, including wildfires (Figure 5.1) combined with potential contribution from marine biogenic sources. BTs for that period show consistent contribution from the Western interior of Alaska with periodic influence from the Arctic Ocean. In addition, the stable carbon signature for the summer samples (Figure C.1) has an enriched signal which may indicate contribution from marine sources or may indicate atmospheric processing (Kirillova, et al. 2013). In particular, the biogenic and secondary organic aerosol would both be non-combustion sources that would not affect BC concentrations.

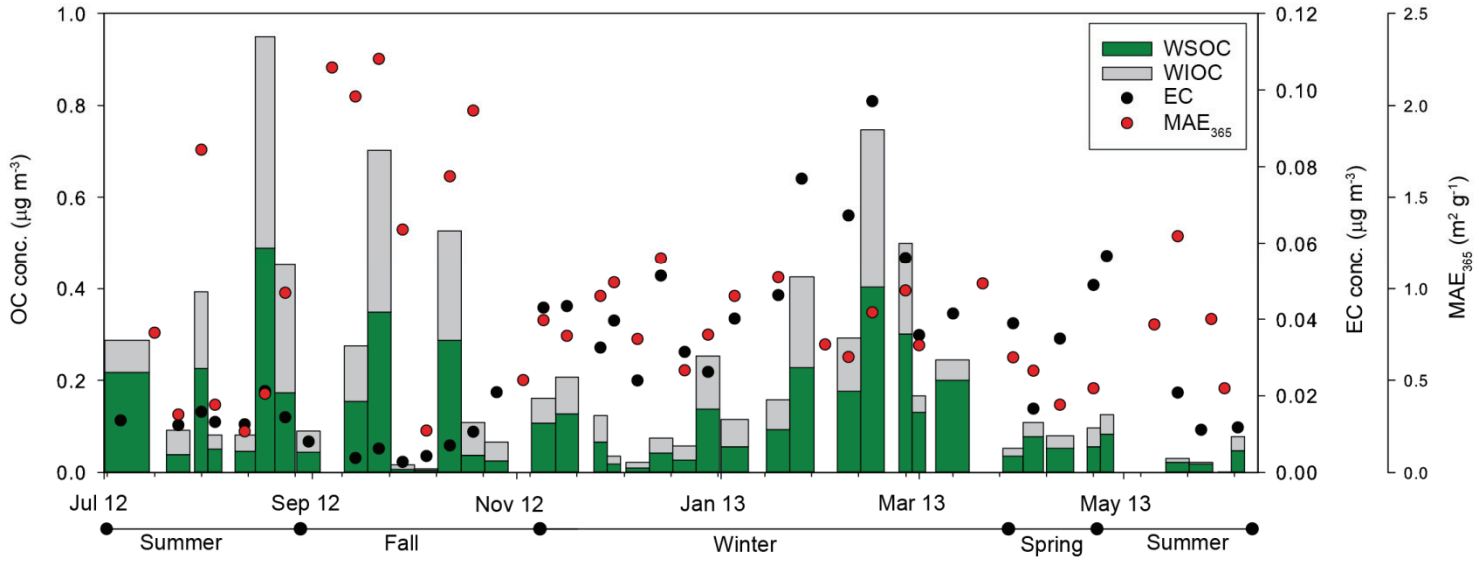

Figure 5.2: Year-round water-soluble organic carbon (WSOC), water-insoluble organic carbon (WIOC), and mass absorption efficiency at 365nm (MAE_{365}) values during the sampling campaign for Barrow, AK from 2012-201

Radiocarbon Source Apportionment

Fossil carbon contributions to TOC (OC plus EC) averaged 51.6 ± 15.3% for the year. Fossil carbon accounted for as much as 67.4 ± 3.8% of TOC in the fall and for as little as 37.6 ± 3.8% of TOC in the summer (Figure 5.3, Table 5.1). For the entire sampling campaign (June 2012- May 2013), the average fossil contribution to OC was 44.3 ± 9.8%; in other words, the OC is more contemporary than the EC, which potentially points to higher biogenic contribution. Fossil carbon contributions to OC averaged 44.4 ± 13.8% for the year. Fossil carbon accounted for as much as 61.4 ± 9.8% in the fall to as little as 31.1 ± 9.8% in the spring (Table 5.1). Fossil contribution to summer OC was similarly low as the spring (37.6± 9.8%) while winter experienced relatively equal contributions between contemporary and fossil carbon (49.7± 9.8% fossil).

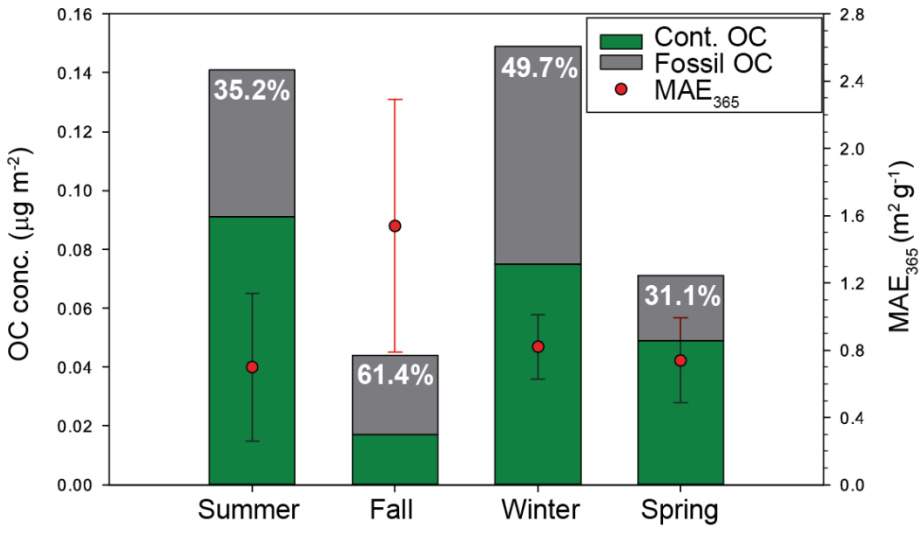

Figure 5.3: Seasonal PM_{10} organic carbon contemporary and fossil concentrations and mass absorption efficiency at 365 nm; % fossil contributions are shown in white.

Table 5.1: Seasonal concentrations of organic carbon (OC), water-soluble organic carbon (WSOC), % WSOC, mass absorption efficiency at 365nm (MAE_{365}), absorption Angstrom exponent (AAE), and % contemporary and fossil contributions to PM_{10} aerosols.

Season	PM_{10} OC Conc. ± s.d. ($\mu g\ m^{-3}$)	PM_{10} WSOC ± s.d. ($\mu g\ m^{-3}$)	% WSOC/OC	PM_{10} MAE_{365} ± s.d. ($m^2\ g^{-3}$)	PM_{10} AAE ± s.d.	OC % Cont. ± unc.	OC % Fossil ± unc.	TOC % Cont. ± unc.	TOC % Fossil ± unc.
Summer	0.14 ±0.26	0.08 ±0.13	58%	0.70 ±0.44	3.21 ±1.78	64.8 ± 9.8	35.2 ±9.8	62.4 ± 3.8	37.6 ±3.8
Fall	0.04 ±0.27	0.02 ±0.14	46%	1.54 ±0.75	3.39 ±1.42	38.6 ± 9.8	61.4 ±9.8	32.6 ± 3.8	67.4 ±3.8
Winter	0.15 ±0.19	0.09 ±0.11	59%	0.82 ±0.19	4.76 ±2.28	50.3 ± 9.8	49.7 ±9.8	50.6 ± 3.8	49.4 ±3.8
Spring	0.07 ±0.03	0.05 ±0.02	70%	0.74 ±0.25	2.91 ±1.02	68.9 ± 9.8	31.1 ±9.8	48.0 ± 3.8	52.0 ±3.8

Optical Properties

PM_{10} MAE_{365} seasonal values ranged from 0.70 m^2 g^{-1} to 1.54 m^2 g^{-1} in the summer and fall, respectively, and average AAE values ranging from 2.91 ± 1.02 to 4.76 ± 2.28 in the spring and winter respectively (Table 5.1, Figure 5.3). PM_{10} MAE_{365} values are in good agreement with previously reported Arctic MAE values of 0.83 ± 0.15 m^2 g^{-1} and 0.27 ± 0.08 m^2 g^{-1}, at 470 and 530 nm wavelengths, respectively (McNaughton, et al. 2011). Despite exhibiting the lowest OC and WSOC average concentrations, the average MAE_{365} during the fall is significantly greater than all other seasons (p-value < 0.001). Previous studies have indicated that WSOC emitted from biomass burning leads to higher MAE_{365} values (Cheng, et al. 2011), but recently, it has been shown that solid fossil fuels, including lignite and high volatility bituminous coals can exhibit similar absorption in the near-UV range as woodsmoke (Olson, et al. 2015). Fossil carbon contribution to OC was the highest in the fall (61.7 ± 9.8%) when the highest MAE_{365} values were observed, but the stable carbon signature is not enriched as would be expected with solid fuels (Figure C.1). The seasons with the largest percent contributions from contemporary carbon, spring and summer, exhibited the lowest average MAE_{365} values (Table 5.1). This is consistent with biogenic rather than biomass combustion sources dominating in spring and summer, which could possibly be masked in year with greater wildfire contributions. Fall was also the most variable season, with a 50% standard deviation, while MAE_{365} values in the winter and spring were more consistent. MAE_{365} measurements show that BrC is present in Barrow in all seasons and will contribute to the overall radiative balance of the region; any underestimation of this contribution will lead to inaccurate warming in climate models for the region. There is little data to compare these results with, therefore

further sampling is needed to determine if theses annual results are typical for this region or an anomaly.

Conclusions

This study provides the first year-round data set for organic carbon, WSOC, and MAE_{365} for the North American Arctic region. OC concentrations did not follow the well-established seasonal trends for Arctic BC. Highest seasonal concentrations for OC were seen in the summer and winter months, which is similar to a study from the late 1990s in Finland (Ricard, et al. 2002). WSOC also peaked in the summer and winter; however the spring had the highest percent WSOC (70%) potentially pointing to aged aerosols influencing Barrow during this time. The fall had the lowest average OC concentrations but the highest MAE_{365} values, coinciding with the highest contribution of fossil sources to OC at 61.4 ± 9.8%. Radiocarbon analysis results showed greater contributions of fossil carbon than contemporary carbon to TOC (both the OC and EC fractions) for the summer, and fall, while contributions of fossil and contemporary carbon were approximately even during the winter and spring. This is possibly due to the influence of secondary and biogenic sources of OC, which would not be seen in the EC fraction. Future studies are needed with higher time resolution and additional chemical characterization in order to further understand these contemporary biogenic and biomass combustion OC sources.

Acknowledgments and Data

Financial support for this campaign was provided by the United States Department of Energy (Atmospheric Radiation Measurement Field Campaign no. 2010-

05876) and the C. Gus Glasscock, Jr. Endowed Fund for Excellence in Environmental Sciences. We would like to thank George Cobb and Baylor University for use of the PM_{10} sampler. We would also like to thank Walter Brower and Jimmy Ivanoff of the Ukpeagvik Inupiat Corporation for sample collection and field assistance as well as Fred Helsel, Dan Lucero, and Jeffrey Zirzow and the Sandia National Laboratory for site access and preparation. We would also like to thank Jeffrey A. Back and the Baylor University Center for Reservoir and Aquatic Systems Research for assistance with WSOC analysis. Supporting data can be found in the supporting information.

References

Anderson, C., J.E. Dibb, R.J. Griffin, and M.H. Bergin (2008), Simultaneous measurements of particulate and gas-phase water-soluble organic carbon concentrations at remote and urban-influenced locations, *Geophys. Res. Lett.*, 35(13), doi:10.1029/2008gl033966.

Bahadur, R., P.S. Praveen, Y.Y. Xu, and V. Ramanathan (2012), Solar absorption by elemental and brown carbon determined from spectral observations109(43), 17366-17371, doi:10.1073/pnas.1205910109.

Barrett, T.E., E.M. Robinson, S. Usenko, and R.J. Sheesley (2015), Source Contributions to Wintertime Elemental and Organic Carbon in the Western Arctic Based on Radiocarbon and Tracer Apportionment, *Environ. Sci. Technol.*, 49(19), 11631-11639, doi:10.1021/acs.est.5b03081.

Barrett, T.E., and R.J. Sheesley (2014), Urban impacts on regional carbonaceous aerosols: Case study in central Texas *Journ. Of Air and Waste Man. Assoc.* 64(8), 917-926, doi:10.1080/10962247.2014.904252.

Birch, M.E., and R.A. Cary (1996), Elemental carbon-based method for monitoring occupational exposures to particulate diesel exhaust, *Aerosol Sci. Technol.*, 25(3), 221-241, doi:10.1080/02786829608965393.

Breider, T.J., L.J. Mickley, D.J. Jacob, Q. Wang, J.A. Fisher, R.Y.W. Chang, and B. Alexander (2014), Annual distributions and sources of Arctic aerosol components, aerosol optical depth, and aerosol absorption119(7), 4107-4124.

Budhavant, K., A. Andersson, C. Bosch, M. Krusa, E.N. Kirillova, R.J. Sheesley, P.D. Safai, P.S.P. Rao, and O. Gustafsson (2015), Radiocarbon-based source apportionment of elemental carbon aerosols at two South Asian receptor observatories over a full annual cycle, *Environ. Res. Lett.*, 10(6), doi:10.1088/1748-9326/10/6/064004.

Chen, Y., and T.C. Bond (2010), Light absorption by organic carbon from wood combustion. *Atmos. Chem. And Phys.*10(4), 1773-1787.

Cheng, Y., et al. (2011), Mass absorption efficiency of elemental carbon and water-soluble organic carbon in Beijing, China, *Atmos. Chem. Phys.*, 11(22), 11497-11510, doi:10.5194/acp-11-11497-2011.

Doherty, S.J., S.G. Warren, T.C. Grenfell, A.D. Clarke, and R.E. Brandt (2010), Light-absorbing impurities in Arctic snow10(23), 11647-11680, doi:10.5194/acp-10-11647-2010.

Draxler, R.R., and G.D. Rolph (2010), HYSPLIT (HYbrid Single-Particle Lagrangian Integrated Trajectory) model access via NOAA ARL READY Website (http://ready.arl.noaa.gov/HYSPLIT.php), edited, Silver Spring, MD, NOAA Air Resources Laboratory.

Eckhardt, S., A. Stohl, S. Beirle, N. Spichtinger, P. James, C. Forster, C. Junker, T. Wagner, U. Platt, and S.G. Jennings (2003), The North Atlantic Oscillation controls air pollution transport to the Arctic3(5), 1769-1778, doi:10.5194/acp-3-1769-2003.

Feng, Y., V. Ramanathan, and V.R. Kotamarthi (2013), Brown carbon: a significant atmospheric absorber of solar radiation?13(17), 8607-8621, doi:10.5194/acp-13-8607-2013.

Gustafsson, O., M. Krusa, Z. Zencak, R.J. Sheesley, L. Granat, E. Engstrom, P.S. Praveen, P.S.P. Rao, C. Leck, and H. Rodhe (2009), Brown Clouds over South Asia: Biomass or Fossil Fuel Combustion?, *Science*, 323(5913), 495-498, doi:10.1126/science.1164857.

Hu, Q.-H., Z.-Q. Xie, X.-M. Wang, H. Kang, and P. Zhang (2013), Levoglucosan indicates high levels of biomass burning aerosols over oceans from the Arctic to Antarctic3, 3119, doi:10.1038/srep03119

Kawamura, K., H. Kasukabe, and L.A. Barrie (2010), Secondary formation of water-soluble organic acids and α-dicarbonyls and their contributions to total carbon and water-soluble organic carbon: Photochemical aging of organic aerosols in the Arctic spring115(D21), D21306, doi:10.1029/2010jd014299.

Kirchstetter, T.W., T. Novakov, and P.V. Hobbs (2004), Evidence that the spectral dependence of light absorption by aerosols is affected by organic carbon109(D21), doi:10.1029/2004jd004999.

Kirillova, E.N., A. Andersson, J. Han, M. Lee, and Ö. Gustafsson (2014), Sources and light absorption of water-soluble organic carbon aerosols in the outflow from northern China14(3), 1413-1422, doi:10.5194/acp-14-1413-2014.

L'Heureux, M., A. Butler, B. Jha, A. Kumar, and W. Wang (2010), Unusual extremes in the negative phase of the Arctic Oscillation during 200937(10), n/a-n/a, doi:10.1029/2010gl043338.

Laskin, A., J. Laskin, and S.A. Nizkorodov (2015), Chemistry of Atmospheric Brown Carbon, doi:10.1021/cr5006167.

Law, K.S., and A. Stohl (2007), Arctic air pollution: Origins and impacts, *Science*, 315(5818), 1537-1540, doi:10.1126/science.1137695.

Lewis, C.W., G.A. Klouda, and W.D. Ellenson (2004), Radiocarbon measurement of the biogenic contribution to summertime PM-2.5 ambient aerosol in Nashville, TN, *Atmos. Environ.*, 38(35), 6053-6061, doi:10.1016/j.atmosenv.2004.06.011.

Li, C., P. Chen, S. Kang, F. Yan, Z. Hu, B. Qu, and M. Sillanpää (2016), Concentrations and light absorption characteristics of carbonaceous aerosol in PM2.5 and PM10 of Lhasa city, the Tibetan Plateau127, 340-346, doi:http://dx.doi.org/10.1016/j.atmosenv.2015.12.059.

Lu, Z., et al. (2015), Light Absorption Properties and Radiative Effects of Primary Organic Aerosol Emissions49(8), 4868-4877, doi:10.1021/acs.est.5b00211.

McNaughton, C.S., et al. (2011), Absorbing aerosol in the troposphere of the Western Arctic during the 2008 ARCTAS/ARCPAC airborne field campaigns11(15), 7561-7582, doi:10.5194/acp-11-7561-2011.

Ricard, V., J.L. Jaffrezo, V.M. Kerminen, R.E. Hillamo, M. Sillanpaa, S. Ruellan, C. Liousse, and H. Cachier (2002), Two years of continuous aerosol measurements in northern Finland107(D11), ACH 10-11-ACH 10-17, doi:10.1029/2001jd000952.

Sharma, S., E. Andrews, L.A. Barrie, J.A. Ogren, and D. Lavoue (2006), Variations and sources of the equivalent black carbon in the high Arctic revealed by long-term observations at Alert and Barrow: 1989-2003, *J. Geophys. Res.-Atmos.*, 111(D14), doi:10.1029/2005jd006581.

Sharma, S., M. Ishizawa, D. Chan, D. Lavoue, E. Andrews, K. Eleftheriadis, and S. Maksyutov (2013), 16-year simulation of Arctic black carbon: Transport, source contribution, and sensitivity analysis on deposition, *J. Geophys. Res.-Atmos.*, 118(2), 943-964, doi:10.1029/2012jd017774.

Sharma, S., D. Lavoué, H. Cachier, L.A. Barrie, and S.L. Gong (2004), Long-term trends of the black carbon concentrations in the Canadian Arctic109(D15), D15203, doi:10.1029/2003jd004331.

Sheesley, R.J., A. Andersson, and O. Gustafsson (2011), Source characterization of organic aerosols using Monte Carlo source apportionment of PAHs at two South Asian receptor sites, *Atmos. Environ.*, 45(23), 3874-3881, doi:10.1016/j.atmosenv.2011.01.031.

Sheesley, R.J., E. Kirillova, A. Andersson, M. Krusa, P.S. Praveen, K. Budhavant, P.D. Safai, P.S.P. Rao, and O. Gustafsson (2012), Year-round radiocarbon-based source apportionment of carbonaceous aerosols at two background sites in South Asia, *J. Geophys. Res.-Atmos.*, 117, doi:10.1029/2011jd017161.

von Schneidemesser, E., J.J. Schauer, G.S.W. Hagler, and M.H. Bergin (2009), Concentrations and sources of carbonaceous aerosol in the atmosphere of Summit, Greenland, *Atmos. Environ.*, 43(27), 4155-4162, doi:10.1016/j.atmosenv.2009.05.043.

Wang, Q., et al. (2011), Sources of carbonaceous aerosols and deposited black carbon in the Arctic in winter-spring: implications for radiative forcing, *Atmos. Chem. Phys.*, 11(23), 12453-12473, doi:10.5194/acp-11-12453-2011.

Wu, A., W. Hsieh, A. Shabbar, G. Boer, and F. Zwiers (2006), The nonlinear association between the Arctic Oscillation and North American winter climate, *Clim Dyn*, 26(7-8), 865-879, doi:10.1007/s00382-006-0118-8.

Yan, C., et al. (2015), Chemical characteristics and light-absorbing property of water-soluble organic carbon in Beijing: Biomass burning contributions121, 4-12, doi:http://dx.doi.org/10.1016/j.atmosenv.2015.05.005.

Yttri, K.E., C.L. Myhre, S. Eckhardt, M. Fiebig, C. Dye, D. Hirdman, J. Strom, Z. Klimont, and A. Stohl (2014), Quantifying black carbon from biomass burning by means of levoglucosan - a one-year time series at the Arctic observatory Zeppelin, *Atmos Chem Phys*, 14(12), 6427-6442, doi:10.5194/acp-14-6427-2014.

Zaveri, R.A., et al. (2012), Overview of the 2010 Carbonaceous Aerosols and Radiative Effects Study (CARES), *Atmos. Chem. Phys.*, 12(16), 7647-7687, doi:10.5194/acp-12-7647-2012.

Zhang, X., Z. Liu, A. Hecobian, M. Zheng, N.H. Frank, E.S. Edgerton, and R.J. Weber (2012), Spatial and seasonal variations of fine particle water-soluble organic carbon (WSOC) over the southeastern United States: implications for secondary organic aerosol formation12(14), 6593-6607, doi:10.5194/acp-12-6593-2012.

Zotter, P., et al. (2014), Diurnal cycle of fossil and nonfossil carbon using radiocarbon analyses during CalNex, *J. Geophys. Res.-Atmos.*, 119(11), 6818-6835, doi:10.1002/2013jd021114.

CHAPTER SIX

Annual Contributions of Fossil Fuel Combustion and Biomass Burning Sources to Atmospheric Elemental Carbon in the North American Arctic Using Radiocarbon Abundance Measurements

Introduction

It is well documented that the Arctic has undergone warming at an alarming rate over the past century, warming nearly 2 °C since 1970 (Odemark, et al. 2012; Sand, et al. 2013a; Pistone, Eisenman, and Ramanathan 2014). At the same time, anthropogenic activity is expected to increase in this region, leading to an increase in aerosols emissions including short-lived climate forcers such as black carbon (BC), organic carbon (OC), along with precursors such as SO_2, NO_x, and non-methane volatile organic compounds (NMVOCs) (Peters, et al. 2011).

Increased emission sources of BC within the Arctic could potentially have significant effects on the region's climate. BC has both direct and indirect effects on the earth's radiative budget and is the most efficient light absorber in the visible spectrum among atmospheric aerosols (Massabò, et al. 2015). In order for climate models to assess the direct radiative forcing of BC, optical properties such as the absorption coefficient (b_{abs}) and mass absorption cross-section (MAC) are of utmost importance (Arctic Monitoring and Assessment Programme 2015). MAC values reported in the literature vary widely from 2-25 $m^2\ g^{-1}$; therefore, site-specific MAC values are needed when determining the direct radiative impacts of BC (Bond and Bergstrom 2006; Ram and Sarin 2009; Wang, et al. 2013). An average MAC value of $7.4 \pm 0.7\ m^2\ g^{-1}$ has previously

been reported for the western Arctic during the spring of 2008 (McNaughton, et al. 2011). The mixing state of the BC particle has been shown to affect MAC. For example, when BC is internally mixed with sulfate and OC, light can be focused into the core of the BC particle, resulting in absorption that is 2-2.5 times higher than when externally mixed (Bond and Bergstrom 2006; Cheng, et al. 2011; Hara, et al. 2003). It has also been shown that BC source, along with increased BC to sulfate emissions ratio, can impact the warming potential of BC, with BC resulting from fossil fuel sources with large BC to sulfate ratios are approximately 100% more efficient at absorbing sunlight than plumes dominated by biomass burning sources (Ramana, et al. 2010). Annual trends in MAC and BC to sulfate ratios will be presented here for Barrow, a long-term Arctic monitoring site, to improve understanding of the variability of this parameter in the Arctic.

The mode by which BC impacts Arctic climate varies by season. While the direct absorption of incoming solar radiation is important in the spring and summer months, wintertime BC is of interest due to deposition on snow and ice, potentially contributing to accelerated spring melt. Winter and spring typically have the highest concentrations of BC, while wildfire events can impact summer BC. Model predictions show a mean decrease in Arctic snow albedo from BC deposition of 0.4% in the winter and 0.6% in the spring (Q. Wang, et al. 2011) Atmospheric BC concentrations in the Arctic are influenced by a variety of factors, including changes in source regions driven by the Arctic Oscillation, seasonal changes in meteorology and seasonal changes in regional emissions.

Global climate models mostly underestimate the atmospheric BC burden in the Arctic when compared to measurement data, partly due to missing emission sources and incorrect spatial and temporal distributions of emissions in emission inventories used in

the models (Sharma, et al. 2013; Eckhardt, et al. 2015). For example, a recent study of current modeling capabilities for simulating BC in the Arctic revealed that the mean underestimate of equivalent BC at Barrow is a factor of 2 (Eckhardt, et al. 2015); the goal of the current observational study is to incorporate source apportionment, aerosol characterization and atmospheric transport modeling to inform models by identifying the driving factors in ambient concentrations at a long-term Arctic monitoring site. Previous wintertime comparisons between models and observations have identified larger discrepancies for the modeled fossil combustion contributions to BC (up to 62% in late winter), and a good agreement for biomass/biofuel combustion contribution to BC (Barrett, et al. 2015).

The current study will apply the natural abundance of radiocarbon (^{14}C) as a source apportionment tool to determine the annual contributions of fossil fuel sources and contemporary sources of BC in Barrow, AK. Here, contemporary carbon is defined as all elemental carbon (EC) derived from both anthropogenic and natural biomass combustion processes (residential biomass combustion, agricultural fires, biofuel, and wildfires) while EC refers to light-absorbing carbon evolved from thermal-optical methods (Petzold, et al. 2013; Birch and Cary 1996). In addition to ^{14}C, the stable carbon isotopic signature (^{13}C) can be used as a dual isotope model to further define sources of EC, such as C3 vs. C4 plants, gaseous fossil sources (flaring), and liquid fossil sources (petroleum, oil, and gasoline) (Huang, et al. 2006; A. Andersson, et al. 2015; Winiger, et al. 2015). Radiocarbon analysis and apportionment is increasingly being used to apportion EC and is of high interest to understand sources of EC at long-term Arctic monitoring sites. Winiger, et al. (2015) reported an average biomass contribution of 57 ± 21% to EC at the

Zeppelin Observatory (Svalbard, Norway), including two days (6/1/2009 and 7/2/2009) with 95% and 98% biomass contribution for January through March of 2009. Barrett, et al. (2015) reported an average biomass contribution of 38 ± 9% for midwinter (Dec. 28, 2012 through Feb. 15, 2013) increasing to 51 ± 6% for the late winter (Feb. 25 through Mar. 11, 2013) at Barrow, AK. These winter studies confirm predicted differences in source regions for European and North American Arctic sites, however, it is important to understand the annual differences across these Arctic sites as well. Previous source apportionment studies in the Arctic have relied on models and emissions databases for year-round EC source characterization (Stohl, et al. 2013; Q. Wang, et al. 2011). This study provides dual isotope analysis of the EC fraction of atmospheric particulate matter (PM_{10}, aerodynamic diameter of 10 μm or less) samples from a year-long study (2012-2013) in Barrow, AK to determine the contributions of fossil fuel and contemporary sources to atmospheric EC. Seasonal trends in BC to sulfate ratios and MAC values will be determined and combined with source and back trajectory analysis. The combination of ^{14}C, $\delta^{13}C$, sulfate, MAC, and back trajectory analysis is applied to understand the impact of emission sources and source regions on the ambient concentrations and optical properties of EC in the North American Arctic on an annual basis.

Methods

Sample Collection

A yearlong sampling campaign was conducted at the Department of Energy Atmospheric Radiation Measurement (ARM) Climate Research Facility, 7.4 km northeast of the village of Barrow, AK, (71°19'23.73" N, 156°36'56.70" W) on the North

Slope of Alaska (NSA) from July 16, 2012 to June 4, 2013. Samples were collected continuously with no exclusion based on local wind direction. The campaign was designed to monitor local and regional influences on ambient concentration and physical properties.

Aerosol samples were collected on pre-combusted quartz fiber filters (QFF, Tissuquartz^{TM} Filters 2500 QAT-UP, 20 x 25 cm.) using a Tisch high volume PM_{10} sampler (TE-6070, Tisch Environmental, Cleves, Ohio). All samples were stored in aluminum foil packets and storage bags in a freezer prior to and post sampling. Filter blanks were collected at least once a month or when sampler maintenance was conducted. All blanks were handled in the same manner as samples.

EC Measurement and Isolation

For each sample, a 1.5 cm^2 aliquot of filter was cut and analyzed on a thermal optical transmittance (TOT) carbon analyzer (Sunset Laboratory, Tigard, OR) using the National Institute of Occupational Safety and Health (NIOSH) 5040 method (Birch and Cary 1996) to determine the organic carbon (OC) and elemental carbon (EC) loading of each filter. Briefly, OC is converted to CO_2 during sample heating in a 100% He atmosphere, while EC is converted to CO_2 under an oxidizing mixture of 10% O_2 and 90% He v/v. The CO_2 is then reduced to methane and measured using a flame ionization detector (FID). The initial transmittance of the laser through the filter is used to determine the split between OC and EC, and to correct for pyrolyzed carbon (PyrC) formed during the charring of organic carbon in the 100% He atmosphere. For EC concentration measurements, triplicate analysis was done every tenth filter. EC

concentration uncertainty is reported as the relative standard deviation of triplicate analysis, which was 17%.

EC isolation for radiocarbon analysis. Multiple PM10 samples were composited for radiocarbon analysis. This compositing was accomplished considering season and source region (based on back trajectory analysis). Samples were composited to achieve 60 μg of EC, with equal mass from each sample. To perform isotope analysis on EC, it must be separated from the OC fraction of the aerosol sample. This separation was achieved by trapping the evolved CO2 gas produced during EC combustion (Chen, et al. 2013). In order to remove water and other potential contaminants (halogen- and sulfur-containing gases) from the resulting CO2, the gas was passed through two traps, magnesium perchlorate, and silver wool heated to 600 °C. The CO2 was then cryo-trapped using liquid nitrogen at a temperature of -150 °C and sealed in glass ampules (Chen, et al. 2013). Sealed ampules were shipped to the National Oceanic Sciences Accelerator Mass Spectrometry facility (Woods Hole, MA, USA) where reduction of CO2 to graphite and carbon isotope measurements ($^{14}C/^{12}C$ and $^{13}C/^{12}C$) were performed. The inadvertent inclusion of a fraction of the PyrC with the EC isolate is possible during the EC isolation step, which could affect the isotopic signature of the EC fraction (Chen, et al. 2013; A. Andersson, et al. 2015; Budhavant, et al. 2015; Gustafsson, et al. 2009; Barrett, et al. 2015); therefore it is necessary that a sensitivity study be performed when using the TOT method. For the current study, sensitivity analysis shows a maximum underestimation of fossil contribution to EC by 10-25% (Appendix B). The TOT isolation method used in the current study uses the same operational definition of EC that is currently used in EC emissions inventories (Bond, et al. 2013; Stohl, et al. 2015),

allowing for direct comparisons between currently used EC emission inventories and this and other studies using the TOT method (Budhavant, et al. 2015).

Radiocarbon Source Apportionment

Radiocarbon results are reported as fraction modern (Fm). Radiocarbon source apportionment uses the large difference in end members between fossil (no radiocarbon) and contemporary (radiocarbon present) sources of EC to determine the percent contributions of each source to the total EC burden. The $\Delta^{14}C$ end member used to determine contemporary carbon contributions was +107.5‰, based on wood burning for temperate regions in 2010 (Zotter, et al. 2014). In a recent study, Mouteva, et al. (2015) suggested an end member value of +131 ± 52‰ (with $\Delta^{14}C$ values for BC ranging from 81 to 168‰) for contemporary contributions to BC and +103 ± 23‰ for contemporary contributions to total carbon, based on wood burning events in interior Alaska during the summer of 2013. However, when applied to our samples end member of +131‰ revealed little difference from the +107.5‰ (~2%); therefore, reported contemporary contributions in this paper are from the +107.5‰ end member in order to remain consistent with previously reported radiocarbon results in Barrett, et al. (2015). An end member of -1000‰ was used for fossil contributions (R. J. Sheesley, et al. 2012; Budhavant, et al. 2015). End members were applied using the following mass balance:

$$\Delta^{14}C\text{-}EC = (\Delta^{14}C_{biomass})(F_{biomass}) + (\Delta^{14}C_{fossil})(1\text{-}F_{biomass})$$

The fossil carbon contribution (F_{fossil}) is ($1\text{-}F_{biomass}$).

Normalization of Annual and Seasonal Averages

The methods used in Chapter Five for the normalization of annual and seasonal averages were also used in this chapter. Briefly, in order to account for different sampling duration ranging from seven to ten days, a normalization was applied based on sample duration. Seasonal radiocarbon measurements are also normalized by composite based on sample duration. The normalized values are used in the seasonal analysis and radiocarbon source apportionment throughout this chapter. Seasonal averages were calculated based on the following seasonal definitions: summer (> 15 hrs. daylight), winter (<12 hrs. daylight) and the transitional seasons of spring and fall with 12-15 hrs. of daylight.

Ion Chromatography

Ion chromatography was performed on aqueous extracts of the particulate matter samples in order to quantify sulfate concentrations. Water extractions followed previously established methods from Barrett and Sheesley (2014) for water soluble organic carbon with a slight modification decreasing the extraction volume to 25 mL. After extraction, the aqueous extracts were analyzed using ion chromatography on a Dionex ICS-2100 IC system equipped with an IonPac AS18 Hydroxide-Selective Anion-Exchange column (ThermoScientific, USA) under the following parameters: 25 µl sample injection volume, isocratic gradient with 23mM potassium hydroxide eluent at 30 °C and a suppressor current of 57mA. Total run time was 34 minutes.

Mass Absorption Coefficient of EC

Previous studies have shown the equivalence of light attenuation, ATN, from the carbon analyzer and the Aethalometer when measurement wavelength is the same,

therefore, ATN from the carbon analyzer can be used in the determination of the absorption coefficient, b_{abs}, by the same approach as used with the Aethalometer (Ram and Sarin 2009; Cheng, et al. 2011). When utilizing the NIOSH 5040 method, ATN is equivalent to the initial absorbance of the 678 nm laser through the sampled filter. ATN is used in the following equations to determine b_{abs} and MAC:

$$b_{abs}\ (\mathrm{Mm^{-1}}) = \mathrm{ATN} \times \mathrm{A/V}$$

Where A represents the sampled filter area used in the carbon analyzer (mm^2) and V is the volume of air sampled (m^3). The absorption coefficient is then used to determine MAC:

$$\mathrm{MAC}\ (\mathrm{m^2\ g^{-1}}) = b_{abs}/\mathrm{EC}$$

Where EC_s is the filter loading of the sample ($\mu g\ C\ cm^{-2}$). Multiple scattering effects and shadowing effects have been shown to be associated with filter-based measurements of absorption and are typically corrected with two empirical correction factors, C and R(ATN), where:

$$R(ATN) = (1/f - 1) \times \frac{\left[\ln(ATN) - \ln(10)\right]}{\left[\ln(50) - \ln(10)\right]} + 1$$

A value of 1.103 has been used for *f* to correct for MAC by Bikkinna, et al. (2016) and Ram and Sarin (2009) and the same approach has been used in this study. A value of C = 2.14 has been applied to this study due to contribution from both biomass and fossil fuel combustion sources (Bikkinna, et al. 2016). Corrected MAC values were calculated using the following equation:

$$MAC_{corrected}\left(m^2 g^{-1}\right) = MAC / \left[C \times R(ATN)\right]$$

Back Trajectory Analysis

Back trajectory analysis performed in Chapter Five is also used to determine source regions of EC for this study. Briefly, ten-day back trajectories originating in Barrow, AK every 6 hours were performed using the HYSPLIT back trajectory software for each day of the sampling campaign. Resulting back trajectories were clustered by radiocarbon composite for source region identification.

Results

Back Trajectory Results

Back trajectory results from Chapter Five are also presented here. Cluster means of sample dates matching the composite strategy for radiocarbon are presented as 10 day back trajectories revealing five major source regions to Barrow, AK: the Russian Arctic, Canadian Arctic, Alaskan Arctic, the Arctic Ocean, and western Alaska (Figure 5.1). All seasons had significant contribution from air masses traveling over the Arctic Ocean. Summer back trajectories consisted of air originating along the Russian Arctic with a heavy influence from western and interior Alaska, especially from August 12 through August 31, 2012. Air masses from the western Alaska source region decreased into the fall, and the Russian Arctic became the dominant source region throughout the remainder of the season. Winter source regions were previously discussed in detail in Chapter Four with two major source regions influencing EC concentrations, the Russian Arctic in mid-winter and the Canadian Arctic in late winter. Spring back trajectories consisted mainly of air masses originating over the Arctic Ocean.

EC Concentrations and Comparison with Model Prediction

For this study, the mean EC burden for 2012-2013 was 0.018 ± 0.003 μg m^{-3}. Previous long-term studies in Barrow have shown a distinct seasonal trend with maximum BC concentrations occurring during the winter and minimum concentrations during the summer with the spring and fall as transitional periods (Sharma, et al. 2006). Seasonal EC concentrations in this study are consistent with this seasonal pattern with the highest average EC concentrations of 0.042 ± 0.007 μg m^{-3} occurring during the winter. EC concentration decreased to 0.034 ± 0.006 μg m^{-3} in the spring, decreasing to 0.020 ± 0.003 μg m^{-3} in the summer and reached a minimum of 0.006 ± 0.001 μg m^{-3} during the fall. As discussed previously, there are still uncertainties associated with predicting surface EC concentrations, especially in the Arctic (Sharma, et al. 2013). When comparing to the current study to the 2010 emissions inventory of Stohl, et al. (2013), the model under-predicts average EC concentrations compared to measured surface EC concentrations by 110% for the spring and over-predicts fall EC concentrations by 60%. These large discrepancies from the 2010 model and the presented results may be due to a combination of an underestimation of fossil EC emission sources within the model or an increase in fossil fuel combustion between the two time periods. Variability in meteorological conditions, such as deposition and atmospheric transport patterns, could also be responsible for the differences. The model accurately predicts summer EC concentrations within 20% and winter EC within 2%. Based off of this comparison, further investigation is needed to determine which modeled parameters differed from the observed conditions. This will also improve the extrapolation of detailed observations from intensive field campaigns to long-term conditions at monitoring sites.

Isotope-Based Characterization and Source Apportionment

Radiocarbon source apportionment of EC revealed that fossil fuel combustion sources are the main contributor to EC throughout the year with an average contribution of 86.2 ± 9.7% (Figure 6.1). During the spring and fall transitional seasons, there is a strong, consistent fossil fuel combustion signal to EC concentrations at Barrow, AK. Fossil EC concentrations of 0.030 ± 0.006 μg m^{-3} and 0.005 ± 0.005 μg m^{-3} (Table 6.1) account for 89.6 ± 9.7% and 91.9 ± 9.7% of the total EC burden for spring and fall respectively (Figure 6.1); despite similarity in fossil contribution, the large differences in ambient concentration of fossil EC indicates very different atmospheric conditions between the two seasons. The domination of fossil fuel sources in the fall is consistent with modeled trends in Stohl, et al. (2013) which predicts decreasing contemporary contributions and increasing fossil contributions throughout the fall and into the winter. The strong fossil signal of EC in the spring, however, is not consistent with previous apportionment models, which show increasing contemporary carbon contributions in the spring (Stohl, et al. 2013). This difference between observed conditions for Spring 213 and modeled conditions may also indicate an anomalous spring season; further model inter-comparison is needed to determine why the observed concentrations had significantly higher EC concentration and fossil contribution than predicated. It is particularly relevant to understand and predict spring EC concentrations as radiative forcing can potentially include both atmospheric and deposition/surface albedo components in the Arctic spring.

Table 6.1: Average seasonal elemental carbon concentrations, average fossil EC concentrations, % fossil EC, mass absorption cross-section (MAC), and elemental carbon to sulfate ratios for Barrow, AK.

Season	Avg. EC Conc. ± unc. ($\mu g\ m^{-3}$)	Fossil EC conc. ± unc. ($\mu g\ m^{-3}$)	EC % Fossil ± unc.	MAC ± s.d.	Avg. EC:Sulfate Ratio ± s.d.
Spring	0.034 ± 0.006	0.030 ± 0.006	89.6 ± 9.7	6.73 ± 0.18	0.05 ± 0.01
Summer	0.020 ± 0.003	0.017 ± 0.003	83.7 ± 9.7	7.83 ± 3.57	0.06 ± 0.03
Fall	0.006 ± 0.001	0.005 ± 0.001	91.9 ± 9.7	18.49 ± 12.22	0.02 ± 0.02
Winter	0.042 ± 0.007	0.034 ± 0.007	80.1 ± 9.7	12.36 ± 4.11	0.11 ± 0.17

Mean fossil contribution to EC was 83.7 ± 9.7% for the summer months during the study period (Figure 6.1). However, during the summer months, two different source regimes impacting EC concentrations: fossil dominated sources in early summer (mid-July to mid-August, Summer 1 Composite), transitioning to more even contributions from fossil and contemporary sources in mid-summer (mid-August to the end of the month, Summer 2 Composite) (Table D.1). For the early summer regime, fossil sources continued to be the major driver of EC, contributing 87.3 ± 9.7% of the total EC burden. For the mid-summer, fossil contribution to EC drops to 52.7 ± 9.7%, which corresponds to back trajectories originating in the interior of Alaska which were influenced by wildfires (Figure 5.1). This decrease to <50% fossil contribution to EC, along with the late winter (Feb. 25 – March 11) contribution of 49.1 ± 5.6% fossil as reported by Barrett, et al. (2015) are the only instances of greater contemporary than fossil contributions to surface level EC.

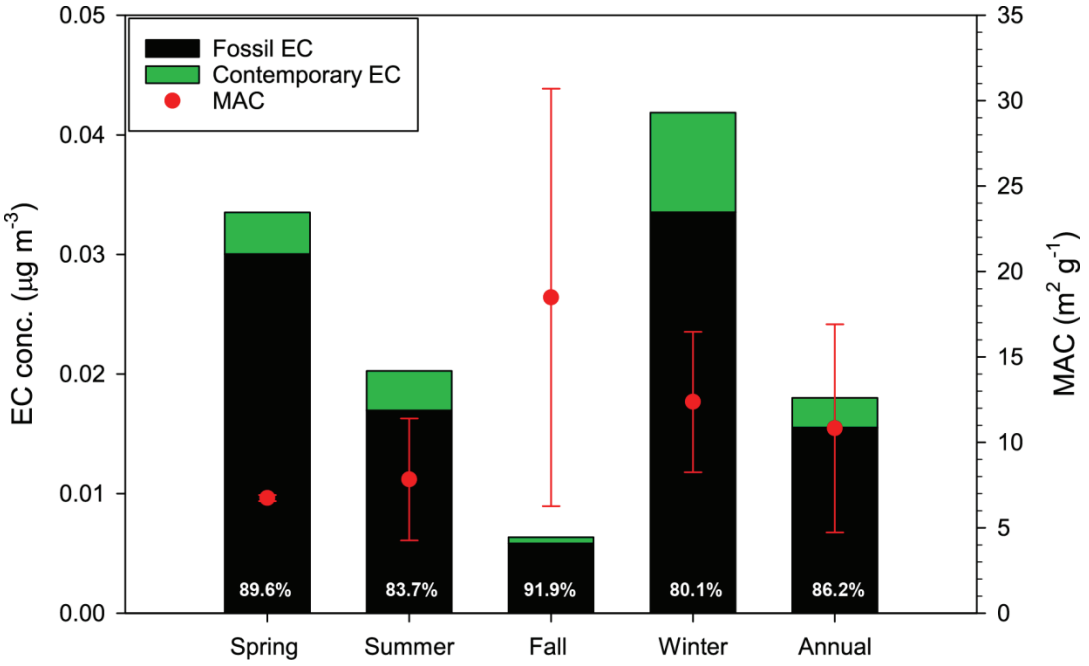

Figure 6.1: Average seasonal and annual contemporary and fossil EC concentrations in Barrow, AK from 2012-2013.

As a complement to the $\Delta^{14}C$ apportionment of EC, characterization of the $\delta^{13}C$ signature was performed. Measurement of $\delta^{13}C$ has previously been used in Arctic EC source apportionment by applying end members for the following combustion sources: C3 plants, coal combustion, and liquid fossil sources (Winiger, et al. 2015). Seasonal $\delta^{13}C$ averages for spring (-26.6 ± 0.8‰), summer (-26.3 ± 0.1‰) and fall (-26.9 ± 0.3‰) are more depleted than the winter (-24.5 ± 2.1‰). Regression of the $\Delta^{14}C$ and $\delta^{13}C$ values reveals a general trend of enrichment in the $\delta^{13}C$ signature as the contribution of contemporary EC increases (Figure 6.2, r^2 = 0.44). Figure 6.2 also indicates more enriched $\delta^{13}C$ values for the late winter period (-22.3 ± 0.7‰) indicating a shift in fossil fuel combustion sources, possibly from flaring and liquid petroleum to coal combustion. This switch coincides with a shift in major source region, from the Russian Arctic to the Canadian Arctic (Figure 4.1).

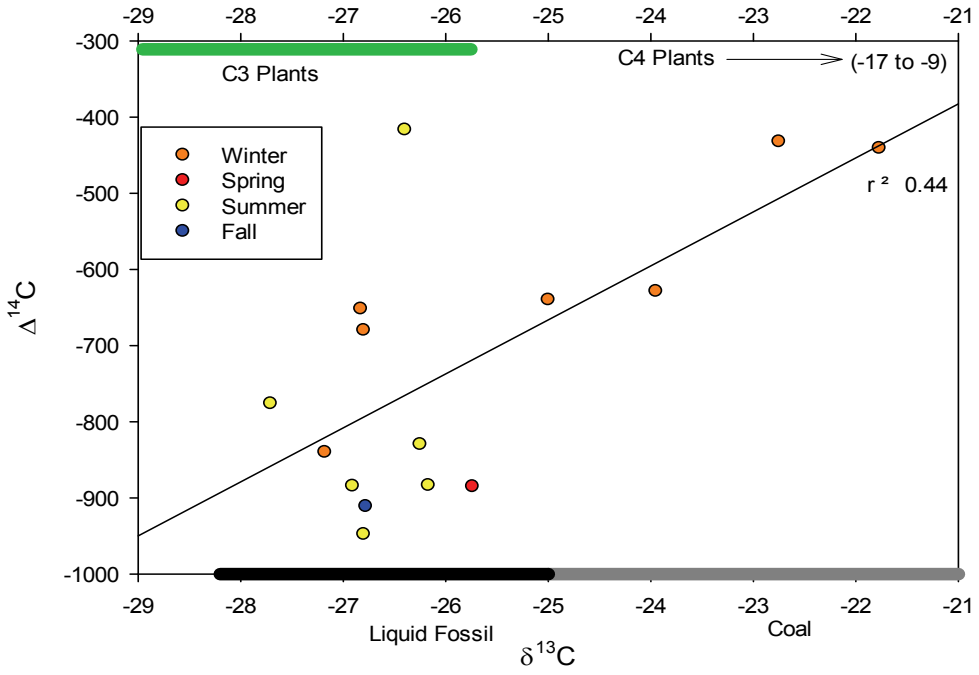

Figure 6.2: $\Delta^{14}C$ and $\delta^{13}C$ signatures of samples from Barrow, AK during the study period. Green, black, and gray bars along the x-axes represent the $\delta^{13}C$ for C3 plants, liquid fossil, and coal sources.

EC Optical Properties and Sulfate Concentrations

The average annual MAC value of EC in the NSA was 10.69 ± 5.95 m^2 g^{-1}, however the high standard deviation indicates that an annual average may not be a good representation of the Arctic MAC. Average MAC values in the NSA were highest in the fall and winter with values of 18.49 ± 12.22 and 12.36 ± 4.11 m^2 g^{-1} respectively. The summer has an average MAC value of 7.83 ± 3.57 m^2 g^{-1}, while spring exhibited the lowest average MAC value of 6.73 ± 0.18 m^2 g^{-1} (Figure 6.1). Average springtime MAC values are in good agreement with previously reported MAC values of 7.4 ± 0.7 m^2 g^{-1} MAC (at 660 nm) for the western Arctic in the Spring of 2008 (McNaughton, et al. 2011). Analysis of mixing state of Arctic aerosols in Svalbard, Norway revealed that under the Arctic haze conditions, soot particles were externally mixed with sulfate

particles while internal mixing was observed during non-haze background conditions (Hara, et al. 2003). A more recent analysis of BC over the Arctic Ocean in September of 2014 showed that greater than 50% of BC detected by an SP2 were internally mixed (Taketani, et al. 2016). Based on the fact that internal mixing of aerosols can enhance absorption by 2-2.5x, it is reasonable to assume that spring time EC aerosols at Barrow are externally mixed with sulfate, while the majority of EC during the fall and winter is internally mixed with sulfate and other aerosol components. High MAC values in the fall and winter could support the notion that EC derived from fossil fuel combustion is more efficient at absorbing solar radiation (Ramana, et al. 2010), however, MAC values from the spring, which had an 89.6% fossil contribution to EC, do not follow this trend. This indicates that merely ascribing MAC by source is too simplistic to predict MAC in the Arctic. EC:Sulfate ratios peaked in the winter (0.11) and were the lowest in the fall (0.02) and showed no correlation with MAC values (Table 6.1, Figure D.3). A recent study has shown that absorption parameter values may be better predicted by photochemical age, which could help explain the high fossil/low MAC observations during the spring (Garg, et al. 2016). MAC values ranging from 6 to 15 m^2 g^{-1} have been used to determine BC concentrations in the Arctic; our results indicate that the seasonal MAC values should be used rather than the application of a single MAC value for BC determination and its effect on snow (Hegg, et al. 2009; Hadley and Kirchstetter 2012)

Sulfate concentrations were highly variable throughout the year ranging from 0.07 to 1.44 μg m^{-3}. The spring exhibited the highest seasonal average concentration of 0.74 ± 0.38 μg m^{-3} and the lowest seasonal concentration, 0.20 ± 0.33 μg m^{-3} in the fall. Despite having the highest average sulfate concentration, the spring exhibited the lowest MAC

(5.62 ± 1.08 m^2 g^{-1}). Increased sulfate concentrations in the spring coincide with the Arctic Haze as expected. During the spring, EC and sulfate were highly correlated (r^2 = 0.81), with very weak correlations during winter, summer and fall (Figure D.1). The strong correlation between EC and sulfate in the spring along with the $\delta^{13}C$ signature points to a strong influence from coal combustion during this time. Sulfate and MAE were highly correlated during the fall and winter (r^2= 0.69 and r^2= 0.89, respectively) indicating possible absorption enhancement from internally mixed EC and sulfate aerosols (Figure D.2).

Conclusions

This study provides the first year-round assessment of fossil fuel combustion and biomass burning sources to EC in the North American Arctic. Fossil contributions consistently dominated the EC burden, contributing as much as 92% of total EC, with an annual contribution of 86.2 ± 5.3% (average ± standard deviation). The contribution of biomass combustion was much more sporadic and event driven, as evidenced by two short periods in late summer (August 12-31, 2012) and the late winter (February 25-March 11, 2013) which had > 50% contribution from biomass combustion. Light absorption of EC is the most efficient during the fall and winter, which is important due to deposition on snow and ice, and could potentially contribute to faster spring melts. However, the MAC was 63% lower in spring than the winter; indicating that intensive spring campaigns on optical properties of Arctic aerosols may not be applicable for year round predictions of aerosols radiative forcing in the region. Absorption by EC is possibly enhanced by internal mixing with sulfate during the fall and winter as seen in the high MAC values during these seasons, while EC is assumed to be externally mixed

during the spring haze event due to low MAC values. These results provide a tightly constrained source apportionment that can be used to improve emissions data currently used in global climate models. Continued long-term sampling and radiocarbon analysis at Barrow is desirable in order to determine if the fossil contributions seen during this study are consistent, or if there is significant variation from year to year.

References

Andersson, A., J. Deng, K. Du, M. Zheng, C. Yan, M. Sköld, and Ö. Gustafsson (2015), Regionally-Varying Combustion Sources of the January 2013 Severe Haze Events over Eastern China, *Environmental Science & Technology*, *49*(4), 2038-2043.

Arctic Monitoring and Assessment Programme, A. (2015), AMAP Assessment 2015: Black carbon and ozone as Arctic climate forcers, edited, p. 116, Arctic Monitoring and Assessment Programme, Oslo, Norway.

Barrett, T. E., E. M. Robinson, S. Usenko, and R. J. Sheesley (2015), Source Contributions to Wintertime Elemental and Organic Carbon in the Western Arctic Based on Radiocarbon and Tracer Apportionment, *Environmental Science & Technology*, *49*(19), 11631-11639.

Bikkinna, S., N. Rastogi, M. M. Sarin, A. Singh, and D. Singh (2016), Mass absorption efficiency of light absorbing organic aerosols from source region of paddy-residue burning emissions in the Indo-Gangetic Plain, *Atmospheric Environment*, *125*, 360-370.

Birch, M. E., and R. A. Cary (1996), Elemental carbon-based method for monitoring occupational exposures to particulate diesel exhaust, *Aerosol Science and Technology*, *25*(3), 221-241.

Bond, T. C., and R. W. Bergstrom (2006), Light absorption by carbonaceous particles: An investigative review, *Aerosol Science and Technology*, *40*(1), 27-67.

Bond, T. C., et al. (2013), Bounding the role of black carbon in the climate system: A scientific assessment, *Journal of Geophysical Research-Atmospheres*, *118*(11), 5380-5552.

Budhavant, K., A. Andersson, C. Bosch, M. Krusa, E. N. Kirillova, R. J. Sheesley, P. D. Safai, P. S. P. Rao, and O. Gustafsson (2015), Radiocarbon-based source apportionment of elemental carbon aerosols at two South Asian receptor observatories over a full annual cycle, *Environ. Res. Lett.*, *10*(6).

Chen, B., et al. (2013), Source Forensics of Black Carbon Aerosols from China, *Environmental Science & Technology*, *47*(16), 9102-9108.

Cheng, Y., et al. (2011), Mass absorption efficiency of elemental carbon and water-soluble organic carbon in Beijing, China, *Atmospheric Chemistry and Physics*, *11*(22), 11497-11510.

Draxler, R. R., and G. D. Rolph (2010), HYSPLIT (HYbrid Single-Particle Lagrangian Integrated Trajectory) model access via NOAA ARL READY Website (http://ready.arl.noaa.gov/HYSPLIT.php), edited, Silver Spring, MD, NOAA Air Resources Laboratory.

Eckhardt, S., et al. (2015), Current model capabilities for simulating black carbon and sulfate concentrations in the Arctic atmosphere: a multi-model evaluation using a comprehensive measurement data set, *Atmos. Chem. Phys.*, *15*(16), 9413-9433.

Garg, S., B. P. Chandra, V. Sinha, R. Sarda-Esteve, V. Gros, and B. Sinha (2016), Limitation of the Use of the Absorption Angstrom Exponent for Source Apportionment of Equivalent Black Carbon: a Case Study from the North West Indo-Gangetic Plain, *Environmental Science & Technology*, *50*(2), 814-824.

Gustafsson, O., M. Krusa, Z. Zencak, R. J. Sheesley, L. Granat, E. Engstrom, P. S. Praveen, P. S. P. Rao, C. Leck, and H. Rodhe (2009), Brown Clouds over South Asia: Biomass or Fossil Fuel Combustion?, *Science*, *323*(5913), 495-498.

Huang, L., J. R. Brook, W. Zhang, S. M. Li, L. Graham, D. Ernst, A. Chivulescu, and G. Lu (2006), Stable isotope measurements of carbon fractions (OC/EC) in airborne particulate: A new dimension for source characterization and apportionment, *Atmospheric Environment*, *40*(15), 2690-2705.

Massabò, D., et al. (2015), Multi-wavelength optical determination of black and brown carbon in atmospheric aerosols, *Atmospheric Environment*, *108*(0), 1-12.

McNaughton, C. S., et al. (2011), Absorbing aerosol in the troposphere of the Western Arctic during the 2008 ARCTAS/ARCPAC airborne field campaigns, *Atmospheric Chemistry and Physics*, *11*(15), 7561-7582.

Mouteva, G. O., et al. (2015), Black carbon aerosol dynamics and isotopic composition in Alaska linked with boreal fire emissions and depth of burn in organic soils, *Global Biogeochemical Cycles*, 2015GB005247.

Odemark, K., S. B. Dalsoren, B. H. Samset, T. K. Berntsen, J. S. Fuglestvedt, and G. Myhre (2012), Short-lived climate forcers from current shipping and petroleum activities in the Arctic, *Atmospheric Chemistry and Physics*, *12*(4), 1979-1993.

Peters, G. P., T. B. Nilssen, L. Lindholt, M. S. Eide, S. Glomsrod, L. I. Eide, and J. S. Fuglestvedt (2011), Future emissions from shipping and petroleum activities in the Arctic, *Atmospheric Chemistry and Physics*, *11*(11), 5305-5320.

Petzold, A., et al. (2013), Recommendations for reporting "black carbon" measurements, *Atmos. Chem. Phys.*, *13*(16), 8365-8379.

Pistone, K., I. Eisenman, and V. Ramanathan (2014), Observational determination of albedo decrease caused by vanishing Arctic sea ice, *Proceedings of the National Academy of Sciences of the United States of America*, *111*(9), 3322-3326.

Ram, K., and M. M. Sarin (2009), Absorption Coefficient and Site-Specific Mass Absorption Efficiency of Elemental Carbon in Aerosols over Urban, Rural, and High-Altitude Sites in India, *Environmental Science & Technology*, *43*(21), 8233-8239.

Ramana, M. V., V. Ramanathan, Y. Feng, S. C. Yoon, S. W. Kim, G. R. Carmichael, and J. J. Schauer (2010), Warming influenced by the ratio of black carbon to sulphate and the black-carbon source, *Nat. Geosci.*, *3*(8), 542-545.

Sand, M., T. K. Berntsen, J. E. Kay, J. F. Lamarque, O. Seland, and A. Kirkevag (2013), The Arctic response to remote and local forcing of black carbon, *Atmospheric Chemistry and Physics*, *13*(1), 211-224.

Sharma, S., E. Andrews, L. A. Barrie, J. A. Ogren, and D. Lavoue (2006), Variations and sources of the equivalent black carbon in the high Arctic revealed by long-term observations at Alert and Barrow: 1989-2003, *Journal of Geophysical Research-Atmospheres*, *111*(D14).

Sharma, S., M. Ishizawa, D. Chan, D. Lavoue, E. Andrews, K. Eleftheriadis, and S. Maksyutov (2013), 16-year simulation of Arctic black carbon: Transport, source contribution, and sensitivity analysis on deposition, *Journal of Geophysical Research-Atmospheres*, *118*(2), 943-964.

Sheesley, R. J., E. Kirillova, A. Andersson, M. Krusa, P. S. Praveen, K. Budhavant, P. D. Safai, P. S. P. Rao, and O. Gustafsson (2012), Year-round radiocarbon-based source apportionment of carbonaceous aerosols at two background sites in South Asia, *Journal of Geophysical Research-Atmospheres*, *117*.

Stohl, A., Z. Klimont, S. Eckhardt, K. Kupiainen, V. P. Shevchenko, V. M. Kopeikin, and A. N. Novigatsky (2013), Black carbon in the Arctic: the underestimated role of gas flaring and residential combustion emissions, *Atmospheric Chemistry and Physics*, *13*(17), 8833-8855.

Stohl, A., et al. (2015), Evaluating the climate and air quality impacts of short-lived pollutants, *Atmospheric Chemistry and Physics*, *15*(18), 10529-10566.

Wang, Q., et al. (2011), Sources of carbonaceous aerosols and deposited black carbon in the Arctic in winter-spring: implications for radiative forcing, *Atmospheric Chemistry and Physics*, *11*(23), 12453-12473.

Wang, Y., S. Liu, P. Shi, Y. Li, C. Mu, and K. Du (2013), Temporal Variation of Mass Absorption Efficiency of Black Carbon at Urban and Suburban Locations, *Aerosol Air Qual. Res.*, *13*(1), 275-286.

Winiger, P., A. Andersson, K. E. Yttri, P. Tunved, and O. Gustafsson (2015), Isotope-Based Source Apportionment of EC Aerosol Particles during Winter High-Pollution Events at the Zeppelin Observatory, Svalbard, *Environ. Sci. Technol.*, *49*(19), 11959-11966.

Zotter, P., et al. (2014), Diurnal cycle of fossil and nonfossil carbon using radiocarbon analyses during CalNex, *Journal of Geophysical Research-Atmospheres*, *119*(11), 6818-6835.

CHAPTER SEVEN

Conclusions

Source apportionment utilizing ^{14}C abundance was applied to the elemental carbon (Chapters Four and Six) and organic carbon (Chapter Five) fractions of atmospheric particulate matter samples collected at Barrow, AK during a year-round sampling campaign from 2012 to 2013. ^{14}C apportionment of EC revealed that fossil fuel combustion is responsible for the majority of the EC burden throughout the year in the North American Arctic, contributing as much as 92% of the total EC during the early winter. Contemporary sources of elemental carbon (biomass burning sources) were responsible for greater than 50% of the burden for only three periods throughout the year, the late summer (August 2012) with air masses arriving from the interior of Alaska, and during the late winter which coincided with a source region shift from the Russian to the Canadian Arctic.

^{14}C apportionment of OC revealed that contemporary, not fossil, carbon sources contributed the majority of the OC burden in Barrow, AK. Contemporary contributions were below 50% of the OC burden only during the fall, 38.6%, and peaked at 78.8% during the late summer, coinciding with the increased contribution of contemporary carbon to Arctic EC.

In addition to radiocarbon source apportionment, light absorption measurements were performed to give insight on the radiative properties of carbonaceous aerosols in the Arctic. Light absorption measurements of aqueous extracts of organic carbon revealed

that organic carbon light absorption is strongest in the fall and the lowest in the summer. Light absorption of EC peaked in the winter and was the lowest during the spring.

A novel method for calculating the atmospheric lifetime of levoglucosan, a biomass burning organic tracer, was also performed, identifying two different atmospheric processing regimes: high degradation and low degradation (Chapter Four). This method of atmospheric lifetime calculation can be used for tracking the atmospheric processing, or aging, of aerosols in the Arctic.

Contributions to the Scientific Community

This work represents a robust data set that is available to climate modelers to be used as input into global and regional climate models. Global climate models rely on emission inventories to run simulations of atmospheric BC in the Arctic, and most underestimate this burden due to missing emission sources and incorrect spatial and temporal distributions of emission sources. The data presented in Chapters Four through Six provide a more tightly constrained source apportionment that can be used to close the gap between modeled and observed concentrations of Arctic BC. Also, organic carbon is typically treated as light scattering in these models; therefore any underestimation of the light absorption due to BrC will lead to an underestimation of the total light absorption by aerosols. The MAE_{365} values of water-soluble brown carbon can help to address this underestimation of total aerosol light absorption in the Arctic.

The combination of highly accurate source apportionment via radiocarbon abundance of organic and elemental carbon in the Arctic, optical properties of aerosols, and a method for determining the half-life of organic tracers helps to fill many voids in the Arctic scientific community. In a report from the United States Environmental

Protection Agency (EPA) to Congress, the EPA identified high priority research needs for aerosols including research on the impacts of aerosols in snow and ice covered regions such as the Arctic and the Intergovernmental Panel on Climate Change (IPCC) identified spatial and temporal variability of climate change and its impacts in regions of the Arctic as one of the key uncertainties on climate change in the Polar regions. The work of this dissertation directly meets the high priority research needs by providing precise information on spatial and temporal variability of organic and elemental carbon sources and atmospheric processing within the Arctic.

Future Work

While light absorption measurements of WSOC are used as a proxy for BrC absorption, not all BrC is water soluble. Therefore, it would be beneficial to measure the light absorption of solvent extracts of the aerosol samples in order to further our knowledge of light-absorption properties of BrC. Currently, solvent extractions of the samples used in this work are available and the determination of the optical properties of these extracts is ongoing.

The year-round characterization of OC at Barrow, AK reveals that OC concentrations did not follow the well-known seasonal trends of BC for 2012-2013. However, it is not known if this represents an atypical year in the Arctic; therefore more long-term campaigns are needed to address this gap. Additionally, the Arctic Ocean source region influences Barrow during all seasons, introducing a marine/sea ice source of organic aerosols. Further investigation into the marine biogenic emissions in this region is needed.

Further long-term investigation into the source contributions of light-absorbing carbonaceous aerosols using ^{14}C abundance at all five Arctic monitoring stations (Barrow, AK, Tiksi, Russia, Summit, Greenland, Svalbard, Norway, and Alert, Canada) is needed in order to understand the overall contributions of fossil and contemporary carbon across the Arctic. In addition to source characterization, light absorption measurements of BrC and EC are needed. ^{14}C apportionment and the optical properties of aerosols would allow for better constrained climate models in the Arctic, which currently cannot accurately model the observed Arctic warming, improving their ability to model future scenarios of increased/decreased emissions in the region.

APPENDICES

APPENDIX A

Supplemental Material for Urban Impacts on Regional Carbonaceous Aerosols: Case Study in Central Texas

WSOC Analysis

Sample aliquots were placed in 50 ml centrifuge tubes (Bio-Link Scientific, Wimberly, TX) and sonicated in 30 mL of de-ionized water for 15 minutes. All tubes were pre-cleaned by triple rinsing with DI water. The extracts were then centrifuged for 10 minutes and decanted to separate out large filter pieces from the solutions. The extracts were filtered using disposable Iso-Disc PTFE-25-2 Filters with a pore size of 0.2 μm (Supelco Analytical, Bellefonte, PA), the filters and syringe were both triple rinsed with DI water prior to filtration. 60 μl of 6N HCl was then added to remove any CO_2 trapped in the solution. Samples were run in three groups with calibration standards (Potassium Hydrogen Phthalate (KHP, C8H5KO4, 1000 mg C/L) from Ultra Scientific, North Kingstown, RI) (concentrations of: 0, 0.5, 1, 2, 3, 4, and 5 mg L^{-1}) measured prior to analysis of each group (r^2= 0.9992, 0.9996, and 0.9998) and periodically throughout each group. The reporting limit was 0.5 mg L^{-1}. Each sample was analyzed three times using 100 μl injections each time. The reported values are the average of the concentrations of the three injections. All samples were blank subtracted using an average blank value of 0.16 mg L^{-1} prior to conversion to μg m^{-3}.

Absorption Parameters

Filter-Based Samples

The optical attenuation (ATN) of a 678 nm laser source in the TOT analyzer was used in the determination of b_{abs} and MAC for the filter based samples. ATN is defined by the Beer-Lambert law as:

$$ATN = -ln\left(\frac{I_0}{I}\right)$$

where I_0 and I are the transmittance signals before and after thermal optical analysis. ATN from the carbon analyzer is then used to determine b_{abs}:

$$b_{abs}(Mm^{-1}) = ATN \times \frac{A}{V}$$

where *A* is the filter area with particle loading (mm^2) and *V* is the volume of air sampled (m^3). MAC is then calculated as:

$$MAC\ (m^2/g) = \frac{ATN \times A}{EC \times V}\frac{1}{3.6}$$

where EC_s is the filter loading of EC. All MAC calculations in this study have been corrected by an empirical correction factor, *C*= 3.6 (Weingartner, et al. 2003). Previous studies have shown equivalence in ATN as determined by the Aethalometer and the carbon analyzer when the wavelength is kept constant (Cheng, et al. 2011; Ram and Sarin 2009).

WSOC Absorption

Light absorption of the aqueous extracts was measured for 200 to 700 nm on an Agilent 8453 UV-Vis spectrometer (Santa Clara, CA), with deuterium and tungsten halogen light sources. Light absorption of the extracts is defined by Beer-Lambert as:

$$ATN_\lambda = -log_{10}\left(\frac{I}{I_0}\right) = L \times \sum_i \left(C_i \times \varepsilon_{i,\lambda}\right)$$

where I_0 and I are the intensity of the incident and transmitted light, L is the absorbing path length, C_i is the concentration of light absorbing substances in solution, and $\varepsilon_{i,\lambda}$ is the wavelength dependent mass absorption efficiency. The absorption coefficient (b_{abs}) is then calculated from ATN using the following equation:

$$(b_{abs})_\lambda = (ATN_\lambda - ATN_{700}) \times \frac{V_w}{V \times L} \times \ln(10)$$

where V_w is the volume of water used for the extraction (30 ml), V is the volume of air sampled (m^3) and L is the path length (0.01 m). Since there is no absorption for ambient aerosol extracts at 700 nm, ATN_{700} accounts for baseline drift during analysis (Hecobian, et al. 2010; Cheng, et al. 2011). Mass absorption efficiency at a particular wavelength (MAE_λ) is then calculated as:

$$MAE_\lambda = \frac{(b_{abs})_\lambda}{WSOC}$$

Geographic Source Assessment

By combining ambient concentrations with BT clusters, it can be determined whether PM components (OC, EC, WSOC and $PM_{2.5}$) follow any geographical source region patterns. The geographic source assessment (GSA) technique used by Sheesley et al., was used to determine contribution of PM components from each cluster (Rebecca J. Sheesley, et al. 2012). The GSA is calculated as the mean PM components weighted by the fraction of air coming from a certain cluster and the duration of the sampling. Unpaired one-sided t-tests were made to test whether the mean concentrations calculated for each source region were significantly different than the total mean values for PM components (Table A.1).

Table A.1: Results from Geographic Source Assessment (GSA) calculations for organic carbon (OC), elemental carbon (EC), particulate matter 2.5 ($PM_{2.5}$), and water soluble organic carbon (WSOC) for each cluster. P-values (to test the hypothesis that the cluster means are different from the overall means) are shown in ().

Cluster	GSA OC ($\mu g/m^3$) (p-value)	GSA EC ($\mu g/m^3$) (p-value)	GSA $PM_{2.5}$ ($\mu g/m^3$) (p-value)	GSA WSOC ($\mu g/m^3$) (p-value)
Long Range Central Plains	2.15 (0.14)	0.16 (0.38)	5.90 (0.04)	1.30 (0.11)
Regional North	2.45 (0.26)	0.18 (0.31)	6.87 (0.10)	1.61 (0.32)
Texas Coast	2.04 (0.11)	0.15 (0.21)	9.77 (0.35)	1.34 (0.15)
Regional South	2.33 (0.12)	0.13 (0.002)	8.53 (0.21)	1.52 (0.17)

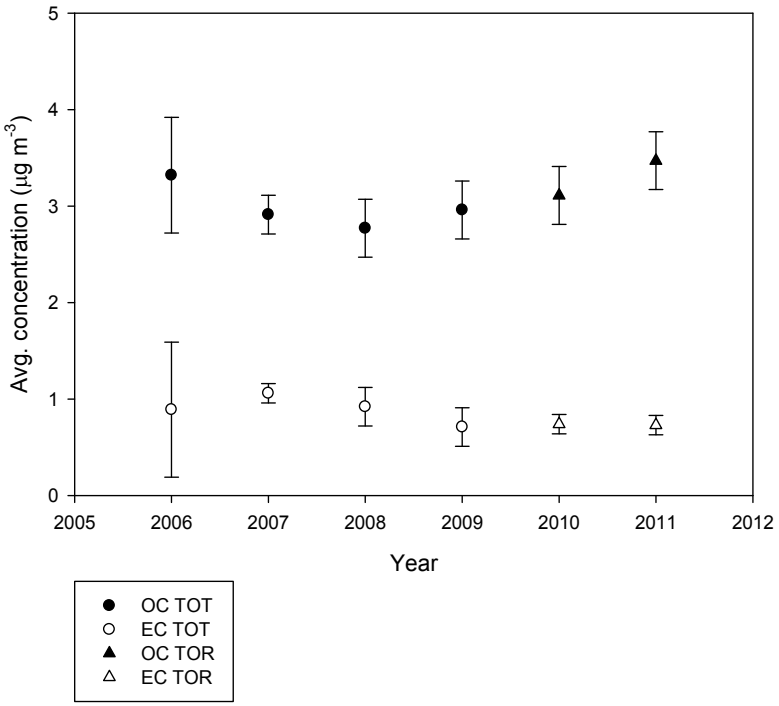

Figure A.1: Average organic carbon (OC) and elemental carbon (EC) concentrations using thermal optical transmittance (TOT) and thermal optical reflectance (TOR) methods for the Houston Clinton monitoring site.

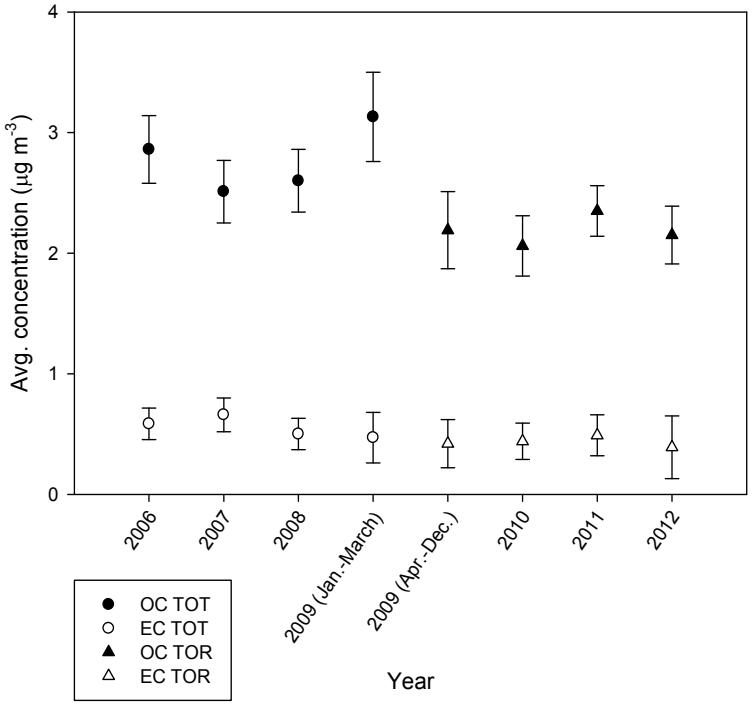

Figure A.2: Average organic carbon (OC) and elemental carbon (EC) concentrations using thermal optical transmittance (TOT) and thermal optical reflectance (TOR) methods for the Dallas Hinton monitoring site.

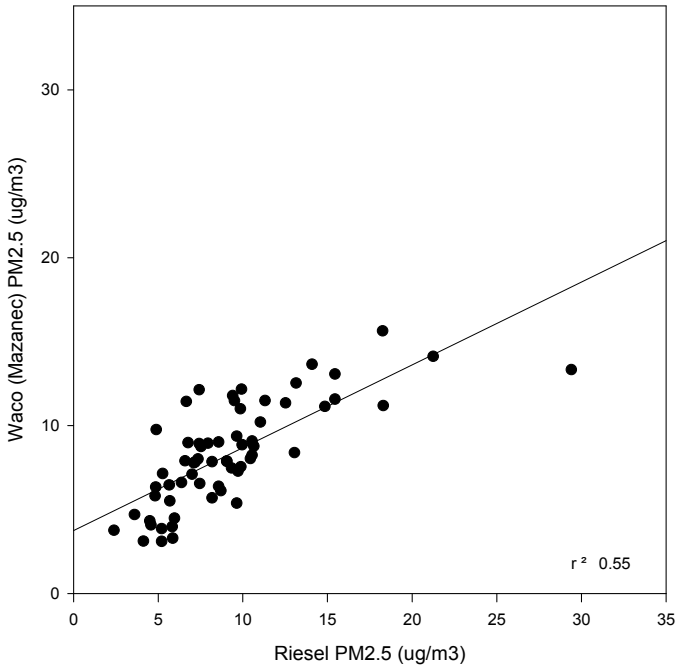

Figure A.3: Comparison of fine particulate matter ($PM_{2.5}$) mass concentrations at the Waco (Mazanec) monitoring station and the Riesel, TX sampling location.

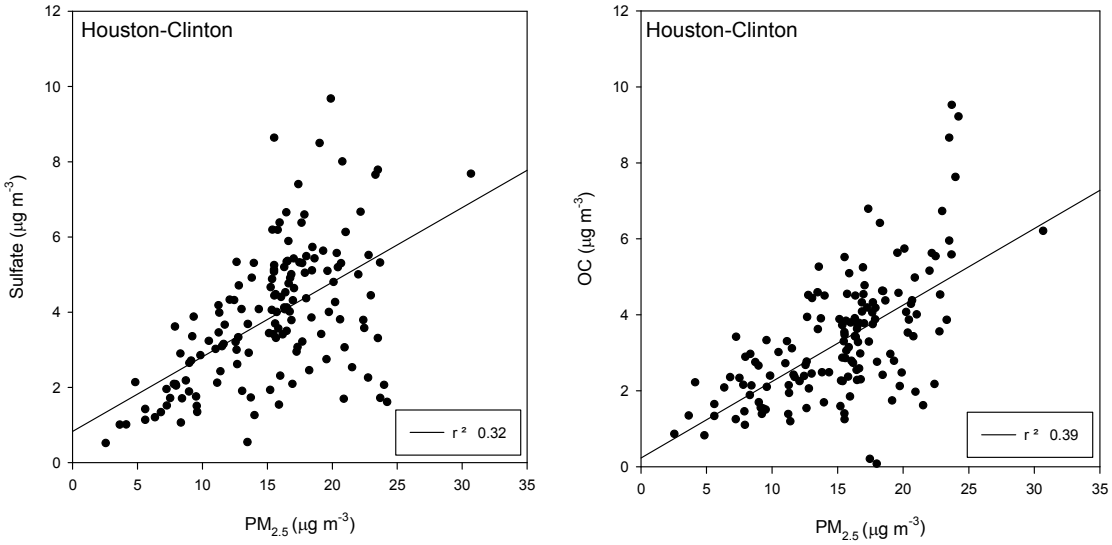

Figure A.4: Regression analysis of sulfate vs. fine particulate matter ($PM_{2.5}$) and organic carbon (OC) vs. $PM_{2.5}$ for Houston Clinton.

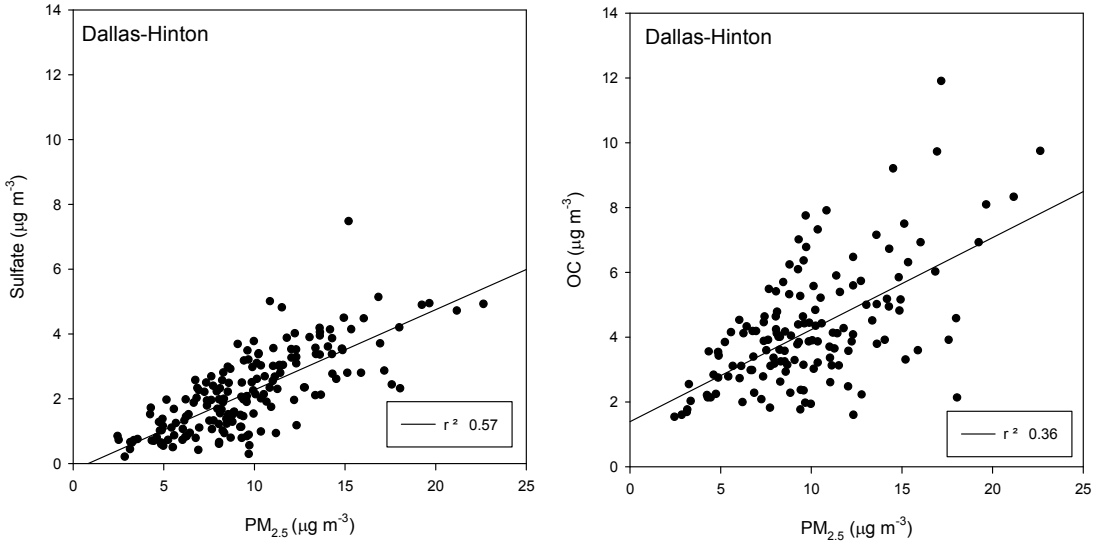

Figure A.5: Regression analysis for sulfate vs. fine particulate matter ($PM_{2.5}$) and organic carbon (OC) vs. $PM_{2.5}$ for Dallas Hinton.

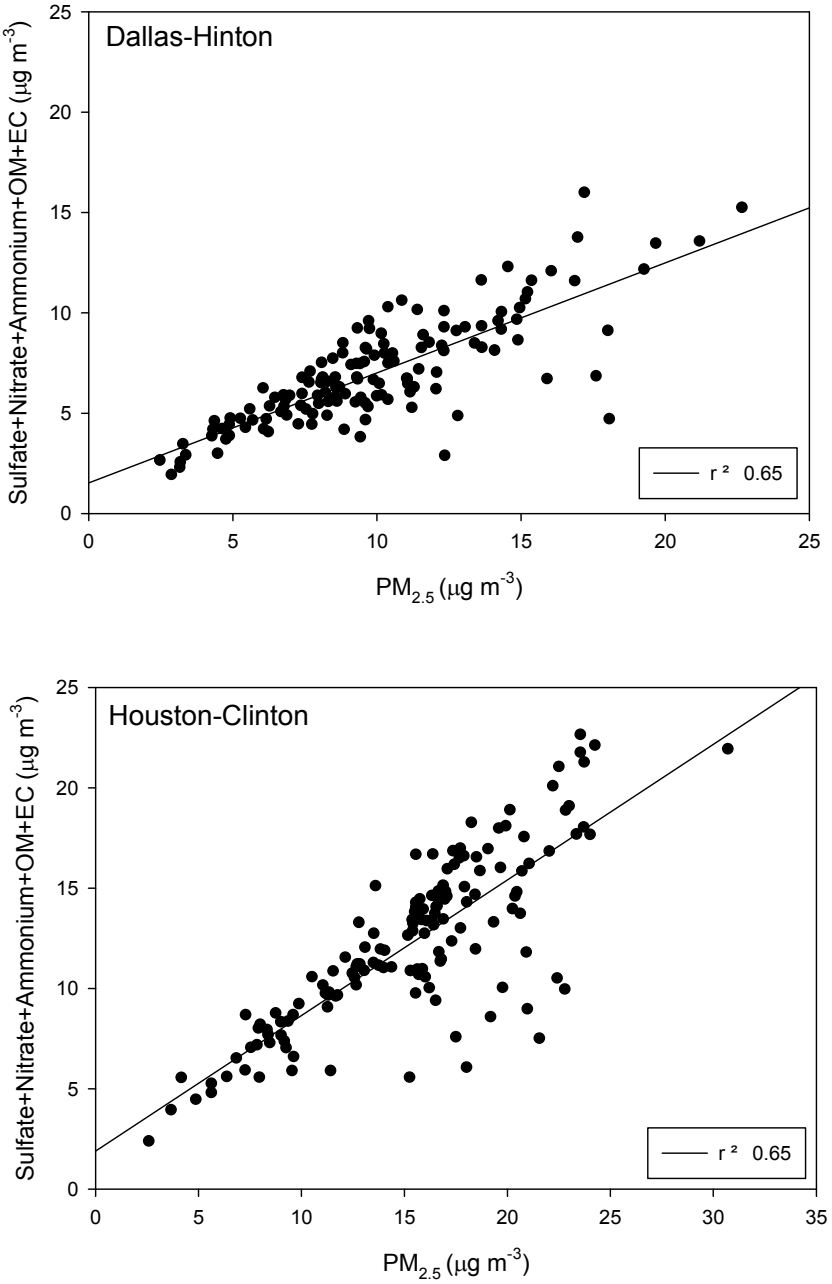

Figure A.6: Regression analysis of sum of sulfate, nitrate, ammonium, organic matter (OM), and elemental carbon (EC) vs. fine particulate matter ($PM_{2.5}$) for Dallas Hinton and Houston Clinton sites.

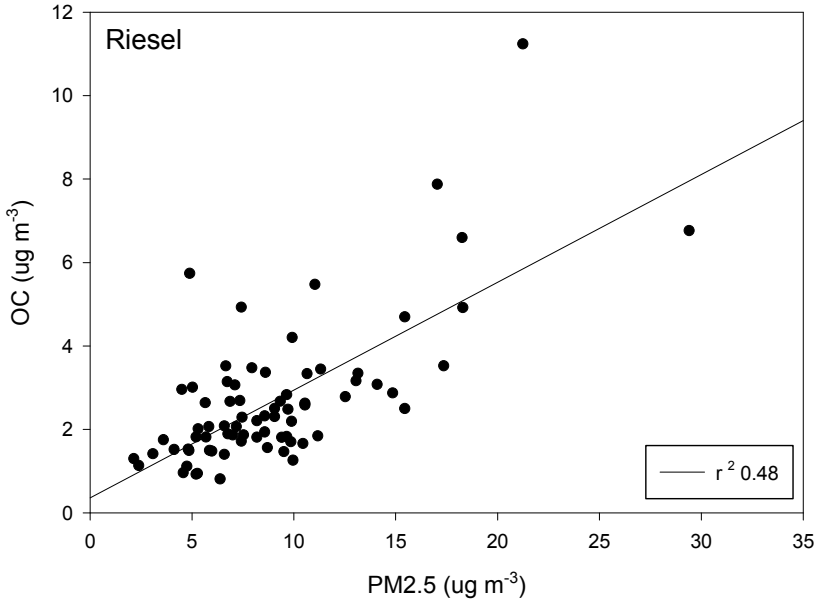

Figure A.7: Regression analysis of OC vs. $PM_{2.5}$ for Riesel, TX.

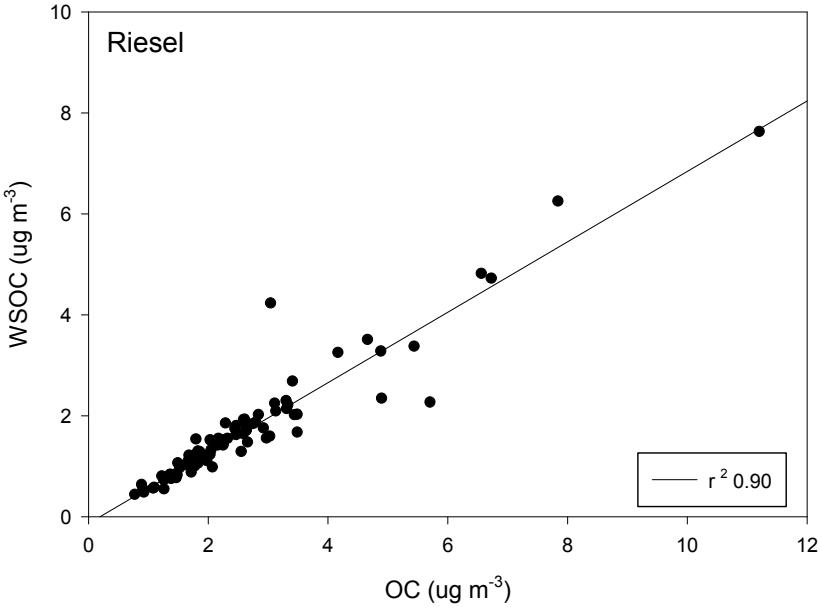

Figure A.8: Regression analysis of WSOC vs. OC for Riesel, TX.

APPENDIX B

Supplemental Material for Source Contributions to Wintertime Elemental and Organic Carbon in the Western Arctic Based on Radiocarbon and Tracer Apportionment

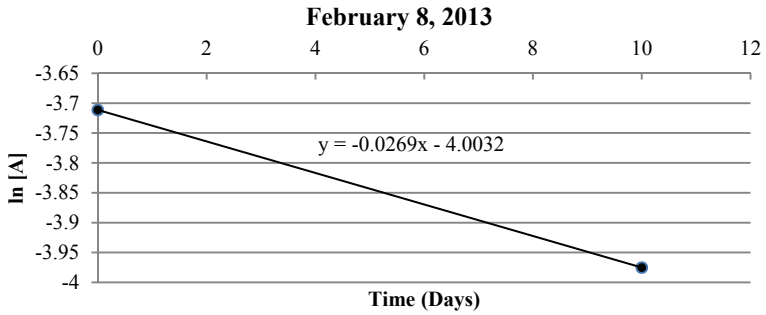

Figure B.1: Graph of *ln* of levoglucosan concentrations at the source (T=0) and the receptor site in Barrow, AK (T=10) for one of the mid-winter samples from the sampling campaign. The slope of the line is equal to -k.

Air volume Normalization

Air volumes were normalized using two co-located instruments (PM2.5 sampler and aethalometer) using the following equation based on the correlation between the two instruments (r^2 =0.91):

$$y = 0.77x-0.002$$

Table B.1: OC and EC Concentrations, Fraction Contemporary, Fraction Fossil, and Fossil and Contemporary Concentrations from Barrow, AK during the study period.

Date	OC (μg m^{-3}) ± uncertainty	OC % Contemporary ± s.e.	OC % Fossil ± s.e.	OC Fossil (μg m^{-3}) ± uncertainty	OC Contemporary (μg m^{-3}) ± uncertainty
12/28/2012-1/5/2013	0.11 ± 0.01	67.5 ± 8.0	32.5 ± 8.0	0.037 ± 0.005	0.076 ± 0.010
1/18-1/25/2013	0.42 ± 0.03	59.9 ± 8.0	40.1 ± 8.0	0.168 ± 0.012	0.252 ± 0.018
2/1-2/8/2013	0.29 ± 0.04	61.3 ± 8.0	38.7 ± 8.0	0.112 ± 0.017	0.177 ± 0.027
2/8-2/15/2013	0.74 ± 0.04	56.3 ± 8.0	43.7 ± 8.0	0.323 ± 0.018	0.417 ± 0.023
2/25-3/1/2013	0.16 ± 0.03	62.6 ± 8.0	37.4 ± 8.0	0.060 ± 0.009	0.100 ± 0.016
3/1-3/11/2013	0.24 ± 0.02	62.6 ± 8.0	37.4 ± 8.0	0.089 ± 0.006	0.149 ± 0.010
Date	EC (μg m^{-3}) ± uncertainty	EC % Contemporary ± s.e.	EC % Fossil ± s.e.	EC Fossil (μg m^{-3}) ± uncertainty	EC Contemporary (μg m^{-3}) ± uncertainty
12/28/2012-1/5/2013	0.04 ± 0.008	33.6 ± 9.2	66.4 ± 9.2	0.013 ± 0.004	0.027 ± 0.002
1/18-1/25/2013	0.077 ± 0.011	32.5 ± 9.2	67.5 ± 9.2	0.052 ± 0.009	0.025 ± 0.004
2/1-2/8/2013	0.067 ± 0.013	28.9 ± 9.2	71.1 ± 9.2	0.048 ± 0.007	0.019 ± 0.003
2/8-2/15/2013	0.097 ± 0.011	31.5 ± 9.2	68.5 ± 9.2	0.067 ± 0.011	0.030 ± 0.005
2/25-3/1/2013	0.036 ± 0.014	50.5 ± 5.6	49.5 ± 5.6	0.018 ± 0.006	0.018 ± 0.006
3/1-3/11/2013	0.041 ± 0.006	51.3 ± 5.6	48.7 ± 5.6	0.021 ± 0.005	0.020 ± 0.005

Target Analyte List

The target analyte list consisted of 28 PAHs: Napthalene*, Acenaphthylene*, Acenapthene*, Fluorene*, Phenanthrene*, Anthracene*, Fluoranthene*, Pyrene*, Benzo[a]anthracene*, Chrysene*, Benzo[b]fluoranthene*, Benzo[k]fluoranthene*, Benzo[a]pyrene*, Benzo[ghi]perylene*, Indeno[1,2,3-cd]pyrene*, Dibenzo[a,h]anthracene*, Benzo[ghi]fluoranthene*, Benzo[e]pyrene*, Perylene*, Retene*, Dibenz[a,e]pyrene*, Coronene*, Picene*, Cyclopenta[1]pyrene *, 1-Methylnaphthalene*, 2-Methylnaphthalene*, 2,6-Dimethylnaphthalene*, 9-Methylanthracene*; 8 steranes and hopanes: ABB-20R-C27-Cholestane*, AAA-20S-C27-Cholestane*, ABB-20R-C28-Methylcholestane*, ABB-20R-C29-Ethylcholestane*, 17A(H)-22,29,30-Trisnorhopane*, 17A(H)-21B(H)-30-Norhopane*, 17A(H)-21B(H)-Hopane*, 17A(H)-21B(H)-22S-Homohopane*; and 25 alkanes: Heptadecane*, Pristane*, Octadecane*, Phytane*, Nonadecane*, Eicosane*, Heneicosane*, Docosane*, Tricosane*, Tetracosane*, Pentacosane*, Hexacosane*, Heptacosane*, Octacosane*, Nonacosane*, Triacontane*, Hentriacontane*, Dotriacontane*, Triatriacontane*, Tetratriacontane*, Pentatriacontane*, Hexatriacontane*, Heptatriacontane*, Octatriacontane*, Nonatriacontane*; as well as levoglucosan.

The isotopically labeled standards were d_{10}-Acenaphthene, d_{10}-Pyrene, d_{12}-Benz[a]anthracene, d_{10}-Phenanthrene, d_{10}-Fluoranthene, d_{12}-Chrysene, d_{12}-Benzo[b] fluoranthene, d_{12}-Benzo[k]fluoranthene, d_{12}-Benzo[a]pyrene, d_{12}-Indeno[1,2,3-cd]pyrene, d_{14}-Dibenz(a,h)anthracene, d_{12}-Coronene, d_{12}-Benzo[e]pyrene, d_4-Cholestane, d_{42}-Eicosane, d_{50}-Tetracosane, d_{58}-Triacontane, d_{66}-Dotriacontane,and d_{74}-Hexatriacontane.

Table B.2: Concentrations of fossil and contemporary EC and OC from the CMB source apportionment.

Date	CMB fossil EC ± uncertainty	CMB Contemporary EC ± uncertainty	CMB fossil OC ± uncertainty	CMB Contemporary OC ± uncertainty
1/18-1/25-2013	0.072 ± 0.012	0.005 ± 0.002	0.089 ± 0.011	0.036 ± 0.017
2/1-2/8/2013	0.053 ± 0.012	0.016 ± 0.006	0.046 ± 0.008	0.11 ± 0.052
2/8-2/15/2013	0.072 ± 0.017	0.027 ± 0.010	0.060 ± 0.010	0.19 ±0.070
2/25-3/1/2013	0.034 ± 0.006	0.003 ± 0.001	0.016 ± 0.003	0.021 ± 0.008

Table B.3: Levoglucosan/EC ratios for different wood smoke emission profiles

	Pine	Pine w/greens	Spruce	Average of Pine w/greens & Spruce	California	Maine	Washington
Levoglucosan/EC	0.92	0.47	0.51	0.49	0.96	0.94	1.80

Table B.4: Calculated half-lives ($\tau_{1/2}$) for 2-day transit times of levoglucosan in the Arctic for different wood smoke emission profiles.

	Pine	Pine w/greens	Spruce	Average of Pine w/greens & Spruce	California	Maine	Washington
EC	$\tau_{1/2}$ (h)	$\tau_{1/2}$ (h)	$\tau_{1/2}$ (h)	$\tau_{1/2}$ (h)	$\tau_{1/2}$ (h)	$\tau_{1/2}$ (h)	$\tau_{1/2}$ (h)
1/18-1/25-2013	20.2	34.3	31.4	32.6	19.6	19.9	14.3
2/1-2/8/2013	133.6	-79.2	-97.9	-87.6	114.7	128.0	36.2
2/8-2/15/2013	106.6	-92.5	-118.8	-104.6	95.1	100.8	34.0
2/25-3/1/2013	20.1	33.8	31.2	32.5	19.6	19.9	14.3

Table B.5: Calculated half-lives ($\tau_{1/2}$) for 5-day transit times of levoglucosan in the Arctic for different wood smoke emission profiles.

EC	Pine $\tau_{1/2}$ (h)	Pine w/greens $\tau_{1/2}$ (h)	Spruce $\tau_{1/2}$ (h)	Average of Pine w/greens & Spruce $\tau_{1/2}$ (h)	California $\tau_{1/2}$ (h)	Maine $\tau_{1/2}$ (h)	Washington $\tau_{1/2}$ (h)
1/18-1/25-2013	50.4	85.8	78.5	81.5	49.1	49.8	35.9
2/1-2/8/2013	334.0	-198.0	-244.6	-218.9	286.8	319.9	90.4
2/8-2/15/2013	266.6	-231.2	-297.1	-261.6	237.7	252.1	84.9
2/25-3/1/2013	50.3	84.6	78.1	81.1	49.0	49.7	35.8

Table B.6: Calculated half-lives ($\tau_{1/2}$) for 10-day transit times of levoglucosan in the Arctic for different wood smoke emission profiles.

EC	Pine $\tau_{1/2}$ (h)	Pine w/greens $\tau_{1/2}$ (h)	Spruce $\tau_{1/2}$ (h)	Average of Pine w/greens & Spruce $\tau_{1/2}$ (h)	California $\tau_{1/2}$ (h)	Maine $\tau_{1/2}$ (h)	Washington $\tau_{1/2}$ (h)
1/18-1/25-2013	100.8	171.5	156.9	163.1	98.2	99.6	71.7
2/1-2/8/2013	668.1	-396.1	-489.3	-437.8	573.6	639.8	180.8
2/8-2/15/2013	533.2	-462.5	-594.1	-523.1	475.3	504.1	169.8
2/25-3/1/2013	100.5	169.1	156.2	162.3	98.0	99.3	71.5

Table B.7: Sensitivity analysis of inadvertent pryolyzed carbon (PyrC) inclusion from 0-25% in EC isolation for isotope analysis.

Date	"True" EC F_{fossil} (%) 0% PyrC	"True" EC F_{fossil} (%) 5% PyrC	"True" EC F_{fossil} (%) 10% PyrC	"True" EC F_{fossil} (%) 15% PyrC	"True" EC F_{fossil} (%) 20% PyrC	"True" EC F_{fossil} (%) 25% PyrC
12/28/2012-1/5/2013	66.4	68.3	70.6	73.3	76.7	80.7
1/18-1/25/2013	67.5	69.0	70.8	72.9	75.4	78.3
2/1-2/8/2013	71.1	72.9	75.0	77.5	80.5	84.1
2/8-2/15/2013	68.5	69.8	71.4	73.3	75.5	78.0
2/25-3/1/2013	49.5	50.2	51.1	52.1	53.5	55.1
3/1-3/11/2013	48.7	49.3	50.1	51.1	52.3	53.7

Table B.8: Total Organic Carbon (TOC) and Elemental Carbon (EC) sample mass (µg C/cm2 to AMS) and TOC and EC fraction modern for samples included in this study. Sample mass and fraction modern for field blanks are also included. At least 100 µg C was submitted for radiocarbon analysis for each sample.

Date	TOC Sample Mass (ug C/cm^2 to AMS)	TOC Fraction Modern	EC Sample Mass (ug C/cm^2 to AMS)	EC Fraction Modern
Field Blank 1	0.53	0.2255 ± 0.0024		
Field Blank 2	0.81	0.3856 ± 0.0050		
12/28/2012-1/5/2013	11.84	0.6344 ± 0.0020	5.01	0.3586 ± 0.0014
1/18-1/25/2013	20.59	0.6113 ± 0.0023	4.38	0.3464 ± 0.0014
2/1-2/8/2013	18.32	0.6045 ± 0.0020	4.08	0.3100 ± 0.0013
2/8-2/15/2013	18.92	0.5862 ± 0.0020	3.38	0.3314 ± 0.0013
2/25-3/1/2013	8.39	0.6459 ± 0.0040	2.82	0.5129 ± 0.0048
3/1-3/11/2013	15.43	0.6642 ± 0.0024	3.85	0.5333 ± 0.0023

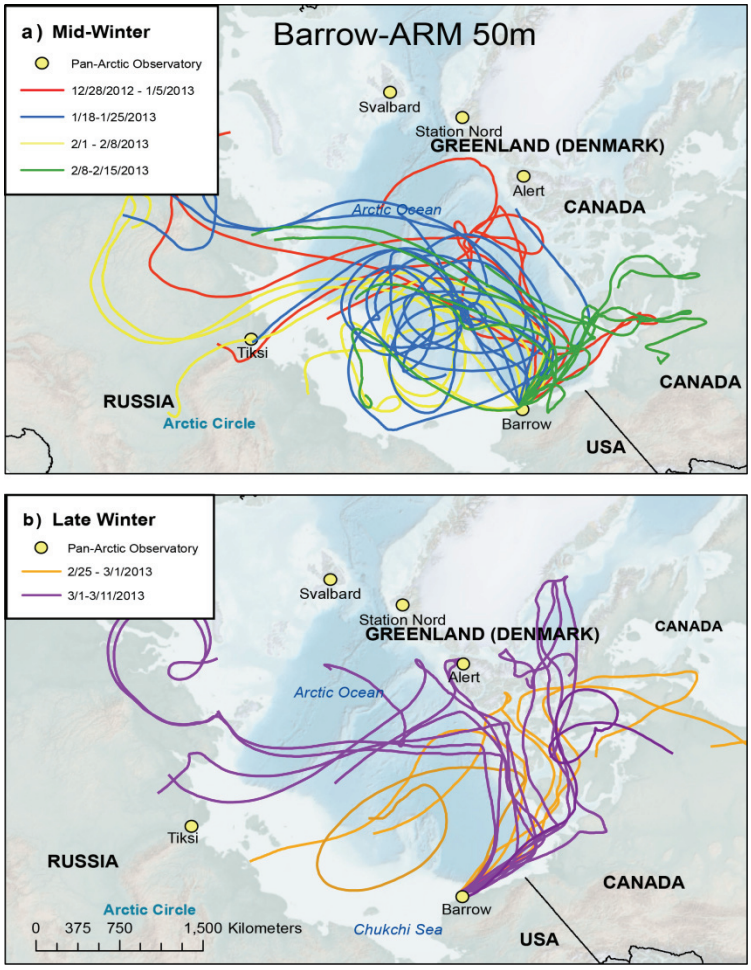

Figure B.2: Back trajectory sensitivity test results for the sampling location with a starting height of 50 meters above ground level.

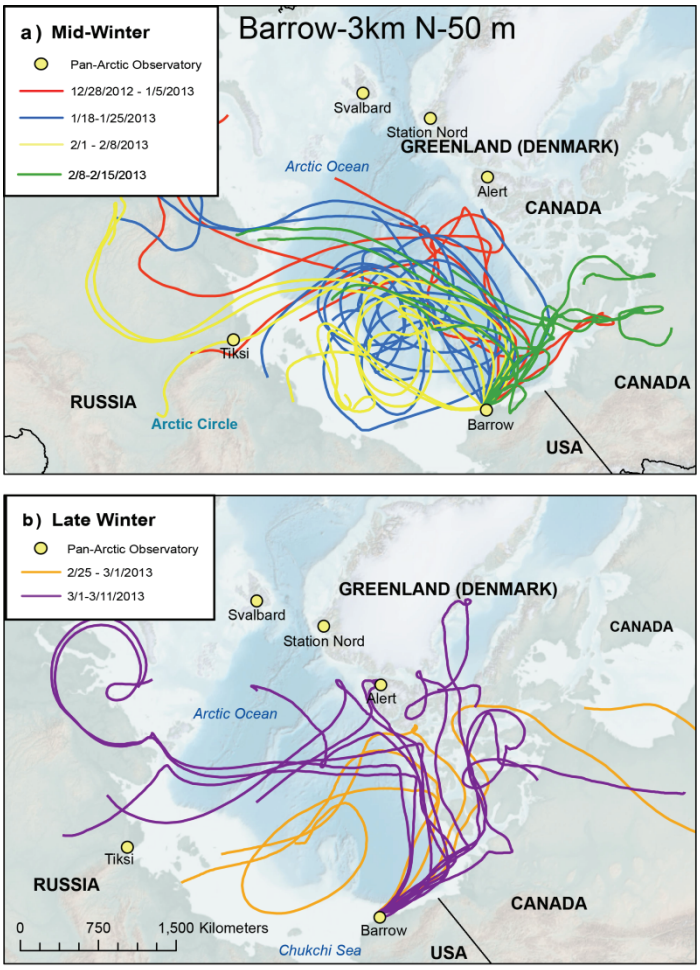

Figure B.3: Back trajectory sensitivity test results from 3 km north of the sampling location with a starting height of 50 meters above ground level.

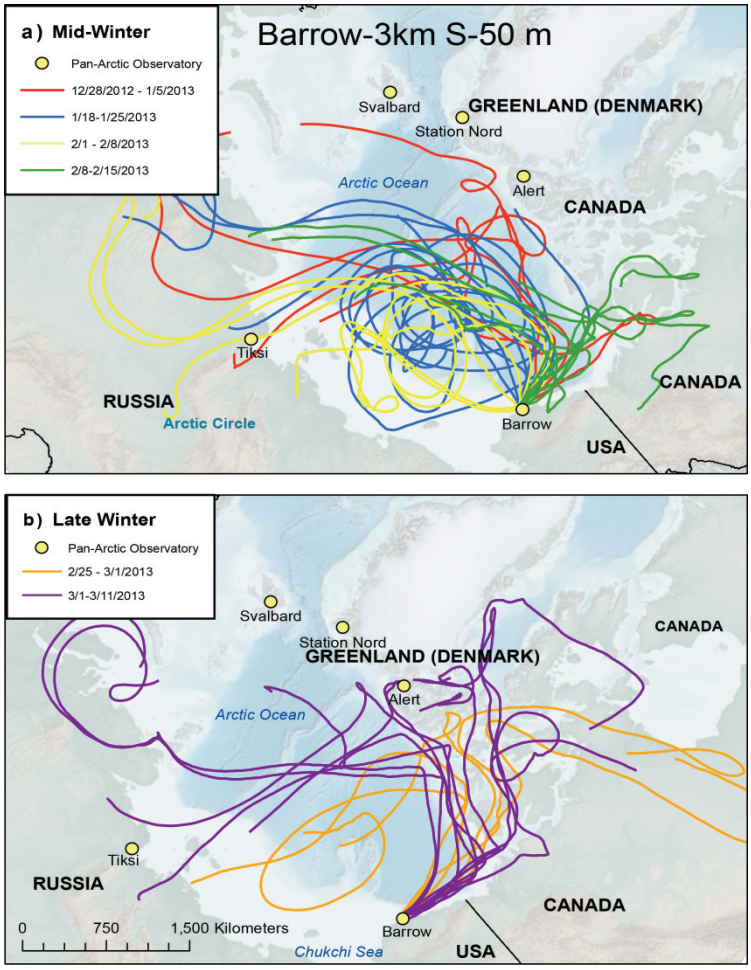

Figure B.4: Back trajectory sensitivity test results from 3 km south of the sampling location with a starting height of 50 meters above ground level.

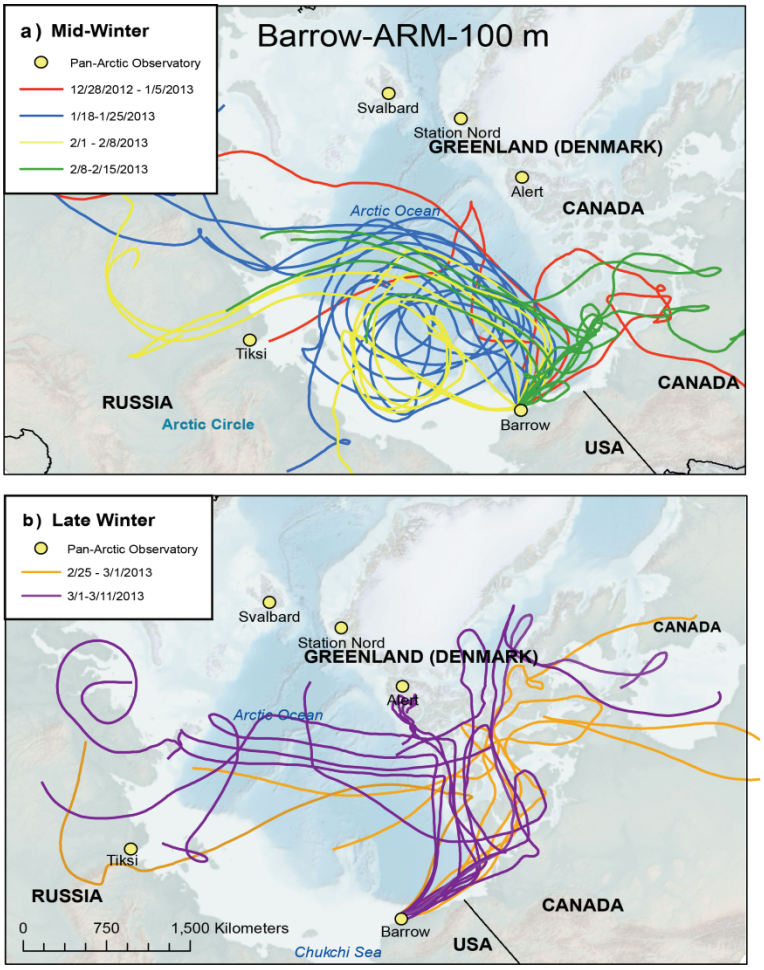

Figure B.5: Back trajectory sensitivity test results for the sampling location with a starting height of 100 meters above ground level.

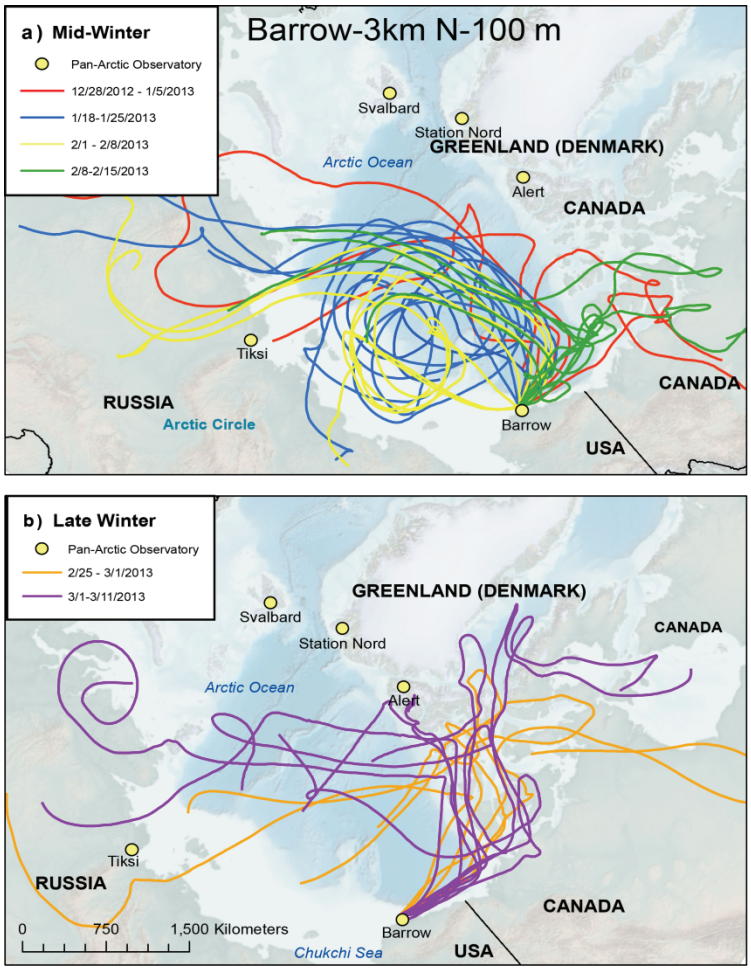

Figure B.6: Back trajectory sensitivity test results from 3 km north of the sampling location with a starting height of 100 meters above ground level.

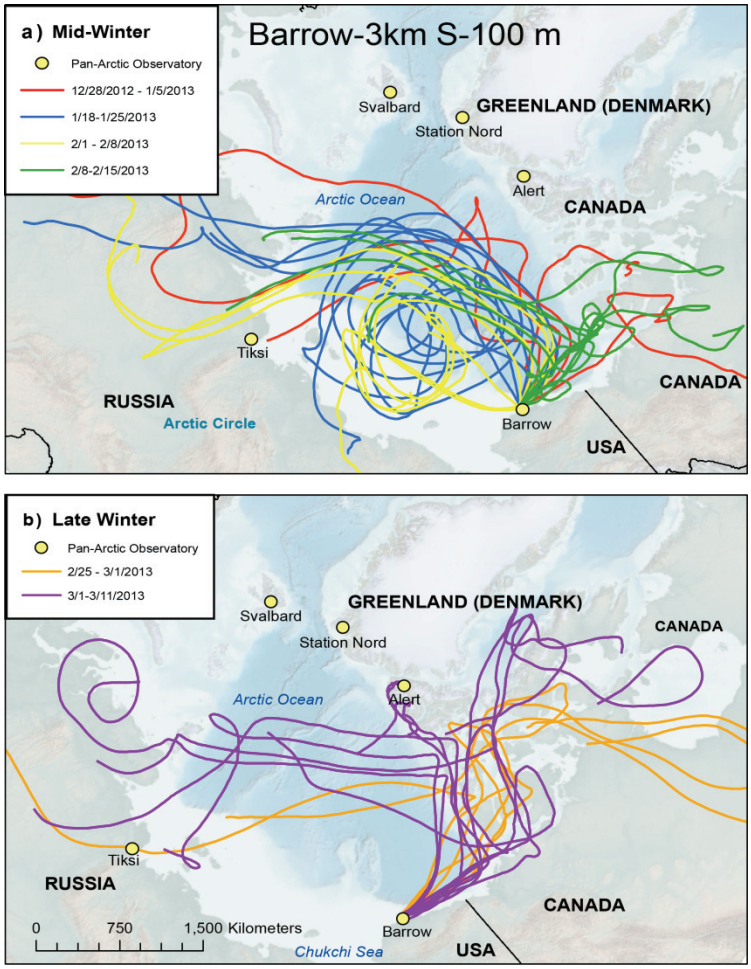

Figure B.7: Back trajectory sensitivity test results from 3 km south of the sampling location with a starting height of 100 meters above ground level.

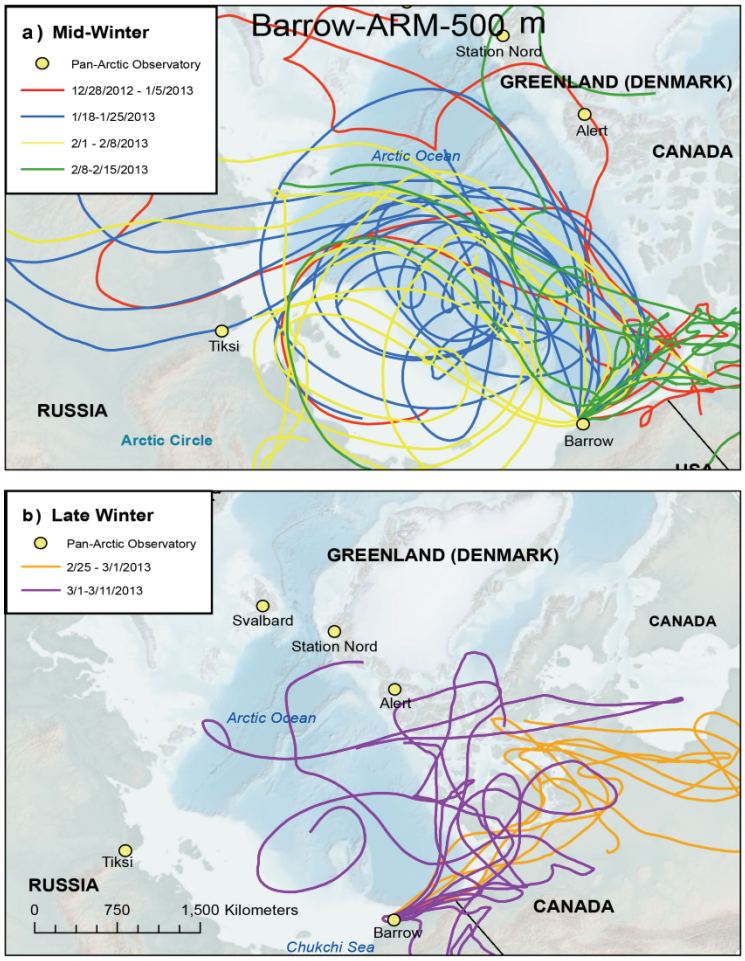

Figure B.8: Back trajectory sensitivity test results for the sampling location with a starting height of 500 meters above ground level.

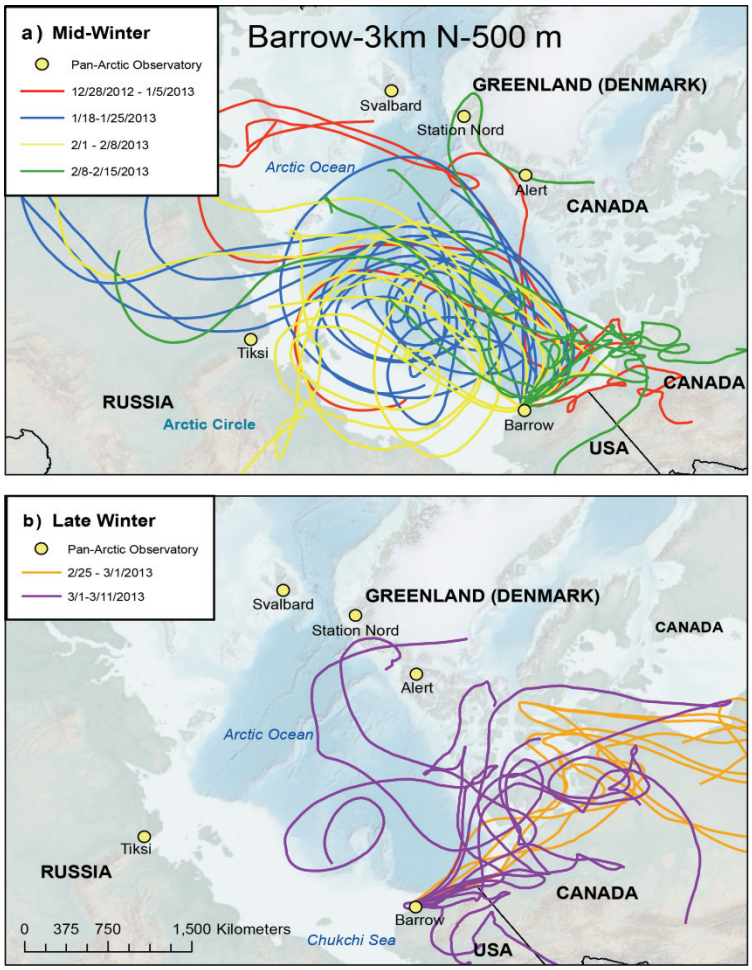

Figure B.9: Back trajectory sensitivity test results from 3 km north of the sampling location with a starting height of 500 meters above ground level.

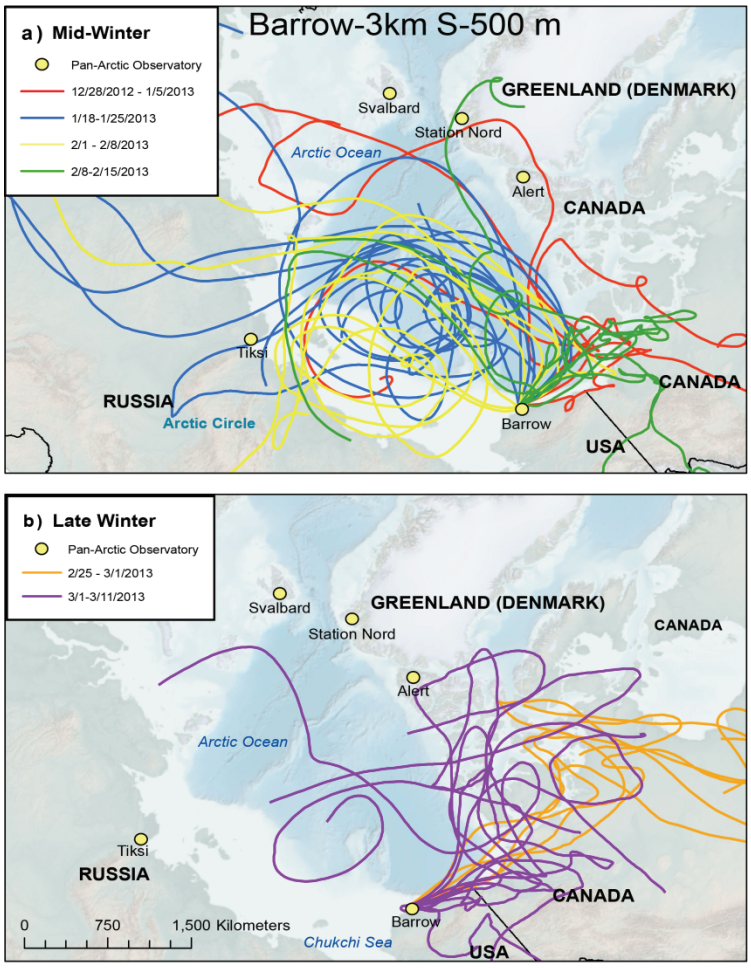

Figure B.10: Back trajectory sensitivity test results from 3 km south of the sampling location with a starting height of 50 meters above ground level.

APPENDIX C

Supplemental Material for Year-round Characterization of Sources and Optical Properties of Arctic Organic Carbon Aerosols in the North Slope Alaska

Table C.1: Composites, samples included, date ranges, back trajectory source regions and contemporary and fossil contributions to OC for each composite.

Composite	Samples Included	Date Range	Back Trajectory Source Regions	% Cont. OC	% Fossil OC
Summer 1	PM10-005 PM10-008	7/16-7/23/12, 8/3-8/12/12	Russian Arctic, Western Alaska	66.7 ± 9.8%	33.3 ± 9.8%
Summer 2	PM10-006 PM10-007 PM10-009 PM10-010 PM10-011	7/23-8/3/12, 8/12-8/31/12	Russian Arctic, Western Alaska, Arctic Ocean, Canadian Arctic	78.8 ± 9.8%	21.2 ± 9.8%
Fall 1	PM10-014#2 PM10-015 PM10-017 PM10-018	9/21-10/5/12, 10/12-10/26/12	Russian Arctic, Western Alaska, Arctic Ocean, Canadian Arctic	38.6 ± 9.8%	61.4 ± 9.8%
Winter 1	PM10-020 PM10-021 PM10-022	11/3-11/26/12	Russian Arctic, Alaskan Arctic, Arctic Ocean	59.5 ± 9.8%	40.5 ± 9.8%
Winter 2	PM10-023 PM10-024 PM10-025 PM10-026	11/26-12/21/12	Russian Arctic, Alaskan Arctic, Arctic Ocean, Canadian Arctic	55.6 ± 9.8%	44.4 ± 9.8%
Spring 1	PM10-038 PM10-040	3/20-3/29/13, 4/4-4/12/13	Russian Arctic, Canadian Arctic, Arctic Ocean	68.9 ± 9.8%	31.1 ± 9.8%
Summer 3	PM10-041 PM10-042	4/12/-4/26/13	Russian Arctic, Western Alaska, Arctic Ocean	60.1 ± 9.8%	39.9 ± 9.8%
Summer 4	PM10-045 PM-046	5/10-5/24/13	Russian Arctic, Western Alaska, Arctic Ocean, Canadian Arctic	78.3 ± 9.8%	21.7 ± 9.8%
Summer 5	PM10-048 PM10-049	5/27-6/4/13	Western Alaska, Alaskan Arctic	60.4 ± 9.8%	39.6 ± 9.8%

Table C.2: Organic carbon, water-soluble organic carbon concentrations, mass absorption efficiency (MAE_{365}), and absorbing Angstrom exponents (AAE) for samples from the sampling campaign. * indicates not available.

Sample ID	Start Date	End Date	OC ($\mu g/m^3$)	OC unc.	WSOC ($\mu g/m^3$)	WSOC unc.	MAE ($m^2\ g^{-1}$)	AAE	Season
BRW-PM10-003	6/29/2012	7/6/2012	0.29	0.027	0.22	0.022	*	*	Summer
BRW-PM10-005	7/16/2012	7/23/2012	0.091	0.037	0.04	0.004	0.76	2.67	Summer
BRW-PM10-006	7/23/2012	7/30/2012	0.392	0.021	0.23	0.023	0.31	6.16	Summer
BRW-PM10-007	7/30/2012	8/3/2012	0.081	0.014	0.05	0.005	1.76	3.14	Summer
BRW-PM10-008	8/3/2012	8/12/2012	0.081	0.024	0.05	0.005	0.37	2.73	Summer
BRW-PM10-009	8/12/2012	8/18/2012	0.949	0.056	0.49	0.049	0.22	6.37	Summer
BRW-PM10-010	8/18/2012	8/24/2012	0.453	0.050	0.17	0.017	0.43	4.17	Summer
BRW-PM10-011	8/24/2013	8/31/2012	0.089	0.026	0.04	0.004	0.97	5.18	Summer
BRW-PM10-013	9/7/2012	9/14/2012	0.275	0.012	0.16	0.016	2.20	2.97	Fall
BRW-PM10-014	9/14/2012	9/21/2012	0.703	0.020	0.35	0.035	2.05	2.39	Fall
BRW-PM10-014#2	9/21/2012	9/28/2012	0.018	0.008	0.01	0.001	2.25	3.26	Fall
BRW-PM10-015	9/28/2012	10/5/2012	0.008	0.010	0.01	0.001	1.32	4.73	Fall
BRW-PM10-016	10/5/2012	10/12/2012	0.527	0.017	0.29	0.029	0.23	3.74	Fall
BRW-PM10-017	10/12/2012	10/19/2012	0.109	0.018	0.04	0.004	1.61	2.61	Fall
BRW-PM10-018	10/19/2012	10/26/2012	0.066	0.010	0.03	0.003	1.97	1.43	Fall
BRW-PM10-020	11/3/2012	11/9/2012	0.161	0.016	0.11	0.011	0.50	3.6	Winter
BRW-PM10-021	11/9/2012	11/16/2012	0.207	0.020	0.13	0.013	0.83	9.59	Winter
BRW-PM10-022	11/16/2012	11/26/2012	0.125	0.024	0.07	0.007	0.74	2.7	Winter
BRW-PM10-023	11/26/2012	11/30/2012	0.036	0.004	0.02	0.002	0.96	6.2	Winter
BRW-PM10-024	11/30/2012	12/7/2012	0.022	0.002	0.01	0.001	1.03	6.63	Winter
BRW-PM10-025	12/7/2012	12/14/2012	0.075	0.006	0.04	0.004	0.73	6.06	Winter
BRW-PM10-026	12/14/2012	12/21/2012	0.058	0.005	0.03	0.003	1.17	3.62	Winter

Sample ID	Start Date	End Date	OC ($\mu g/m^3$)	OC unc.	WSOC ($\mu g/m^3$)	WSOC unc.	MAE ($m^2\ g^{-1}$)	AAE	Season
BRW-PM10-027	12/21/2012	12/28/2012	0.253	0.021	0.14	0.014	0.56	3.46	Winter
BRW-PM10-028	12/28/2012	1/5/2013	0.115	0.008	0.06	0.006	0.75	2.6	Winter
BRW-PM10-029	1/5/2013	1/18/2013	0.158	0.016	0.09	0.009	0.96	9.22	Winter
BRW-PM10-030	1/18/2013	1/25/2013	0.426	0.027	0.23	0.023	1.06	5.01	Winter
BRW-PM10-032	2/1/2013	2/8/2013	0.293	0.018	0.18	0.018	0.69	3.87	Winter
BRW-PM10-033	2/8/2013	2/15/2013	0.748	0.045	0.40	0.040	0.63	5.21	Winter
BRW-PM10-034	2/15/2013	2/25/2013	0.499	0.038	0.30	0.030	0.87	3.3	Winter
BRW-PM10-035	2/25/2013	3/1/2013	0.166	0.015	0.13	0.013	0.99	1.83	Winter
BRW-PM10-036	3/1/2013	3/11/2013	0.244	0.018	0.20	0.020	0.69	3.3	Winter
BRW-PM10-038	3/20/2013	3/29/2013	0.052	0.005	0.04	0.004	1.03	3.96	Spring
BRW-PM10-039	3/29/2013	4/4/2013	0.108	0.011	0.08	0.008	0.63	2.84	Spring
BRW-PM10-040	4/4/2013	4/12/2013	0.079	0.018	0.05	0.005	0.55	1.92	Spring
BRW-PM10-041	4/12/2013	4/22/2013	0.097	0.006	0.06	0.006	0.37	3.54	Summer
BRW-PM10-042	4/22/2013	4/26/2013	0.125	0.011	0.08	0.008	0.46	1.62	Summer
BRW-PM10-045	5/10/2013	5/17/2013	0.030	0.012	0.02	0.002	0.80	1.35	Summer
BRW-PM10-046	5/17/2013	5/24/2013	0.022	0.011	0.02	0.002	1.29	1.94	Summer
BRW-PM10-049	5/31/2013	6/4/2013	0.079	0.032	0.05	0.005	0.46	1.39	Summer

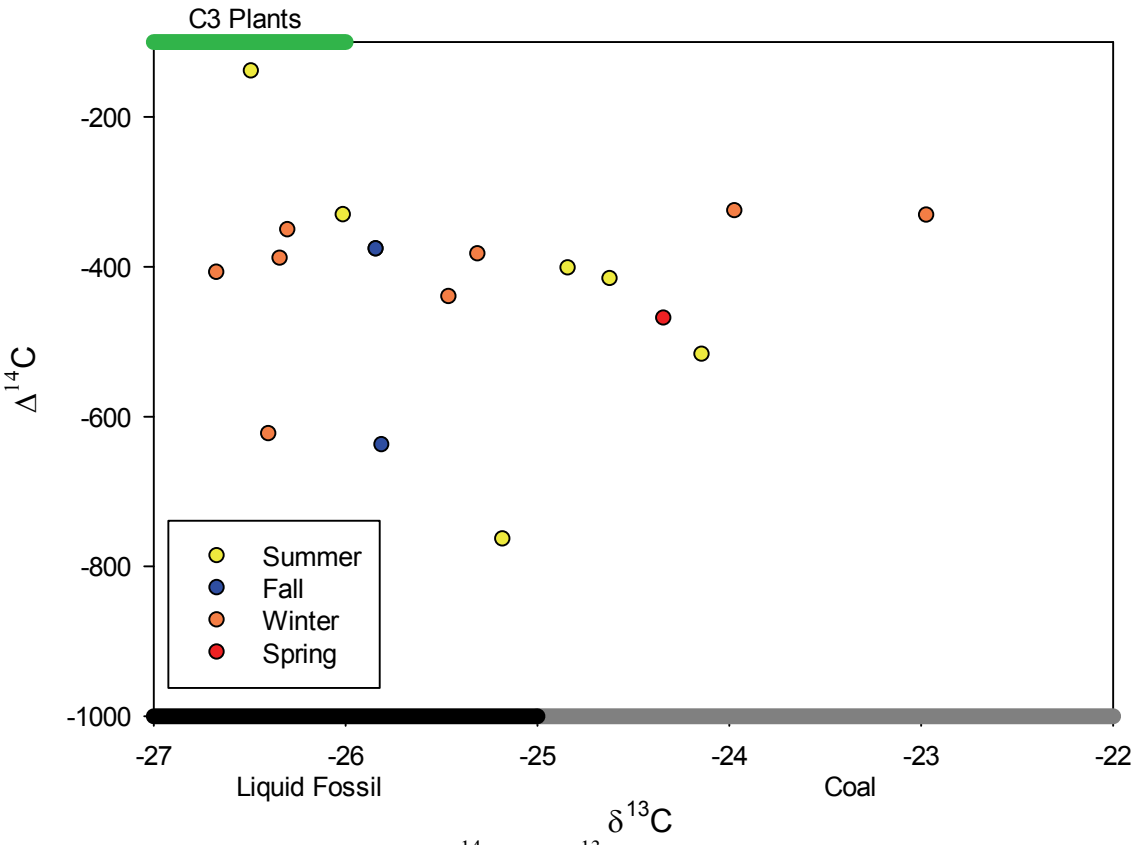

Figure C.1: Scatter plot of $\Delta^{14}C$ and $\delta^{13}C$ for total organic carbon (TOC).

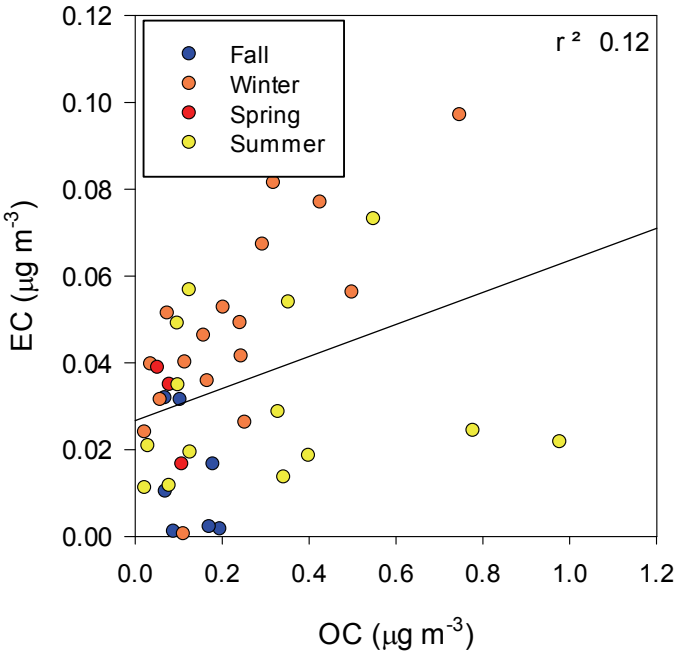

Figure C.2: Regression of organic carbon (OC) and elemental carbon (EC) for Barrow, AK.

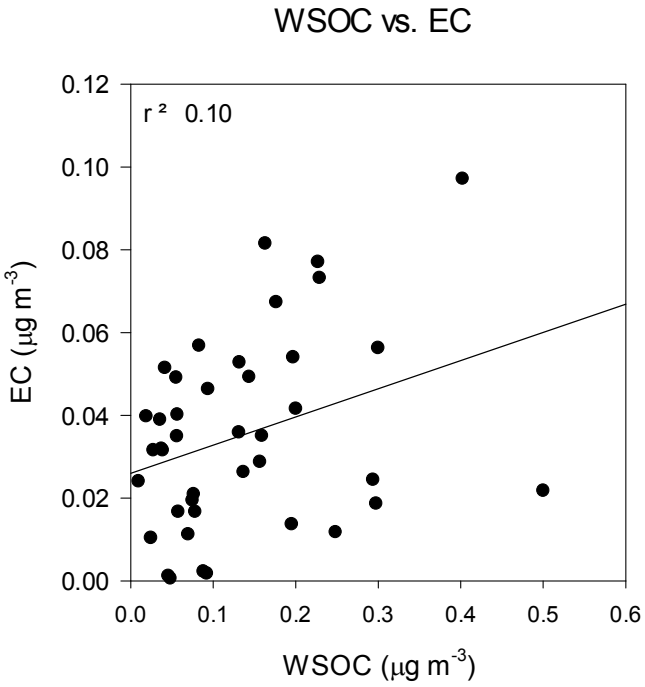

Figure C.3: Regression of water-soluble organic carbon (WSOC) and elemental carbon (EC) for Barrow, AK.

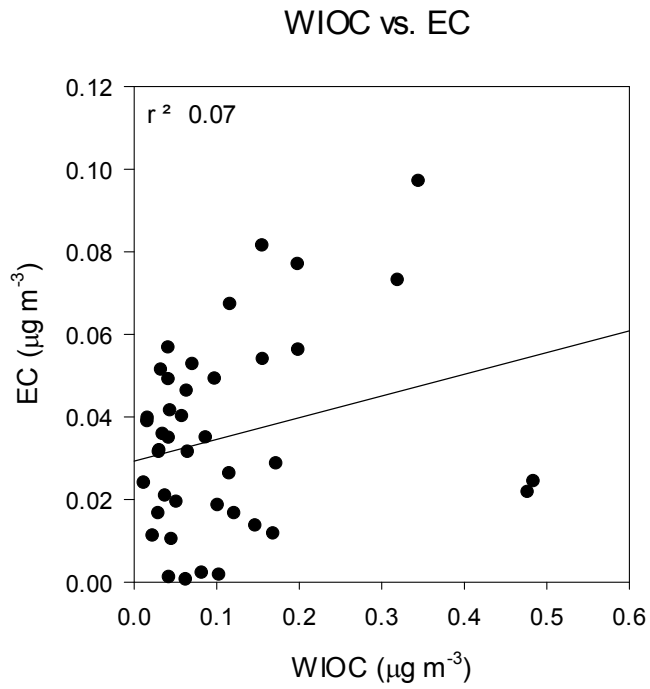

Figure C.4: Regression of water-insoluble organic carbon (WIOC) and elemental carbon (EC) for Barrow, AK.

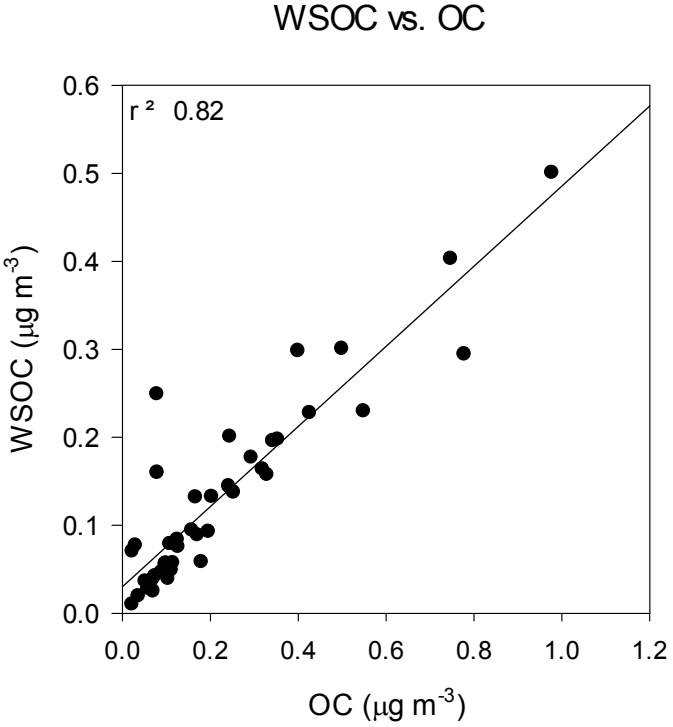

Figure C.5: Regression of organic carbon (OC) and water-soluble organic carbon (WSOC) for Barrow, AK

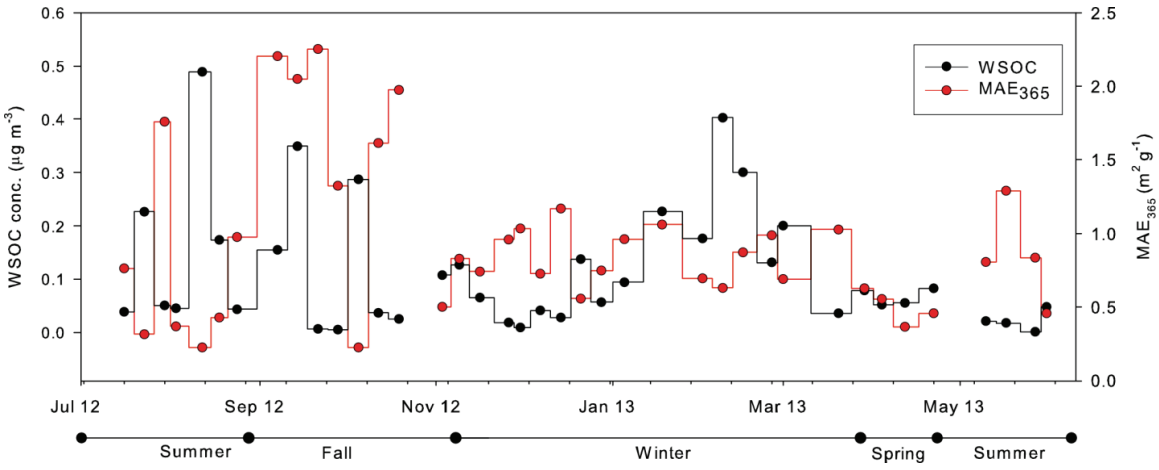

Figure C.6: Water-soluble organic carbon (WSOC) and mass absorption efficiency at 365 nm (MAE_{365}) timeline for the duration of the sampling campaign.

APPENDIX D

Supporting Information for Annual Contributions of Fossil Fuel Combustion and Biomass Burning Sources to Atmospheric Elemental Carbon in the North American Arctic Using Radiocarbon Abundance Measurements

Table D.1: Composites, samples included, date ranges, back trajectory source regions and contemporary and fossil contributions to OC for each composite.

Composite	Samples Included	Date Range	Back Trajectory Source Regions	% Cont. OC	% Fossil OC
Summer 1	PM10-005 PM10-008	7/16-7/23/12, 8/3-8/12/12	Russian Arctic, Western Alaska	15.4 ± 9.8%	84.6 ± 9.8%
Summer 2	PM10-006 PM10-007 PM10-009 PM10-010 PM10-011	7/23-8/3/12, 8/12-8/31/12	Russian Arctic, Western Alaska, Arctic Ocean, Canadian Arctic	52.7 ± 9.8%	47.3 ± 9.8%
Fall 1	PM10-014#2 PM10-015 PM10-017 PM10-018	9/21-10/5/12, 10/12-10/26/12	Russian Arctic, Western Alaska, Arctic Ocean, Canadian Arctic	8.1 ± 9.8%	91.9 ± 9.8%
Winter 1	PM10-020 PM10-021 PM10-022	11/3-11/26/12	Russian Arctic, Alaskan Arctic, Arctic Ocean	14.4 ± 9.8%	85.6 ± 9.8%
Winter 2	PM10-023 PM10-024 PM10-025 PM10-026	11/26-12/21/12	Russian Arctic, Alaskan Arctic, Arctic Ocean, Canadian Arctic	8.0 ± 9.8%	92.0 ± 9.8%
Spring 1	PM10-038 PM10-040	3/20-3/29/13, 4/4-4/12/13	Russian Arctic, Canadian Arctic, Arctic Ocean	10.4 ± 9.8%	89.6 ± 9.8%
Summer 3	PM10-041 PM10-042	4/12/-4/26/13	Russian Arctic, Western Alaska, Arctic Ocean	10.5 ± 9.8%	89.5 ± 9.8%
Summer 4	PM10-045 PM-046	5/10-5/24/13	Russian Arctic, Western Alaska, Arctic Ocean, Canadian Arctic	10.4 ± 9.8%	89.6 ± 9.8%
Summer 5	PM10-048 PM10-049	5/27-6/4/13	Western Alaska, Alaskan Arctic	20.2 ± 9.8%	79.8 ± 9.8%

Table D.2: Elemental carbon concentrations and mass absorption efficiencies for samples collected during the sampling campaign.

Sample ID	Start Date	End Date	EC Conc. ($\mu g\ m^{-2}$)	EC unc.	MAC ($m^2\ g^{-1}$)	Season
BRW-PM10-003	6/29/2012	7/6/2012	0.014	0.002	6.47	Summer
BRW-PM10-005	7/16/2012	7/23/2012	0.012	0.002	7.57	Summer
BRW-PM10-006	7/23/2012	7/30/2012	0.016	0.003	10.99	Summer
BRW-PM10-007	7/30/2012	8/3/2012	0.013	0.002	6.53	Summer
BRW-PM10-008	8/3/2012	8/12/2012	0.013	0.002	8.39	Summer
BRW-PM10-009	8/12/2012	8/18/2012	0.021	0.004	13.54	Summer
BRW-PM10-010	8/18/2012	8/24/2012	0.014	0.002	16.48	Summer
BRW-PM10-011	8/24/2013	8/31/2012	0.008	0.001	8.09	Summer
BRW-PM10-014#2	9/21/2012	9/28/2012	0.003	0.001	13.09	Fall
BRW-PM10-015	9/28/2012	10/5/2012	0.004	0.001	7.31	Fall
BRW-PM10-017	10/12/2012	10/19/2012	0.011	0.002	35.06	Fall
BRW-PM10-018	10/19/2012	10/26/2012	0.021	0.004	13.44	Fall
BRW-PM10-020	11/3/2012	11/9/2012	0.043	0.007	11.31	Winter
BRW-PM10-021	11/9/2012	11/16/2012	0.043	0.007	17.62	Winter
BRW-PM10-022	11/16/2012	11/26/2012	0.033	0.006	14.04	Winter
BRW-PM10-023	11/26/2012	11/30/2012	0.040	0.007	7.71	Winter
BRW-PM10-024	11/30/2012	12/7/2012	0.024	0.004	7.33	Winter
BRW-PM10-025	12/7/2012	12/14/2012	0.051	0.009	9.29	Winter
BRW-PM10-026	12/14/2012	12/21/2012	0.031	0.005	9.04	Winter
BRW-PM10-028	12/28/2012	1/5/2013	0.040	0.007	11.67	Winter
BRW-PM10-030	1/18/2013	1/25/2013	0.077	0.013	14.53	Winter
BRW-PM10-032	2/1/2013	2/8/2013	0.067	0.011	13.30	Winter
BRW-PM10-033	2/8/2013	2/15/2013	0.097	0.017	21.39	Winter
BRW-PM10-035	2/25/2013	3/1/2013	0.036	0.006	8.94	Winter

Sample ID	Start Date	End Date	EC Conc. ($\mu g\ m^{-2}$)	EC unc.	MAC ($m^2\ g^{-1}$)	Season
BRW-PM10-036	3/1/2013	3/11/2013	0.041	0.007	14.54	Winter
BRW-PM10-038	3/20/2013	3/29/2013	0.039	0.007	6.61	Spring
BRW-PM10-040	4/4/2013	4/12/2013	0.035	0.006	6.86	Spring
BRW-PM10-041	4/12/2013	4/22/2013	0.049	0.008	5.03	Summer
BRW-PM10-042	4/22/2013	4/26/2013	0.057	0.010	6.21	Summer
BRW-PM10-045	5/10/2013	5/17/2013	0.024	0.004	6.52	Summer
BRW-PM10-046	5/17/2013	5/24/2013	0.021	0.004	4.65	Summer
BRW-PM10-048	5/27/2013	5/31/2013	0.001	0.000	5.21	Summer
BRW-PM10-049	5/31/2013	6/4/2013	0.012	0.002	3.88	Summer

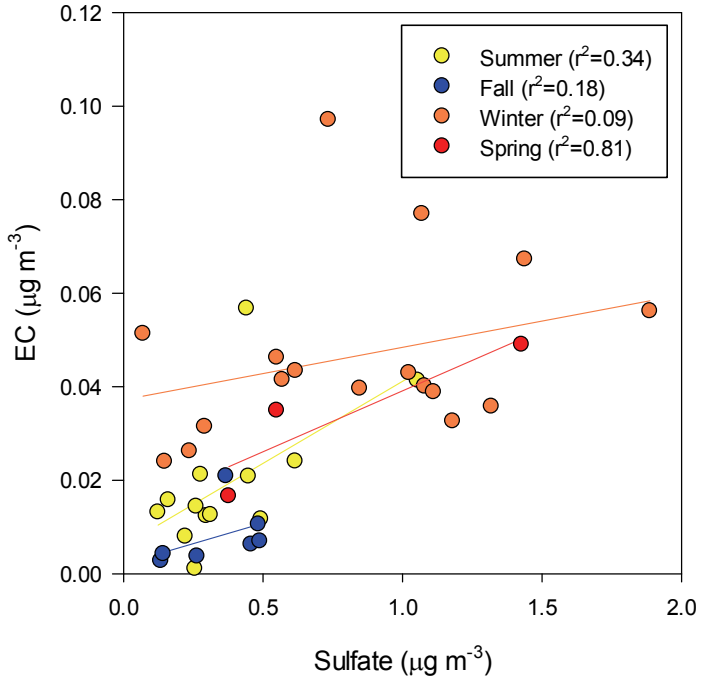

Figure D.1: Sulfate vs. EC concentrations for each season.

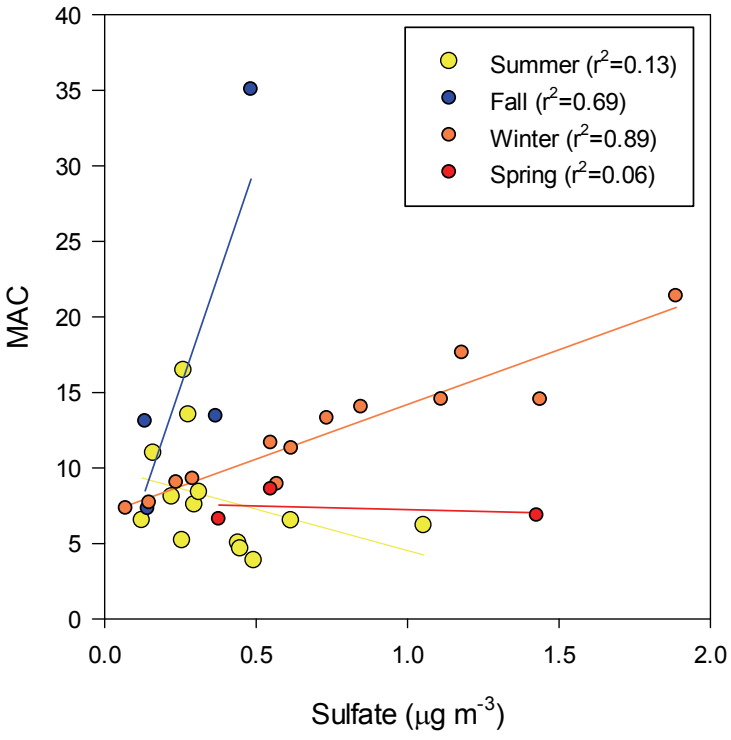

Figure D.2: Sulfate vs. MAC for each season.

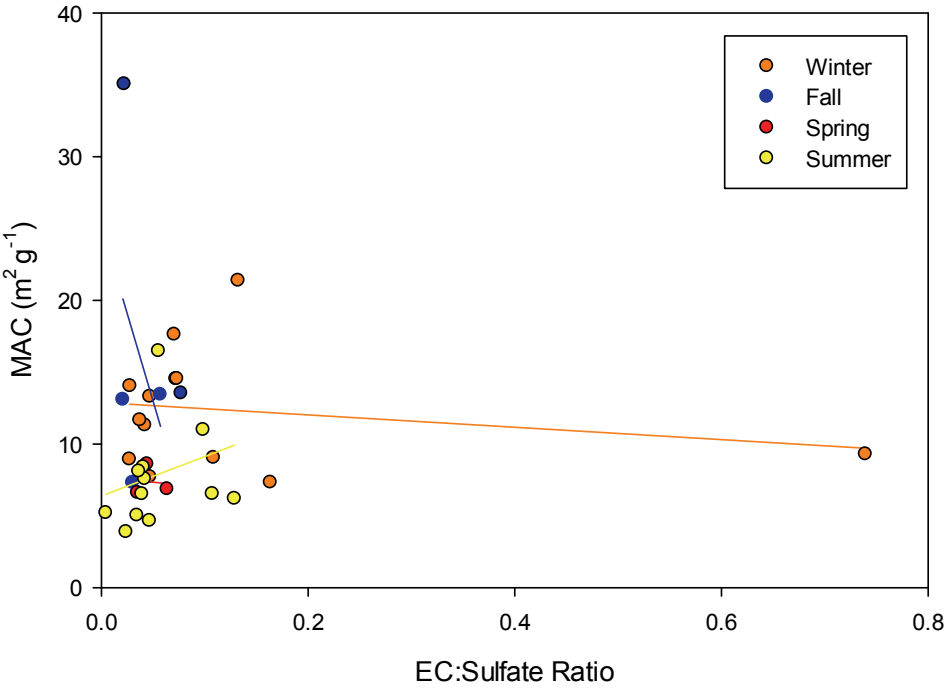

Figure D.3: Correlation of EC:Sulfate ratios and MAC for each season.

BIBLIOGRAPHY

"2011 Traffic Maps." 2012. Accessed August 9, 2013. http://www.txdot.gov/inside-txdot/division/transportation-planning/maps/traffic.html.

Anderson, C., et al. 2008. "Simultaneous Measurements of Particulate and Gas-Phase Water-Soluble Organic Carbon Concentrations at Remote and Urban-Influenced Locations." *Geophysical Research Letters* 35, no. 13 (Jul). http://dx.doi.org/10.1029/2008gl033966.

Anderson, T. L., et al. 2003. "Climate Forcing by Aerosols - a Hazy Picture." *Science* 300, no. 5622 (May): 1103-1104. http://dx.doi.org/10.1126/science.1084777.

Andersson, A., et al. 2011. "C-14-Based Source Assessment of Soot Aerosols in Stockholm and the Swedish Emep-Aspvreten Regional Background Site." *Atmospheric Environment* 45, no. 1 (Jan): 215-222. http://dx.doi.org/10.1016/j.atmosenv.2010.09.015.

Andersson, A, et al. 2015. "Regionally-Varying Combustion Sources of the January 2013 Severe Haze Events over Eastern China." *Environmental Science & Technology* 49, no. 4 (Feb 17): 2038-2043. http://dx.doi.org/10.1021/es503855e.

Andreae, M. O., and A. Gelencser. 2006. "Black Carbon or Brown Carbon? The Nature of Light-Absorbing Carbonaceous Aerosols." *Atmospheric Chemistry and Physics* 6 (Jul): 3131-3148. http://dx.doi.org /WOS:000239346600001.

Arctic Monitoring and Assessment Programme, AMAP. 2015. *Amap Assessment 2015: Black Carbon and Ozone as Arctic Climate Forcers*. Vol. vii. Oslo, Norway: Arctic Monitoring and Assessment Programme.

Asa-Awuku, Akua, et al. 2011. "Airborne Cloud Condensation Nuclei Measurements During the 2006 Texas Air Quality Study." *Journal of Geophysical Research-Atmospheres* 116 (Jun 1). http://dx.doi.org/10.1029/2010jd014874.

Bahadur, R., et al. 2012. "Solar Absorption by Elemental and Brown Carbon Determined from Spectral Observations." *Proceedings of the National Academy of Sciences of the United States of America* 109, no. 43 (Oct): 17366-17371. http://dx.doi.org/10.1073/pnas.1205910109.

Bahreini, R., et al. 2009. "Organic Aerosol Formation in Urban and Industrial Plumes near Houston and Dallas, Texas." *Journal of Geophysical Research-Atmospheres* 114 (Aug). http://dx.doi.org/10.1029/2008jd011493.

Barrett, T. E., et al. 2015. "Source Contributions to Wintertime Elemental and Organic Carbon in the Western Arctic Based on Radiocarbon and Tracer Apportionment." *Environmental Science & Technology* 49, no. 19 (Oct 6): 11631-9. http://dx.doi.org/10.1021/acs.est.5b03081.

Barrett, T.E., and R. J. Sheesley. 2014. "Urban Impacts on Regional Carbonaceous Aerosols: Case Study in Central Texas." *Journal of the Air & Waste Management Association* 64, no. 8 (2014/08/03): 917-926. Accessed 2015/04/21. http://dx.doi.org/10.1080/10962247.2014.904252.

Bates, T. S., et al. 2008. "Boundary Layer Aerosol Chemistry During Texaqs/Gomaccs 2006: Insights into Aerosol Sources and Transformation Processes." *Journal of Geophysical Research-Atmospheres* 113 (Nov). http://dx.doi.org/D00f0110.1029/2008jd010023.

Berkowitz, C. M., C. W. Spicer, and P. V. Doskey. 2005. "Hydrocarbon Observations and Ozone Production Rates in Western Houston During the Texas 2000 Air Quality Study." *Atmospheric Environment* 39, no. 19 (Jun): 3383-3396. http://dx.doi.org/10.1016/j.atmosenv.2004.12.007.

Bikkinna, S., et al. 2016. "Mass Absorption Efficiency of Light Absorbing Organic Aerosols from Source Region of Paddy-Residue Burning Emissions in the Indo-Gangetic Plain." *Atmospheric Environment* 125: 360-370. http://dx.doi.org/10.1016/j.atmosenv.2015.07.017.

Birch, M. E., and R. A. Cary. 1996. "Elemental Carbon-Based Method for Monitoring Occupational Exposures to Particulate Diesel Exhaust." *Aerosol Science and Technology* 25, no. 3 (Oct): 221-241. http://dx.doi.org/10.1080/02786829608965393.

Bond, T. C., and R. W. Bergstrom. 2006. "Light Absorption by Carbonaceous Particles: An Investigative Review." *Aerosol Science and Technology* 40, no. 1 (Jan): 27-67. http://dx.doi.org/10.1080/02786820500421521.

Bond, T. C., et al. 2013. "Bounding the Role of Black Carbon in the Climate System: A Scientific Assessment." *Journal of Geophysical Research-Atmospheres* 118, no. 11 (Jun 16): 5380-5552. http://dx.doi.org/Doi 10.1002/Jgrd.50171.

Bond, T. C., et al. 2004. "A Technology-Based Global Inventory of Black and Organic Carbon Emissions from Combustion." *Journal of Geophysical Research-Atmospheres* 109, no. D14 (Jul). http://dx.doi.org/10.1029/2003jd003697.

Browse, J., et al. 2013. "Impact of Future Arctic Shipping on High-Latitude Black Carbon Deposition." *Geophysical Research Letters* 40, no. 16 (Aug): 4459-4463. http://dx.doi.org/10.1002/grl.50876.

Budhavant, K., et al. 2015. "Radiocarbon-Based Source Apportionment of Elemental Carbon Aerosols at Two South Asian Receptor Observatories over a Full Annual Cycle." *Environmental Research Letters* 10, no. 6 (Jun). http://dx.doi.org/10.1088/1748-9326/10/6/064004.

Carlton, A. G., et al. 2010. "To What Extent Can Biogenic Soa Be Controlled?" *Environmental Science & Technology* 44, no. 9 (May): 3376-3380. http://dx.doi.org/10.1021/es903506b.

Chen, B., et al. 2013. "Source Forensics of Black Carbon Aerosols from China." *Environmental Science & Technology* 47, no. 16 (Aug): 9102-9108. http://dx.doi.org/10.1021/es401599r.

Chen, B., et al. 2012. "Emission and Transport of Carbonaceous Aerosols in Urbanized Coastal Areas in China." *Aerosol and Air Quality Research* 12, no. 3 (Jun): 371-378. http://dx.doi.org/10.4209/aaqr.2011.08.0131.

Chen, Y., and T. C. Bond. 2010. "Light Absorption by Organic Carbon from Wood Combustion." *Atmospheric Chemistry and Physics* 10, no. 4: 1773-1787. http://dx.doi.org WOS:000274851500018.

Chen, Y. J., et al. 2012. "Pm2.5 Source Apportionment in the Southeastern U.S.: Spatial and Seasonal Variations During 2001-2005." *Journal of Geophysical Research-Atmospheres* 117 (Apr). http://dx.doi.org/10.1029/2011jd016572.

Cheng, Y., et al. 2011. "Mass Absorption Efficiency of Elemental Carbon and Water-Soluble Organic Carbon in Beijing, China." *Atmospheric Chemistry and Physics* 11, no. 22: 11497-11510. http://dx.doi.org/10.5194/acp-11-11497-2011.

Chow, J. C. 1995. "Measurement Methods to Determine Compliance with Ambient Air Quality Standards for Suspended Particles." *Journal of the Air & Waste Management Association* 45, no. 5 (1995/05/01): 320-382. http://dx.doi.org/10.1080/10473289.1995.10467369.

Chow, J. C., et al. 2001. "Comparison of Improve and Niosh Carbon Measurements." *Aerosol Science and Technology* 34, no. 1 (Jan): 23-34. http://dx.doi.org/10.1080/027868201300081923.

Chow, J. C., et al. 2009. "Aerosol Light Absorption, Black Carbon, and Elemental Carbon at the Fresno Supersite, California." *Atmospheric Research* 93, no. 4 (Aug): 874-887. http://dx.doi.org/10.1016/j.atmosres.2009.04.010.

Chung, C. E., et al. 2005. "Global Anthropogenic Aerosol Direct Forcing Derived from Satellite and Ground-Based Observations." *Journal of Geophysical Research-Atmospheres* 110, no. D24 (Dec). http://dx.doi.org/10.1029/2005jd006356.

Chung, S. H., and J. H. Seinfeld. 2005. "Climate Response of Direct Radiative Forcing of Anthropogenic Black Carbon." *Journal of Geophysical Research-Atmospheres* 110, no. D11 (Jun). http://dx.doi.org/10.1029/2004jd005441.

Currie, L. A., et al. 2002. "A Critical Evaluation of Interlaboratory Data on Total, Elemental, and Isotopic Carbon in the Carbonaceous Particle Reference Material, Nist Srm 1649a." *Journal of Research of the National Institute of Standards and Technology* 107, no. 3 (May-Jun): 279-298. http://dx.doi.org //000176575100004

Doherty, S. J., et al. 2010. "Light-Absorbing Impurities in Arctic Snow." *Atmospheric Chemistry and Physics* 10, no. 23 (2010): 11647-11680. http://dx.doi.org/10.5194/acp-10-11647-2010.

Draxler, R.R, and G.D. Rolph. 2010. "Hysplit (Hybrid Single-Particle Lagrangian Integrated Trajectory) Model Access Via Noaa Arl Ready Website (Http://Ready.Arl.Noaa.Gov/Hysplit.Php)."

Draxler, R.R., and G.D. Rolph. 2010. *Hysplit (Hybrid Single-Particle Lagrangian Integrated Trajectory) Model Access Via Noaa Arl Ready Website (Http://Ready.Arl.Noaa.Gov/Hysplit.Php)*. Silver Spring, MD: NOAA Air Resources Laboratory.

Dusek, U., et al. 2014. "Evaluation of a Two-Step Thermal Method for Separating Organic and Elemental Carbon for Radiocarbon Analysis." *Atmospheric Measurement Techniques* 7, no. 7: 1943-1955. http://dx.doi.org/10.5194/amt-7-1943-2014.

Eckhardt, S., et al. 2015. "Current Model Capabilities for Simulating Black Carbon and Sulfate Concentrations in the Arctic Atmosphere: A Multi-Model Evaluation Using a Comprehensive Measurement Data Set." *Atmos. Chem. Phys.* 15, no. 16: 9413-9433. http://dx.doi.org/10.5194/acp-15-9413-2015.

Eckhardt, S., et al. 2003. "The North Atlantic Oscillation Controls Air Pollution Transport to the Arctic." *Atmos. Chem. Phys.* 3, no. 5: 1769-1778. http://dx.doi.org/10.5194/acp-3-1769-2003.

Office of Air Quality Planning & Standards. 2004. *Cmb8.2 User's Manual. Report Number Epa-452/R-04-011,* by EPA. Research Triangle Park, NC.

Fan, J. W., et al. 2005. "Simulations of Fine Particulate Matter (Pm2.5) in Houston, Texas." *Journal of Geophysical Research-Atmospheres* 110, no. D16 (Aug). http://dx.doi.org/D1620310.1029/2005jd005805.

Feng, Y., V. Ramanathan, and V. R. Kotamarthi. 2013. "Brown Carbon: A Significant Atmospheric Absorber of Solar Radiation?" *Atmos. Chem. Phys.* 13, no. 17: 8607-8621. http://dx.doi.org/10.5194/acp-13-8607-2013.

Fine, P. M., G. R. Cass, and B. R. T. Simoneit. 2002. "Chemical Characterization of Fine Particle Emissions from the Fireplace Combustion of Woods Grown in the Southern United States." *Environmental Science & Technology* 36, no. 7 (Apr 1): 1442-1451. http://dx.doi.org/10.1021/es0108988.

Fine, P. M., G. R. Cass, and B. R. T. Simoneit. 2004. "Chemical Characterization of Fine Particle Emissions from the Fireplace Combustion of Wood Types Grown in the Midwestern and Western United States." *Environmental Engineering Science* 21, no. 3 (May-Jun): 387-409. http://dx.doi.org/10.1089/109287504323067021.

Fu, P., K. Kawamura, and L. A. Barrie. 2009. "Photochemical and Other Sources of Organic Compounds in the Canadian High Arctic Aerosol Pollution During Winter-Spring." *Environmental Science & Technology* 43, no. 2 (Jan): 286-292. http://dx.doi.org/10.1021/es803046q.

Fu, Pingqing, et al. 2009. "Isoprene, Monoterpene, and Sesquiterpene Oxidation Products in the High Arctic Aerosols During Late Winter to Early Summer." *Environmental Science & Technology* 43, no. 11 (2009/06/01): 4022-4028. Accessed 2015/01/06. http://dx.doi.org/10.1021/es803669a.

Fuglestvedt, Jan S., et al. 2014. "Climate Penalty for Shifting Shipping to the Arctic." *Environmental Science & Technology* 48, no. 22 (Nov 18): 13273-13279. http://dx.doi.org/10.1021/es502379d.

Garg, Saryu, et al. 2016. "Limitation of the Use of the Absorption Angstrom Exponent for Source Apportionment of Equivalent Black Carbon: A Case Study from the North West Indo-Gangetic Plain." *Environmental Science & Technology* 50, no. 2 (2016/01/19): 814-824. http://dx.doi.org/10.1021/acs.est.5b03868.

Gustafsson, O., et al. 2009. "Brown Clouds over South Asia: Biomass or Fossil Fuel Combustion?" *Science* 323, no. 5913 (Jan): 495-498. http://dx.doi.org/10.1126/science.1164857.

Hadley, O. L., and T. W. Kirchstetter. 2012. "Black-Carbon Reduction of Snow Albedo." *Nature Climate Change* 2, no. 6 (Jun): 437-440. http://dx.doi.org/10.1038/nclimate1433.

Hara, K., et al. 2003. "Mixing States of Individual Aerosol Particles in Spring Arctic Troposphere During Astar 2000 Campaign." *Journal of Geophysical Research: Atmospheres* 108, no. D7: n/a-n/a. http://dx.doi.org/10.1029/2002jd002513.

Harmel, R. D., J. V. Bonta, and C. W. Richardson. 2007. "The Original Usda-Ars Experimental Watersheds in Texas and Ohio: Contributions from the Past and Visions for the Future." *Transactions of the Asabe* 50, no. 5 (Sep-Oct): 1669-1675. http://dx.doi.org//WOS:000251033300020.

Harmel, R. D., et al. 2003. "Long-Term Precipitation Analyses for the Central Texas Blackland Prairie." *Transactions of the Asae* 46, no. 5 (Sep-Oct): 1381-1388. http://dx.doi.org //WOS:000186733000009.

Harmel, R. D., et al. 2006. "Runoff and Soil Loss Relationships for the Texas Blackland Prairies Ecoregion." *Journal of Hydrology* 331, no. 3-4 (Dec): 471-483. http://dx.doi.org/10.1016/j.jhydrol.2006.05.033.

Heal, M. R. 2014. "The Application of Carbon-14 Analyses to the Source Apportionment of Atmospheric Carbonaceous Particulate Matter: A Review." *Analytical and Bioanalytical Chemistry* 406, no. 1 (Jan): 81-98. http://dx.doi.org/10.1007/s00216-013-7404-1.

Hecobian, A., et al. 2010. "Water-Soluble Organic Aerosol Material and the Light-Absorption Characteristics of Aqueous Extracts Measured over the Southeastern United States." *Atmospheric Chemistry and Physics* 10, no. 13: 5965-5977. http://dx.doi.org/10.5194/acp-10-5965-2010.

Hegg, D. A., et al. 2009. "Source Attribution of Black Carbon in Arctic Snow." *Environmental Science & Technology* 43, no. 11 (Jun): 4016-4021. http://dx.doi.org/10.1021/es803623f.

Hoffer, A., et al. 2006. "Optical Properties of Humic-Like Substances (Hulis) in Biomass-Burning Aerosols." *Atmospheric Chemistry and Physics* 6 (Aug): 3563-3570. http://dx.doi.org//WOS:000240205400004.

Hoffmann, D., et al. 2010. "Atmospheric Stability of Levoglucosan: A Detailed Laboratory and Modeling Study." *Environmental Science & Technology* 44, no. 2 (Jan 15): 694-699. http://dx.doi.org/10.1021/es902476f.

Hopke, Philip K. 2016. "Review of Receptor Modeling Methods for Source Apportionment." *Journal of the Air & Waste Management Association* 66, no. 3 (2016/03/03): 237-259. http://dx.doi.org/10.1080/10962247.2016.1140693.

Hu, Qi-Hou, et al. 2013. "Levoglucosan Indicates High Levels of Biomass Burning Aerosols over Oceans from the Arctic to Antarctic." *Scientific Reports* 3: 3119. http://dx.doi.org/10.1038/srep03119.

Huang, L., et al. 2006. "Stable Isotope Measurements of Carbon Fractions (Oc/Ec) in Airborne Particulate: A New Dimension for Source Characterization and Apportionment." *Atmospheric Environment* 40, no. 15: 2690-2705. http://dx.doi.org/http://dx.doi.org/10.1016/j.atmosenv.2005.11.062.

Hung, H., et al. 2005. "Temporal and Spatial Variabilities of Atmospheric Polychlorinated Biphenyls (Pcbs), Organochlorine (Oc) Pesticides and Polycyclic Aromatic Hydrocarbons (Pahs) in the Canadian Arctic: Results from a Decade of Monitoring." *Science of the Total Environment* 342, no. 1-3 (Apr 15): 119-144. http://dx.doi.org/10.1016/j.scitotenv.2004.12.058.

Iinuma, Y., et al. 2007. "Source Characterization of Biomass Burning Particles: The Combustion of Selected European Conifers, African Hardwood, Savanna Grass, and German and Indonesian Peat." *Journal of Geophysical Research-Atmospheres* 112, no. D8 (Apr). http://dx.doi.org/10.1029/2006jd007120.

IPCC. 2007. *Climate Change 2007: Impacts, Adaptation and Vulnerability. Contribution of Working Group Ii to the Fourth Assessment Report of the Intergovernmental Panel on Climate Change*, edited by M.L Parry, et al.: Cambridge University Press.

IPCC. 2013. *Climate Change 2013: The Physical Science Basis. Contribution of Working Group I to the Fifth Assessment Report of the Intergovernmental Panel on Climate Change*: Cambridge University Press.

Kawamura, Kimitaka, Hideki Kasukabe, and Leonard A. Barrie. 2010. "Secondary Formation of Water-Soluble Organic Acids and A-Dicarbonyls and Their Contributions to Total Carbon and Water-Soluble Organic Carbon: Photochemical Aging of Organic Aerosols in the Arctic Spring." *Journal of Geophysical Research: Atmospheres* 115, no. D21: D21306. http://dx.doi.org/10.1029/2010jd014299.

Kirchstetter, T. W., T. Novakov, and P. V. Hobbs. 2004. "Evidence That the Spectral Dependence of Light Absorption by Aerosols Is Affected by Organic Carbon." *Journal of Geophysical Research-Atmospheres* 109, no. D21 (Nov). http://dx.doi.org/10.1029/2004jd004999.

Kirillova, E.N. 2013. "Dual Isotope (^{13}c -^{14}c) Studies of Water-Soluble Organic Carbon (Wsoc) Aerosols in South and East Asia." Dissertation, Stockholm University.

Kirillova, E. N., et al. 2014. "Sources and Light Absorption of Water-Soluble Organic Carbon Aerosols in the Outflow from Northern China." *Atmos. Chem. Phys.* 14, no. 3: 1413-1422. http://dx.doi.org/10.5194/acp-14-1413-2014.

Kirillova, E. N., et al. 2010. "Natural Abundance C-13 and C-14 Analysis of Water-Soluble Organic Carbon in Atmospheric Aerosols." *Analytical Chemistry* 82, no. 19 (Oct): 7973-7978. http://dx.doi.org/10.1021/ac1014436.

Kirillova, E. N., et al. 2013. "13c- and 14c-Based Study of Sources and Atmospheric Processing of Water-Soluble Organic Carbon (Wsoc) in South Asian Aerosols." *Journal of Geophysical Research: Atmospheres* 118, no. 2: 614-626. http://dx.doi.org/10.1002/jgrd.50130.

Koch, D., and J. Hansen. 2005. "Distant Origins of Arctic Black Carbon: A Goddard Institute for Space Studies Modele Experiment." *Journal of Geophysical Research-Atmospheres* 110, no. D4 (Feb). http://dx.doi.org/10.1029/2004jd005296.

Kroll, Jesse H., and John H. Seinfeld. 2008. "Chemistry of Secondary Organic Aerosol: Formation and Evolution of Low-Volatility Organics in the Atmosphere." *Atmospheric Environment* 42, no. 16: 3593-3624. http://dx.doi.org/http://dx.doi.org/10.1016/j.atmosenv.2008.01.003.

Kuwayama, T., et al. 2013. "Particulate Matter Emissions Reductions Due to Adoption of Clean Diesel Technology at a Major Shipping Port." *Aerosol Science and Technology* 47, no. 1: 29-36. http://dx.doi.org/10.1080/02786826.2012.720049.

L'Heureux, Michelle, et al. 2010. "Unusual Extremes in the Negative Phase of the Arctic Oscillation During 2009." *Geophysical Research Letters* 37, no. 10: n/a-n/a. http://dx.doi.org/10.1029/2010gl043338.

Laskin, Alexander, Julia Laskin, and Sergey A. Nizkorodov. 2015. "Chemistry of Atmospheric Brown Carbon." *Chemical Reviews* (2015/02/26). http://dx.doi.org/10.1021/cr5006167.

Law, K. S., and A. Stohl. 2007. "Arctic Air Pollution: Origins and Impacts." *Science* 315, no. 5818 (Mar): 1537-1540. http://dx.doi.org/10.1126/science.1137695.

Lewis, C. W., G. A. Klouda, and W. D. Ellenson. 2004. "Radiocarbon Measurement of the Biogenic Contribution to Summertime Pm-2.5 Ambient Aerosol in Nashville, Tn." *Atmospheric Environment* 38, no. 35 (Nov): 6053-6061. http://dx.doi.org/10.1016/j.atmosenv.2004.06.011.

Li, Chaoliu, et al. 2016. "Concentrations and Light Absorption Characteristics of Carbonaceous Aerosol in Pm2.5 and Pm10 of Lhasa City, the Tibetan Plateau." *Atmospheric Environment* 127: 340-346. http://dx.doi.org/http://dx.doi.org/10.1016/j.atmosenv.2015.12.059.

Li, Q. F., et al. 2012. "Field Evaluation of Particulate Matter Measurements Using Tapered Element Oscillating Microbalance in a Layer House." *Journal of the Air & Waste Management Association* 62, no. 3 (Mar): 322-335. http://dx.doi.org/10.1080/10473289.2011.650316.

Lin, Lin, Milton L. Lee, and Delbert J. Eatough. 2010. "Review of Recent Advances in Detection of Organic Markers in Fine Particulate Matter and Their Use for Source Apportionment." *Journal of the Air & Waste Management Association* 60, no. 1 (Jan): 3-25. http://dx.doi.org/10.3155/1047-3289.60.1.3.

Lin, W. W., et al. 2011. "Acute Respiratory Inflammation in Children and Black Carbon in Ambient Air before and During the 2008 Beijing Olympics." *Environmental Health Perspectives* 119, no. 10 (Oct): 1507-1512. http://dx.doi.org/10.1289/ehp.1103461.

Lu, Zifeng, et al. 2015. "Light Absorption Properties and Radiative Effects of Primary Organic Aerosol Emissions." *Environmental Science & Technology* 49, no. 8 (2015/04/21): 4868-4877. http://dx.doi.org/10.1021/acs.est.5b00211.

Massabò, D., et al. 2015. "Multi-Wavelength Optical Determination of Black and Brown Carbon in Atmospheric Aerosols." *Atmospheric Environment* 108, no. 0: 1-12. http://dx.doi.org/http://dx.doi.org/10.1016/j.atmosenv.2015.02.058.

Massoli, P., et al. 2009. "Aerosol Optical and Hygroscopic Properties During Texaqs-Gomaccs 2006 and Their Impact on Aerosol Direct Radiative Forcing." *Journal of Geophysical Research-Atmospheres* 114 (Apr). http://dx.doi.org/10.1029/2008jd011604.

McComiskey, A., et al. 2008. "Direct Aerosol Forcing: Calculation from Observables and Sensitivities to Inputs." *Journal of Geophysical Research-Atmospheres* 113, no. D9 (May). http://dx.doi.org/10.1029/2007jd009170.

McNaughton, C. S., et al. 2011. "Absorbing Aerosol in the Troposphere of the Western Arctic During the 2008 Arctas/Arcpac Airborne Field Campaigns." *Atmospheric Chemistry and Physics* 11, no. 15 (2011): 7561-7582. http://dx.doi.org/10.5194/acp-11-7561-2011.

Mouteva, G. O., et al. 2015. "Black Carbon Aerosol Dynamics and Isotopic Composition in Alaska Linked with Boreal Fire Emissions and Depth of Burn in Organic Soils." *Global Biogeochemical Cycles*: 2015GB005247. http://dx.doi.org/10.1002/2015gb005247.

Nallathamby, P. D., et al. 2014. "Qualitative and Quantitative Assessment of Unresolved Complex Mixture in Pm2.5 of Bakersfield, Ca." *Atmospheric Environment* 98 (Dec): 368-375. http://dx.doi.org/DOI 10.1016/j.atmosenv.2014.09.006.

NOAA. 2015. "Daily Arctic Osciallation Index." 2015. http://www.cpc.ncep.noaa.gov/products/precip/CWlink/daily_ao_index/ao_index.html.

Nordenskiöld, A. E. 1883. "Nordenskiöld on the Inland Ice of Greenland." *Science* 2, no. 44 (Dec 7): 732-8. http://dx.doi.org/10.1126/science.ns-2.44.732.

Octaviani, M., et al. 2015. "Atmospheric Transport of Persistent Organic Pollutants to and from the Arctic under Present-Day and Future Climate." *Environ Sci Technol* 49, no. 6 (Mar 17): 3593-602. http://dx.doi.org/10.1021/es505636g.

Odemark, K., et al. 2012. "Short-Lived Climate Forcers from Current Shipping and Petroleum Activities in the Arctic." *Atmospheric Chemistry and Physics* 12, no. 4: 1979-1993. http://dx.doi.org/10.5194/acp-12-1979-2012.

Olson, Michael R., et al. 2015. "Investigation of Black and Brown Carbon Multiple-Wavelength-Dependent Light Absorption from Biomass and Fossil Fuel Combustion Source Emissions." *Journal of Geophysical Research: Atmospheres* 120, no. 13: 6682-6697. http://dx.doi.org/10.1002/2014jd022970.

Overland, J. E., and M. Y. Wang. 2013. "When Will the Summer Arctic Be Nearly Sea Ice Free?" *Geophysical Research Letters* 40, no. 10 (May): 2097-2101. http://dx.doi.org/10.1002/grl.50316.

Peters, G. P., et al. 2011. "Future Emissions from Shipping and Petroleum Activities in the Arctic." *Atmospheric Chemistry and Physics* 11, no. 11 (2011): 5305-5320. http://dx.doi.org/10.5194/acp-11-5305-2011.

Petzold, A., et al. 2013. "Recommendations for Reporting "Black Carbon" Measurements." *Atmos. Chem. Phys.* 13, no. 16: 8365-8379. http://dx.doi.org/10.5194/acp-13-8365-2013.

Pistone, Kristina, Ian Eisenman, and V. Ramanathan. 2014. "Observational Determination of Albedo Decrease Caused by Vanishing Arctic Sea Ice." *Proceedings of the National Academy of Sciences of the United States of America* 111, no. 9 (Mar 4): 3322-3326. http://dx.doi.org/10.1073/pnas.1318201111.

Polidori, A., et al. 2008. "Organic Pm2.5: Fractionation by Polarity, Ftir Spectroscopy, and Om/Oc Ratio for the Pittsburgh Aerosol." *Aerosol Science and Technology* 42, no. 3 (Mar): 233-246. http://dx.doi.org/10.1080/02786820801958767.

Pöschl, Ulrich. 2005. "Atmospheric Aerosols: Composition, Transformation, Climate and Health Effects." *Angewandte Chemie International Edition* 44, no. 46: 7520-7540. http://dx.doi.org/10.1002/anie.200501122.

Quinn, P. K., et al. 2009. "Decadal Trends in Aerosol Chemical Composition at Barrow, Alaska: 1976-2008." *Atmospheric Chemistry and Physics* 9, no. 22: 8883-8888. http://dx.doi.org/10.5194/acp-9-8883-2009.

Ram, K., and M. M. Sarin. 2009. "Absorption Coefficient and Site-Specific Mass Absorption Efficiency of Elemental Carbon in Aerosols over Urban, Rural, and High-Altitude Sites in India." *Environmental Science & Technology* 43, no. 21 (Nov): 8233-8239. http://dx.doi.org/10.1021/es9011542.

Ram, K., and M. M. Sarin. 2010. "Spatio-Temporal Variability in Atmospheric Abundances of Ec, Oc and Wsoc over Northern India." *Journal of Aerosol Science* 41, no. 1 (Jan): 88-98. http://dx.doi.org/10.1016/j.jaerosci.2009.11.004.

Ramana, M. V., et al. 2010. "Warming Influenced by the Ratio of Black Carbon to Sulphate and the Black-Carbon Source." *Nature Geoscience* 3, no. 8 (Aug): 542-545. http://dx.doi.org/10.1038/ngeo918.

Ramanathan, V., and G. Carmichael. 2008. "Global and Regional Climate Changes Due to Black Carbon." *Nature Geoscience* 1, no. 4 (Apr): 221-227. http://dx.doi.org/10.1038/ngeo156.

Ricard, V., et al. 2002. "Two Years of Continuous Aerosol Measurements in Northern Finland." *Journal of Geophysical Research: Atmospheres* 107, no. D11: ACH 10-1-ACH 10-17. http://dx.doi.org/10.1029/2001jd000952.

Russell, L. M., et al. 2009. "Oxygenated Fraction and Mass of Organic Aerosol from Direct Emission and Atmospheric Processing Measured on the R/V Ronald Brown During Texaqs/Gomaccs 2006." *Journal of Geophysical Research-Atmospheres* 114 (Apr). http://dx.doi.org/D00f0510.1029/2008jd011275.

Sand, M., et al. 2013a. "The Arctic Response to Remote and Local Forcing of Black Carbon." *Atmospheric Chemistry and Physics* 13, no. 1: 211-224. http://dx.doi.org/10.5194/acp-13-211-2013.

Sand, M., et al. 2013b. "Arctic Surface Temperature Change to Emissions of Black Carbon within Arctic or Midlatitudes." *Journal of Geophysical Research-Atmospheres* 118, no. 14 (Jul): 7788-7798. http://dx.doi.org/10.1002/jgrd.50613.

Schauer, J. J., et al. 2003. "Ace-Asia Intercomparison of a Thermal-Optical Method for the Determination of Particle-Phase Organic and Elemental Carbon." *Environmental Science & Technology* 37, no. 5 (2003/03/01): 993-1001. http://dx.doi.org/10.1021/es020622f.

Schauer, J. J., et al. 1996. "Source Apportionment of Airborne Particulate Matter Using Organic Compounds as Tracers." *Atmospheric Environment* 30, no. 22 (Nov): 3837-3855. http://dx.doi.org/10.1016/1352-2310(96)00085-4.

Schmidl, Christoph, et al. 2008. "Chemical Characterisation of Fine Particle Emissions from Wood Stove Combustion of Common Woods Growing in Mid-European Alpine Regions." *Atmospheric Environment* 42, no. 1 (Jan): 126-141. http://dx.doi.org/10.1016/j.atmosenv.2007.09.028.

Seinfeld, J. 2008. "Atmospheric Science - Black Carbon and Brown Clouds." *Nature Geoscience* 1, no. 1 (Jan): 15-16. http://dx.doi.org/10.1038/ngeo.2007.62.

Seinfeld, J., and S. N. Pandis. 2016. *Atmopsheric Chemistry and Physics: From Air Pollution to Climate Change*. Third ed. New Jersey: John Wiley & Sons.

Seinfeld, J.H, and S. N. Pandis. 2006. *Atmospheric Chemistry and Physics: From Air Pollution to Climate Change*. New York: Wiley.

Serreze, Mark C., and Roger G. Barry. 2011. "Processes and Impacts of Arctic Amplification: A Research Synthesis." *Global and Planetary Change* 77, no. 1-2 (May): 85-96. http://dx.doi.org/10.1016/j.gloplacha.2011.03.004.

Sharma, S., et al. 2006. "Variations and Sources of the Equivalent Black Carbon in the High Arctic Revealed by Long-Term Observations at Alert and Barrow: 1989-2003." *Journal of Geophysical Research-Atmospheres* 111, no. D14 (Jul 26). http://dx.doi.org/10.1029/2005jd006581.

Sharma, S., et al. 2013. "16-Year Simulation of Arctic Black Carbon: Transport, Source Contribution, and Sensitivity Analysis on Deposition." *Journal of Geophysical Research-Atmospheres* 118, no. 2 (Jan): 943-964. http://dx.doi.org/10.1029/2012jd017774.

Sharma, S., et al. 2004. "Long-Term Trends of the Black Carbon Concentrations in the Canadian Arctic." *Journal of Geophysical Research: Atmospheres* 109, no. D15: D15203. http://dx.doi.org/10.1029/2003jd004331.

Shaw, P. M., et al. 2010. "Arctic Organic Aerosol Measurements Show Particles from Mixed Combustion in Spring Haze and from Frost Flowers in Winter." *Geophysical Research Letters* 37, no. 10: L10803. http://dx.doi.org/10.1029/2010gl042831.

Sheesley, Rebecca. J., et al. 2012. "Year-Round Radiocarbon-Based Source Apportionment of Carbonaceous Aerosols at Two Background Sites in South Asia." *Journal of Geophysical Research-Atmospheres* 117 (May). http://dx.doi.org/10.1029/2011jd017161.

Sheesley, Rebecca. J., et al. 2009. "Tracking Personal Exposure to Particulate Diesel Exhaust in a Diesel Freight Terminal Using Organic Tracer Analysis." *Journal of Exposure Science and Environmental Epidemiology* 19, no. 2 (Feb): 172-186. http://dx.doi.org/10.1038/jes.2008.11.

Sheesley, Rebecca J., August Andersson, and Orjan Gustafsson. 2011. "Source Characterization of Organic Aerosols Using Monte Carlo Source Apportionment of Pahs at Two South Asian Receptor Sites." *Atmospheric Environment* 45, no. 23 (Jul): 3874-3881. http://dx.doi.org/10.1016/j.atmosenv.2011.01.031.

Sheesley, Rebecca J., et al. 2012. "Year-Round Radiocarbon-Based Source Apportionment of Carbonaceous Aerosols at Two Background Sites in South Asia." *J. Geophys. Res.* 117, no. D10: D10202. http://dx.doi.org/10.1029/2011jd017161.

Sheesley, Rebecca J., et al. 2007. "Sensitivity of Molecular Marker-Based Cmb Models to Biomass Burning Source Profiles." *Atmospheric Environment* 41, no. 39 (Dec): 9050-9063. http://dx.doi.org/10.1016/j.atmosenv.2007.08.011.

Shindell, D., and G. Faluvegi. 2009. "Climate Response to Regional Radiative Forcing During the Twentieth Century." *Nature Geoscience* 2, no. 4 (Apr): 294-300. http://dx.doi.org/10.1038/ngeo473.

Snyder, David C., et al. 2009. "Insights into the Origin of Water Soluble Organic Carbon in Atmospheric Fine Particulate Matter." *Aerosol Science and Technology* 43, no. 11 (2009): 1099-1107. http://dx.doi.org/10.1080/02786820903188701.

Srinivas, B., and M. M. Sarin. 2014. "Brown Carbon in Atmospheric Outflow from the Indo-Gangetic Plain: Mass Absorption Efficiency and Temporal Variability." *Atmospheric Environment* 89: 835-843. http://dx.doi.org/http://dx.doi.org/10.1016/j.atmosenv.2014.03.030.

Stohl, A. 2006. "Characteristics of Atmospheric Transport into the Arctic Troposphere." *Journal of Geophysical Research: Atmospheres* 111, no. D11: D11306. http://dx.doi.org/10.1029/2005jd006888.

Stohl, A., et al. 2015. "Evaluating the Climate and Air Quality Impacts of Short-Lived Pollutants." *Atmospheric Chemistry and Physics* 15, no. 18: 10529-10566. http://dx.doi.org/10.5194/acp-15-10529-2015.

Stohl, A., et al. 2013. "Black Carbon in the Arctic: The Underestimated Role of Gas Flaring and Residential Combustion Emissions." *Atmospheric Chemistry and Physics* 13, no. 17: 8833-8855. http://dx.doi.org/10.5194/acp-13-8833-2013.

Sullivan, David W., et al. 2013. "Field Study and Source Attribution for Pm2.5 and Pm10 with Resulting Reduction in Concentrations in the Neighborhood North of the Houston Ship Channel Based on Voluntary Efforts." *Journal of the Air & Waste Management Association* 63, no. 9 (2013/09/01): 1070-1082. Accessed 2013/08/26. http://dx.doi.org/10.1080/10962247.2013.775972.

Taketani, Fumikazu, et al. 2016. "Shipborne Observations of Atmospheric Black Carbon Aerosol Particles over the Arctic Ocean, Bering Sea, and North Pacific Ocean During September 2014." *Journal of Geophysical Research: Atmospheres* 121, no. 4: 1914-1921. http://dx.doi.org/10.1002/2015jd023648.

"Texas Commission on Environmental Quality Monitoring Site Information." 2013. Accessed March 15, 2013. http://www.tceq.texas.gov/cgi-bin/compliance/monops/site_photo.pl.

Thompson, J. E., et al. 2012. "Aerosol Optical Properties at Pasadena, Ca During Calnex 2010." *Atmospheric Environment* 55 (Aug): 190-200. http://dx.doi.org/10.1016/j.atmosenv.2012.03.011.

Turetsky, Merritt R., et al. 2011. "Recent Acceleration of Biomass Burning and Carbon Losses in Alaskan Forests and Peatlands." *Nature Geosci* 4, no. 1: 27-31. http://dx.doi.org/http://www.nature.com/ngeo/journal/v4/n1/abs/ngeo1027.html#supplementary-information.

"Us Environmental Protection Agency. Air Quality System Data Mart [Internet Databse]." 2012. Accessed February 15, 2013. http://www.epa.gov/ttn/airs/aqsdatamart/access/interface.htm.

Usenko, S., et al. 2005. "Trace Analysis of Semivolatile Organic Compounds in Large Volume Samples of Snow, Lake Water, and Groundwater." *Environmental Science & Technology* 39, no. 16 (Aug 15): 6006-6015. http://dx.doi.org/10.1021/es0506511.

von Schneidemesser, Erika, et al. 2009. "Concentrations and Sources of Carbonaceous Aerosol in the Atmosphere of Summit, Greenland." *Atmospheric Environment* 43, no. 27 (Sep): 4155-4162. http://dx.doi.org/10.1016/j.atmosenv.2009.05.043.

Wang, M., et al. 2015. "Carbonaceous Aerosols Recorded in a Southeastern Tibetan Glacier: Analysis of Temporal Variations and Model Estimates of Sources and Radiative Forcing." *Atmospheric Chemistry and Physics* 15, no. 3 (2015): 1191-1204. http://dx.doi.org/10.5194/acp-15-1191-2015.

Wang, M. Y., and J. E. Overland. 2012. "A Sea Ice Free Summer Arctic within 30 Years: An Update from Cmip5 Models." *Geophysical Research Letters* 39 (Sep). http://dx.doi.org/10.1029/2012gl052868.

Wang, Q., et al. 2011. "Sources of Carbonaceous Aerosols and Deposited Black Carbon in the Arctic in Winter-Spring: Implications for Radiative Forcing." *Atmospheric Chemistry and Physics* 11, no. 23: 12453-12473. http://dx.doi.org/10.5194/acp-11-12453-2011.

Wang, Y. G., et al. 2011. "Characterization of Ambient Black Carbon and Wood Burning Particles in Two Urban Areas." *Journal of Environmental Monitoring* 13, no. 7 (Jul): 1919-1926. http://dx.doi.org/10.1039/c1em10117j.

Wang, Yang, et al. 2013. "Temporal Variation of Mass Absorption Efficiency of Black Carbon at Urban and Suburban Locations." *Aerosol and Air Quality Research* 13, no. 1 (Feb): 275-286. http://dx.doi.org/10.4209/aaqr.2012.05.0125.

Warneke, C., et al. 2010. "An Important Contribution to Springtime Arctic Aerosol from Biomass Burning in Russia." *Geophysical Research Letters* 37 (Jan). http://dx.doi.org/10.1029/2009gl041816.

Watson, John G., et al. 2002. "Receptor Modeling Application Framework for Particle Source Apportionment." *Chemosphere* 49, no. 9: 1093-1136. http://dx.doi.org/http://dx.doi.org/10.1016/S0045-6535(02)00243-6.

Weingartner, E., et al. 2003. "Absorption of Light by Soot Particles: Determination of the Absorption Coefficient by Means of Aethalometers." *Journal of Aerosol Science* 34, no. 10 (Oct): 1445-1463. http://dx.doi.org/10.1016/s0021-8502(03)00359-8.

Winiger, P., et al. 2015. "Isotope-Based Source Apportionment of Ec Aerosol Particles During Winter High-Pollution Events at the Zeppelin Observatory, Svalbard." *Environ Sci Technol* 49, no. 19 (Oct 6): 11959-66. http://dx.doi.org/10.1021/acs.est.5b02644.

Winton, Michael. 2006. "Amplified Arctic Climate Change: What Does Surface Albedo Feedback Have to Do with It?" *Geophysical Research Letters* 33, no. 3. http://dx.doi.org/10.1029/2005gl025244.

Wood, E. C., et al. 2010. "Investigation of the Correlation between Odd Oxygen and Secondary Organic Aerosol in Mexico City and Houston." *Atmospheric Chemistry and Physics* 10, no. 18: 8947-8968. http://dx.doi.org/10.5194/acp-10-8947-2010.

Wright, M. E., et al. 2010. "Extensive Aerosol Optical Properties and Aerosol Mass Related Measurements During Tramp/Texaqs 2006-Implications for Pm Compliance and Planning." *Atmospheric Environment* 44, no. 33 (Oct): 4035-4044. http://dx.doi.org/10.1016/j.atmosenv.2008.12.055.

Wu, Aiming, et al. 2006. "The Nonlinear Association between the Arctic Oscillation and North American Winter Climate." *Climate Dynamics* 26, no. 7-8 (2006/06/01): 865-879. http://dx.doi.org/10.1007/s00382-006-0118-8.

Wu, J., et al. 2009. "Exposure of Pm2.5 and Ec from Diesel and Gasoline Vehicles in Communities near the Ports of Los Angeles and Long Beach, California." *Atmospheric Environment* 43, no. 12 (Apr): 1962-1971. http://dx.doi.org/10.1016/j.atmosenv.2009.01.009.

Yan, Caiqing, et al. 2015. "Chemical Characteristics and Light-Absorbing Property of Water-Soluble Organic Carbon in Beijing: Biomass Burning Contributions." *Atmospheric Environment* 121: 4-12. http://dx.doi.org/http://dx.doi.org/10.1016/j.atmosenv.2015.05.005.

Yang, H., Q. F. Li, and J. Z. Yu. 2003. "Comparison of Two Methods for the Determination of Water-Soluble Organic Carbon in Atmospheric Particles." *Atmospheric Environment* 37, no. 6 (Feb): 865-870. http://dx.doi.org/10.1016/s1352-2310(02)00953-6.

Yttri, K. E., et al. 2014. "Quantifying Black Carbon from Biomass Burning by Means of Levoglucosan - a One-Year Time Series at the Arctic Observatory Zeppelin." *Atmospheric Chemistry and Physics* 14, no. 12 (2014): 6427-6442. http://dx.doi.org/10.5194/acp-14-6427-2014.

Zangrando, R., et al. 2013. "Molecular Markers of Biomass Burning in Arctic Aerosols." *Environmental Science & Technology* 47, no. 15 (Aug): 8565-8574. http://dx.doi.org/10.1021/es400125r.

Zaveri, R. A., et al. 2012. "Overview of the 2010 Carbonaceous Aerosols and Radiative Effects Study (Cares)." *Atmospheric Chemistry and Physics* 12, no. 16: 7647-7687. http://dx.doi.org/10.5194/acp-12-7647-2012.

Zhang, H. L., and Q. Ying. 2010. "Source Apportionment of Airborne Particulate Matter in Southeast Texas Using a Source-Oriented 3d Air Quality Model." *Atmospheric Environment* 44, no. 29 (Sep): 3547-3557. http://dx.doi.org/10.1016/j.atmosenv.2010.06.004.

Zhang, H. L., and Q. Ying. 2011. "Secondary Organic Aerosol Formation and Source Apportionment in Southeast Texas." *Atmospheric Environment* 45, no. 19 (Jun): 3217-3227. http://dx.doi.org/10.1016/j.atmosenv.2011.03.046.

Zhang, X. L., et al. 2013. "Sources, Composition and Absorption Angstrom Exponent of Light-Absorbing Organic Components in Aerosol Extracts from the Los Angeles Basin." *Environmental Science & Technology* 47, no. 8 (Apr): 3685-3693. http://dx.doi.org/10.1021/es305047b.

Zhang, X. L., et al. 2011. "Light-Absorbing Soluble Organic Aerosol in Los Angeles and Atlanta: A Contrast in Secondary Organic Aerosol." *Geophysical Research Letters* 38 (Nov). http://dx.doi.org/10.1029/2011gl049385.

Zhang, X., et al. 2012a. "Spatial and Seasonal Variations of Fine Particle Water-Soluble Organic Carbon (Wsoc) over the Southeastern United States: Implications for Secondary Organic Aerosol Formation." *Atmos. Chem. Phys.* 12, no. 14: 6593-6607. http://dx.doi.org/10.5194/acp-12-6593-2012.

Zhang, X., et al. 2012b. "Spatial and Seasonal Variations of Fine Particle Water-Soluble Organic Carbon (Wsoc) over the Southeastern United States: Implications for Secondary Organic Aerosol Formation." *Atmospheric Chemistry and Physics* 12, no. 14: 6593-6607. http://dx.doi.org/10.5194/acp-12-6593-2012.

Zotter, Peter, et al. 2014. "Diurnal Cycle of Fossil and Nonfossil Carbon Using Radiocarbon Analyses During Calnex." *Journal of Geophysical Research-Atmospheres* 119, no. 11 (Jun 16): 6818-6835. http://dx.doi.org/10.1002/2013jd021114.